Technical Report

TR-06-34

Ice sheet hydrology – a review

Peter Jansson, Jens-Ove Näslund
Department of Physical Geography and
Quaternary Geology, Stockholm University

Lars Rodhe, Geological Survey of Sweden

March 2007

Svensk Kärnbränslehantering AB
Swedish Nuclear Fuel
and Waste Management Co
Box 5864
SE-102 40 Stockholm Sweden
Tel 08-459 84 00
+46 8 459 84 00
Fax 08-661 57 19
+46 8 661 57 19

Ice sheet hydrology – a review

Peter Jansson, Jens-Ove Näslund
Department of Physical Geography and
Quaternary Geology, Stockholm University

Lars Rodhe, Geological Survey of Sweden

March 2007

Contents

1. Preface

This report summarizes the *theoretical* knowledge on water flow in and beneath glaciers and ice sheets and how these theories are applied in models to simulate the hydrology of ice sheets. The purpose is to present the state of knowledge and, perhaps more importantly, identify the gaps in our understanding of ice sheet hydrology. Many general concepts in hydrology and hydraulics are applicable to water flow in glaciers. However, the unique situation of having the liquid phase flowing in conduits of the solid phase of the same material, water, is not a commonly occurring phenomena. This situation means that the heat exchange between the phases and the resulting phase changes also have to be accounted for in the analysis. The fact that the solidus in the pressure-temperature dependent phase diagram of water has a negative slope provides further complications. Ice can thus melt or freeze from both temperature and pressure variations or variations in both.

In order to provide details of the current understanding of water flow in conjunction with deforming ice and to provide understanding for the development of ideas and models, emphasis has been put on the mathematical treatments, which are reproduced in detail. Qualitative results corroborating theory or, perhaps more often, questioning the simplifications made in theory, are also given. The overarching problem with our knowledge of glacier hydrology is the gap between the local theories of processes and the general flow of water in glaciers and ice sheets. Water is often channelized in non-stationary conduits through the ice, features which due to their minute size relative to the size of glaciers and ice sheets are difficult to incorporate in spatially larger models. New work is emerging which attempts to bridge the gap between the ice sheet spatial scale modelling and the details of our process understanding.

It is our hope that his report will provide both a broad overview and an in-depth understanding of glacier hydrology to be applied to ice sheets.

In Stockholm,
Peter Jansson, Jens-Ove Näslund, Lars Rodhe

2. The glacier hydrological system

The hydrology of glaciers has been reviewed by several authors (Weertman, 1972; Lang, 1987; Röthlisberger and Lang, 1987; Hooke, 1989; Hubbard and Nienow, 1997; Fountain and Walder, 1998; Schneider, 2000; Boulton *et al.*, 2001; Jansson *et al.*, 2003; Hock and Jansson, 2005; Hock *et al.*, 2005). However, most reviews concern specific topics and do not look at the wide spectrum of the topic, no reviews exist where the current state of knowledge is viewed in the context of ice sheets.

The traditional view of the glacier hydrological system is similar to a combination of a groundwater system and a limestone karst system of shafts and tunnels and consist of supra-, en- and subglacial systems components. Figure 2.1 shows the situation on a typical glacier in summer.

The surface can be divided into two parts, a lower part where the surface consists of solid ice, referred to as the ablation area since a net loss of mass occurs in this area, and where water will run off by mostly channelized surface flow and an upper part, referred to as the accumulation area because a net mass gain occurs, where the surface consists of permeable snow or firn, snow that has survived one year of melting. The snow and firn pack is porous and allows water to percolate into the glacier and accumulate at depth as firn water bodies, equivalent to groundwater bodies whereas ice effectively is impermeable.

On an ice sheet, the snow covered area can be further subdivided into zones

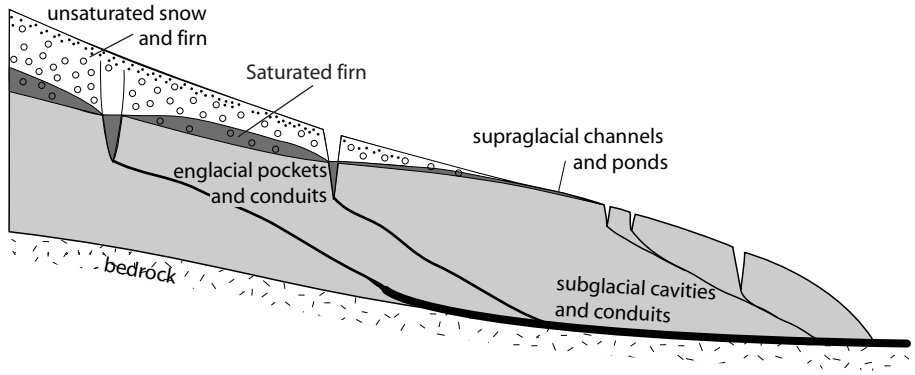

Figure 2.1. The hydrological system of a glacier consist of supra-, en- and subglacial subsystems. After Röthlisberger and Lang (1987).

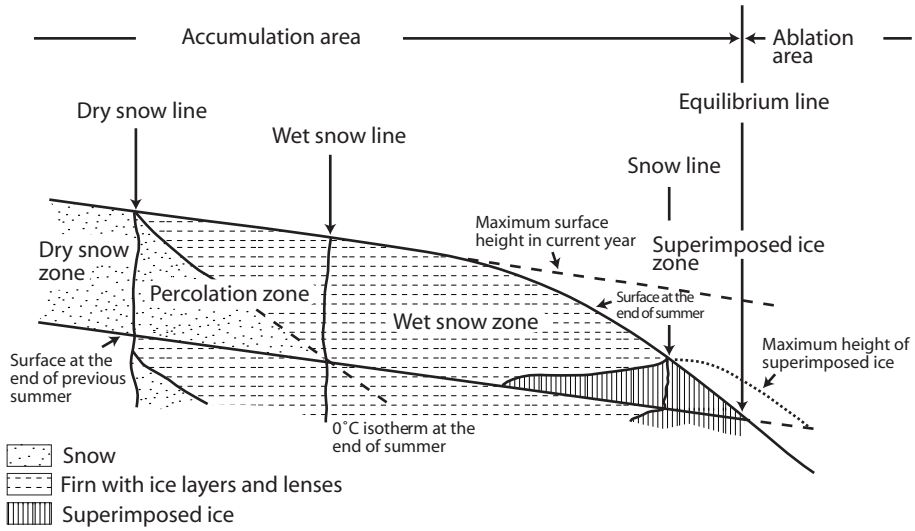

Figure 2.2. The glacier surface can be divided into different facies starting with the cold snow zone through the percolation zone to the wet snow zone. After Benson (1961), Müller (1962) and Paterson (1994).

depending on their thermal conditions (Figure 2.2; Benson, 1961; Müller, 1962; Paterson, 1994). At the center of ice sheets, an example of which is modern Greenland, the snow pack is cold and no surface melting occurs during any part of the year. This is the *dry snow zone*. At some point at lower elevation, surface melting can occur because of warmer conditions caused by the atmospheric temperature lapse rate. Hence there is a zone where percolation occurs increasingly wetting the upper part of the snow pack at lower altitude since the potential for melt increases at lower altitude. This zone is called the *percolation zone*. At some elevation the melting is strong enough to completely warm the snow pack. The zone of completely temperate snow is called the *wet snow zone*. These zones describe the conditions met during parts of the season. During winter most of the ice sheet will be covered by dry snow and development of the different zones initiate as air temperature rises during spring and summer. This also means that the different zones start to develop at lower altitude and move upglacier as the season progresses to reach their uppermost position at the end of the melt season or when the annual temperature cycle has reached maximum temperature. This also indicates that the surface flow system will develop throughout the entire melt season with accompanying effects on runoff and water input to a en- and subglacial drainage system.

The progressive development of different zones can also be followed on smaller glaciers. In the year 2000, mapping of the transient snow lines on Storglaciären Figure 2.3 reveals how the area of exposed ice is enlarged as the winter snow pack thins. As the area of exposed ice increases, the runoff also changes, showing more rapid response with increasing exposed area of ice (*e.g.* Hock *et al.*, 2005). Hence, the seasonality of the snow cover also introduces a seasonality in runoff characteristics

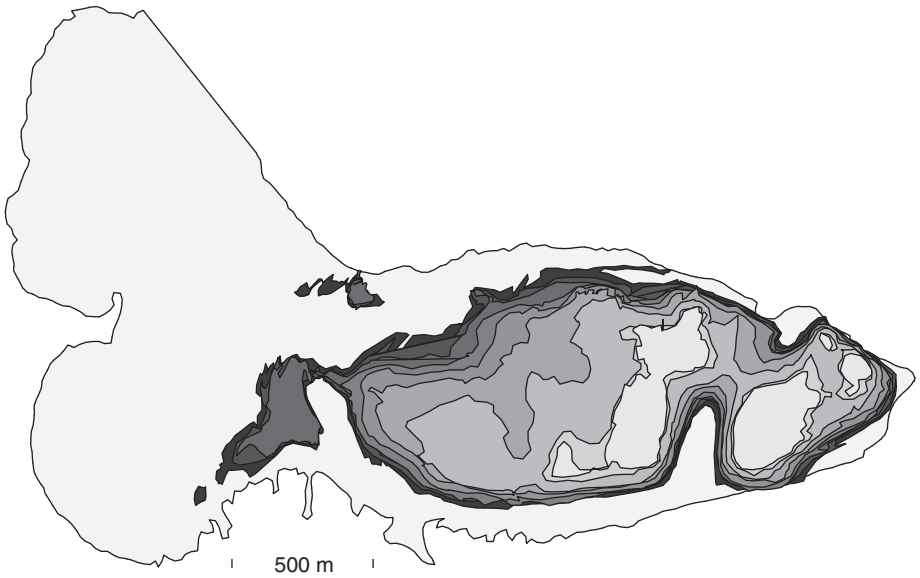

Figure 2.3. The snow line retreats during the course of a melt season. Transient snow lines were mapped during the year 2000 melt season and reveal the progressively larger area of bare ice which allows faster runoff. (Jansson, unpublished data).

from glaciers and ice sheets.

Surface water can enter the en- and subglacial system through crevasses and vertical shafts, moulins. If the ice is temperate it may also be slightly permeable. Water that enters the glacier will flow through an englacial system for some time. Commonly water reaches the bed within a couple of ice thicknesses in distance but englacial drainage can occur over longer distances. Most often this is associated with over-deepened basins.

The basal system can be described as either fast or slow response. In traditional views the fast system can be thought of in terms of a tunnel system and the slow in terms of a linked cavity system or basal water film. We will now describe these systems and their characteristics in more detail.

3. The supraglacial drainage system

The supraglacial drainage system strongly affects the runoff from glaciers and drains large quantities of water that is produced through surface melting and liquid precipitation and which may enter the en- and subglacial systems (*e.g.* Hock and Jansson, 2005; Hock *et al.*, 2005). The water production varies on a seasonal basis by the seasonal variation in temperature. In winter, snow covers all or most of a glacier, a situation which was likely also true of the Weichselian ice sheet even during its retreat phases. As melting starts, water will percolate into underlying cold snow and refreeze. This process warms the snow cover until it is at the melting temperature throughout. Only then will the snow pack release running water to runoff from the glacier. Hence, there is a delay between positive temperature and an increase in runoff from the snow by days or weeks.

The snow pack itself affects runoff after it has reached the melting point and allows water to pass through. Water can only be generated at or very near the snow or ice surface because that is where either liquid precipitation hits the glacier surface or where the exchange in energy between the atmosphere and the glacier can occur. Water thus generated must then percolate through the snow pack before running off on the underlying ice surface. Runoff on the ice surface is channelized and hence much faster, on the order of m/s, than the percolation velocity in snow which can be on the order of m/day (Schneider, 2001). As the summer season progresses, the snow cover decreases in both thickness and in terms of surface area coverage. As the percolation distance, both vertically and horizontally, decreases, partly due to the waning snow cover and partly through development of flow pathways through the snow pack, the response time of runoff to changes in water production decreases (Singh et al., 1997, 2000), the surface system becomes more responsive. This development of the system from one dominated by percolation to one dominated by channelized flow constitutes the major change in the drainage characteristics during late spring and early summer. Figure 2.3 shows the seasonal development of the areal snow cover on Storglaciären through weekly mappings of the snow line. One striking feature is the rapid changes that occur during the early summer as is evident from the development of the transient accumulation area ratio (AAR), calculated as the ratio between the snow covered area to the total surface area of the glacier for each survey.

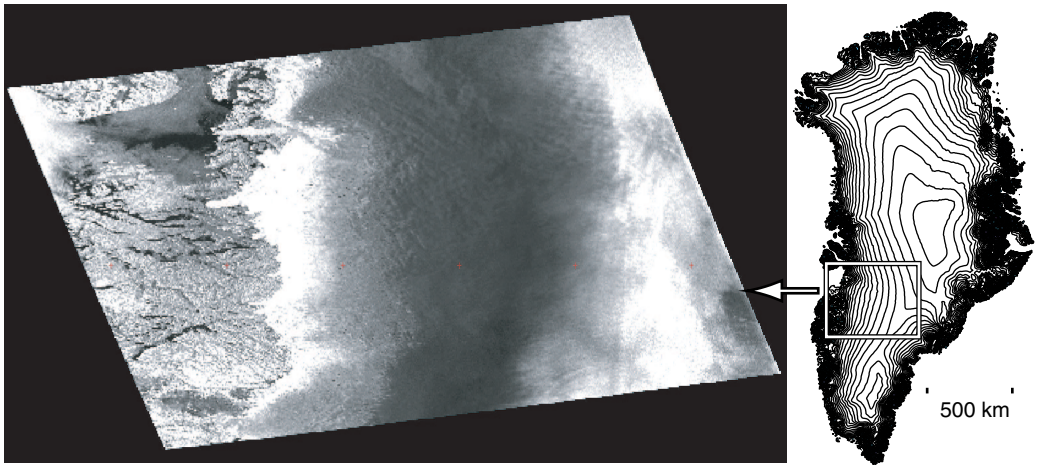

Figure 3.1. Radarsat-1 ScanSAR image of West Greenland (approximate coverage is given by the box on the map of Greenland) showing the different facies of the ice sheet from the exposed ice in the ablation area (white area at the left center of the image) through the superimposed ice, wet snow and percolation zones (darker shades of grey at the center of the image) to the dry snow zone to the far right of the image. The grey areas to the extreme right correspond to lower elevations on the eastern side of the ice divide. Figure provided by I. Brown.

On the Greenland ice sheet the different facies occupy vast areas because of the shallow slope of the ice surface at altitude. Figure 3.1 shows a section of the western central part of the ice sheet east and south of Disco Bay and covers all facies from the ice in the ablation area to the dry snow at the ice divide. The zones are 10–100 km wide.

During summer water generated on the ice surface is quickly discharged out from the glacier through supraglacial streams or recharging the en- and subglacial systems through crevasses and moulins. Water generated in the snow covered area percolates through the snow and firn pack and may accumulate as a groundwater aquifer at the firn-ice transition (ice being practically impermeable). This water constitutes a temporary storage that is filled during the initial melting in late spring and early summer, maintained during the summer season and released during the fall when surface melting decreases. Water from this storage is thus responsible for a substantial winter discharge from the glacier.

Water from the snow- and firn-covered areas is released either through runoff into surface streams on the glacier or into crevasses, common to the accumulation area. On the Greenland ice sheet, crevassed zones are commonplace in the ablation area due to the effects of subglacial topography on the surface morphology of the ice sheet Figure 3.2.

In the case of larger ice sheets, occurrence of surface bodies of water is common. On the western part of the Greenland ice sheet surface lakes covering several square km are common (Figure 3.3, Figures 3.4 and 3.5). These lakes have been found to be

Figure 3.2. Example of surface morphology and crevassed zones (darker areas) near the edge of the western Greenland Ice sheet near Russell Glacier. In the background, the supraglacial lake of Figure 3.5 is visible. The approximate width of the depicted part of the ice sheet front is 6 km.

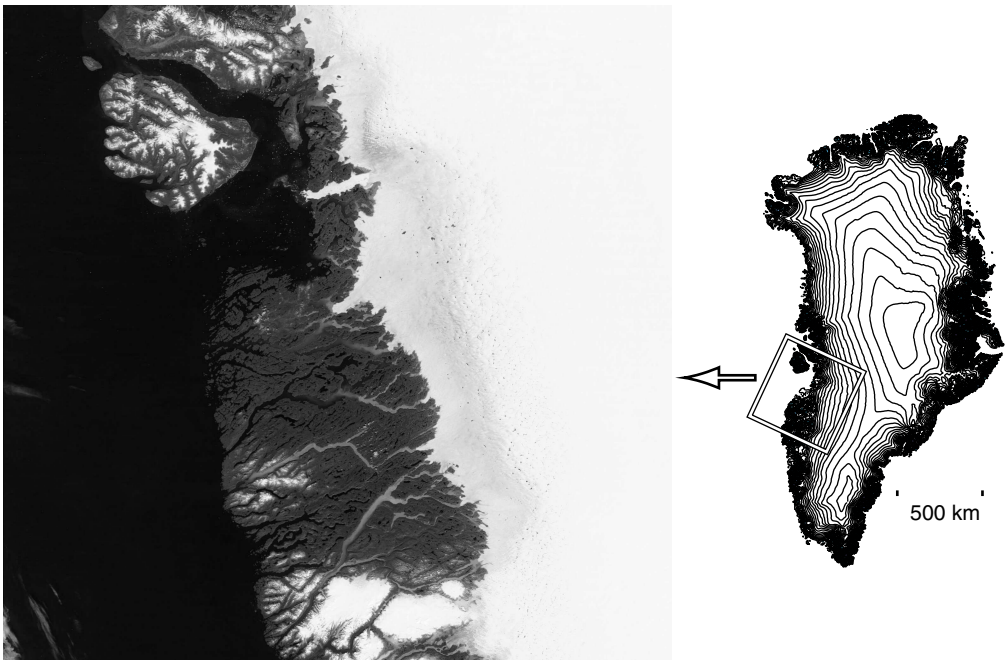

Figure 3.3. Surface lakes on the Greenland ice sheet.

perennial and thus contain water even during winter. The lakes are interconnected by surface drainage and seem to be be stable features. It is possible that this is due to the low surface slopes at higher elevations on the ice sheet which prevents water flow to reach high enough flow speeds to generate enough frictional heat to significantly deepen and steepen the channels in the system.

It seems reasonable to think that the hydrology of our past ice sheets would contain the same features as we can currently see on Greenland and that the same processes would be active. Like the current situation on Greenland, the characteristics would have varied around the ice sheet perimeter since the differences between, say, the southern and northern margins would have be significantly different with more melt occurring in the south. During the retreat of the ice sheet it is also likely that the surface profile was lowered, particularly while the terminus was calving as was the case during retreat in the Baltic basin. A lower profile would make the ablation area larger than during advance for any particular ice sheet configuration and hence produce more runoff from melt. The surface hydrology of the waning Weichselian ice sheet therefore sported similar hydrological systems to those met on the Greenland ice sheet but with flow rates significantly larger.

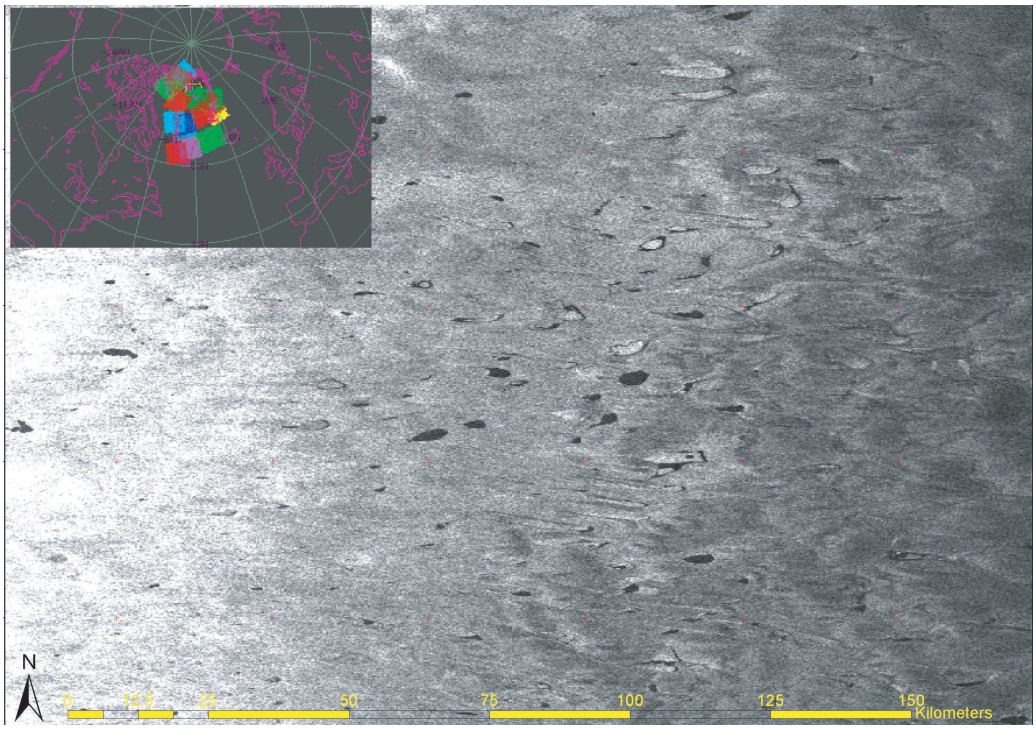

Figure 3.4. Radarsat-1 ScanSAR image of West Greenland showing a section of the ice sheet from the ice in the ablation area to the left through the superimposed ice area to the wet snow zone to the right. Lakes can be seen as black spots because the radar waves are absorbed by liquid water. Some of the lakes have ice floes remaining on the lake surface. Figure provided by I. Brown.

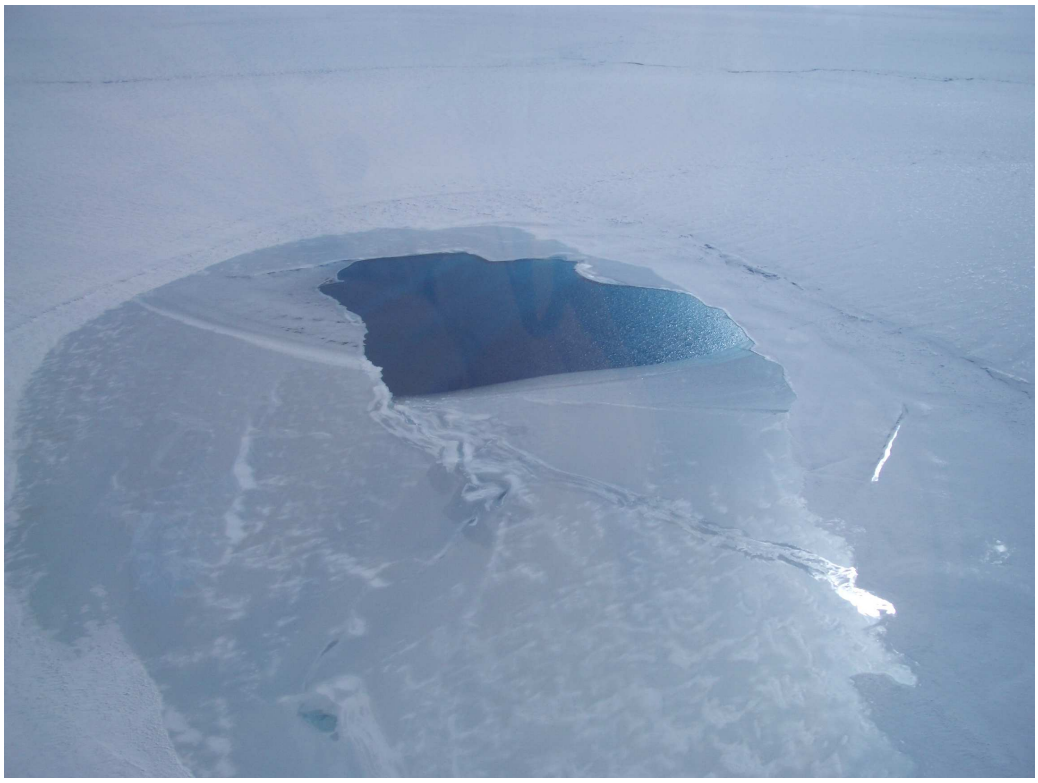

Figure 3.5. A partially frozen supraglacial lake near Russell Glacier, Western Greenland (10 September, 2005, photo: Peter Jansson).

4. The englacial drainage system

4.1 The general flow of water in glaciers

The general conditions for water flow in a glacier was investigated by Shreve (1972) who applied a simple hydraulic model of water-filled pipes to a glacier. In this model we assume pipes are cylindrical and that the closure rate of the cylinder occurs through deformation according to Glen's empirical flow law for ice

$$\dot{\varepsilon} = (\tau/B)^n \tag{4.1}$$

where $\dot{\varepsilon}$ is the strain rate, τ is the shear stress and B and n are the empirical constants. n is typically set to a value of 3 (*e.g.* Hooke, 1981). By dimensional analysis Shreve obtained the following expression for the pressure in the conduit:

$$P_w = P_i + KnB \left| \frac{\dot{r} - M}{r} \right|^{1/n} \text{sign}\,(\dot{r} - M) \tag{4.2}$$

where P_w and P_i are the pressures in the water and ice, respectively, K is a function of the general rate of deformation of the ice beyond the influence of the conduit (if no deformation occurs $K = 1$; Nye, 1953, p. 482), r is the radius of the conduit and $\dot{r}$ is the rate of change of the conduit radius and M is the melt rate of the passage wall. For simplicity, Shreve also made the assumption that P_i could be approximated by the weight of the overlying ice as

$$P_i = \rho_i g\,(H - z) \tag{4.3}$$

where ρ_i is the density of ice, g is the gravitational acceleration, H is the ice thickness and z is the height above the bed of the conduit. Since water moves in the direction of the negative gradient of the potential, Φ, which is given by

$$\Phi = \Phi_0 + P_w + \rho_w g z \tag{4.4}$$

where ρ_w is the density of water. The potential in the system of deforming conduits can be obtained by inserting (4.2) and (4.3) into Equation (4.4):

$$\Phi = \Phi_0 + \rho_i g H + (\rho_w - \rho_i)\, g z + KnB \left| \frac{\dot{r} - M}{r} \right|^{1/n} \text{sign}\,(\dot{r} - M)\ . \tag{4.5}$$

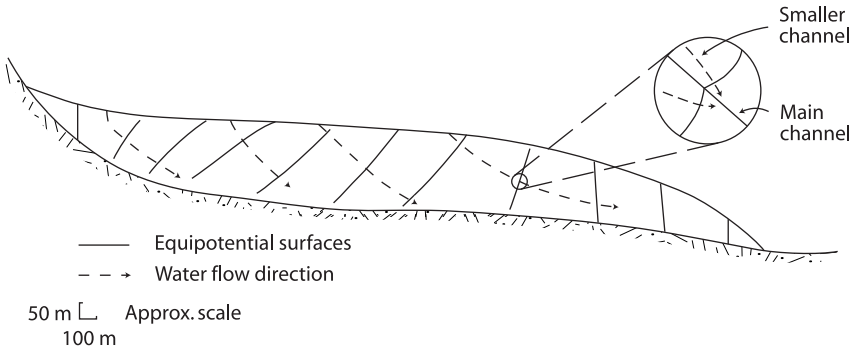

Figure 4.1. By calculating the potential equipotential surfaces, we can plot the general flow of water through the glacier, here in a longitudinal section. After Hooke (1989).

In the englacial system water flow will be perpendicular to the equipotential surfaces. We can estimate the orientation of these surfaces by first differentiating Equation (4.5) with respect to an arbitrary direction, S,

$$\frac{\partial \Phi}{\partial S} = \rho_i g \frac{\partial \left(H - z\right)}{\partial S} + \rho_w g \frac{\partial z}{\partial S} \tag{4.6}$$

Since the conditions on an equipotential surface is that $\partial\Phi/\partial S = 0$, *i.e.* no change in potential with distance, we can determine the orientations of such planes as

$$-\left(\rho_w - \rho_i\right) \frac{\partial z}{\partial S} = \rho_i \frac{\partial H}{\partial S} \tag{4.7}$$

The slope of a the direction S in the x-direction is given by dz/dx. We can therefore multiply 4.7 by dS/dx and rearrange

$$\frac{\partial z}{\partial x} = \frac{\rho_i}{\rho_w - \rho_i} \frac{\partial H}{\partial x} \tag{4.8}$$

By inserting values for the densities we get that

$$\frac{\partial z}{\partial x} = -11 \tan^{-1} \left(\frac{\partial H}{\partial x} \right) \tag{4.9}$$

or that the slope of an equipotential plane (dz/dx) is -11 times the surface slope (dH/dx) and sloping upglacier (Figure 4.1).

Shreve's approach involves a stable ice and water pressure. In reality water pressures vary depending on input from melt and rain as we will se later. However, the idea is probably still valid for longer term perspectives where the average conditions in the hydraulic system is considered.

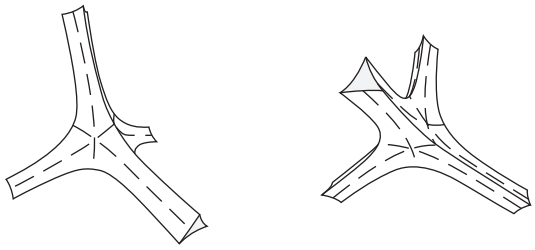

Figure 4.2. Junction between four water veins producing a tetrahedral shape void. (after Nye and Frank, 1973)

4.2 Water flow through ice

Water flow through ice can possibly occur as either Darcian flow through a permeable medium or through larger discrete conduits. We will start by reviewing the possibility of flow through the ice itself.

The extent to which ice is permeable and can can transmit water has been debated. Steineman (1958a,b) suggested that water could exist in temperate ice only in tetrahedral pockets and that water flow through ice was negligible. Numerous early discoverers (cited by Lliboutry, 1971) found that dye poured on the glacier surface could penetrate in between ice crystals in surface ice and in ice in tension such as in a crevasse field but not in regions of compression and on ice tunnel walls (where ice is in compression). This indicated that the occurrence of water pathways was related to the stresses in the ice. Lliboutry (1971), Nye and Mae (1972) and Nye and Frank (1973) showed how small conduits could exist between individual ice crystals, so called three-grain intersections (Figure 4.2). In addition, water can also collect in tetrahedral pockets where four grains intersect. The three-grain intersections and the tetrahedral junctions thus form a network of passages that would allow water to move freely through the temperate ice.

The theoretical equilibrium position of the water phase relative to the grain structure is governed by the relative surface energies of ice–ice and ice–water interfaces. The geometry of the water inclusions can be defined by the dihedral angle φ measured in the liquid between the three surfaces solid–solid, solid–liquid, liquid–solid (Figure 4.3). We also define the specific free energies between a solid–solid interface (grain boundary) and a solid–liquid interface as γ_{ss} and γ_{sl}, respectively. Grain boundaries makes equal angles $(\pi - 1/2\varphi)$ with the two solid–liquid surfaces. We can thus establish

$$2\cos\frac{1}{2}\varphi = \frac{\gamma_{ss}}{\gamma_{sl}} \tag{4.10}$$

as a general condition for the geometry.

Grain boundaries at triple junctions meet at 120 degree under equilibrium conditions. This produces veins with equilateral curvilinear triangular cross-sections (Figure 4.4). By applying the following four principles,

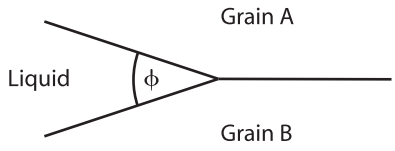

Figure 4.3. Geometry of a unction between two grains and a water vein. (after Nye and Frank, 1973)

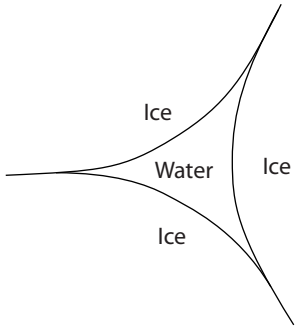

Figure 4.4. Equilateral curvilinear cross-section of a three grain intersection vein (after Nye and Frank, 1973)

(a) the condition formulated in Equation (4.10) on the dihedral angle must be satisfied at all edges where the liquid is in contact with a grain boundary

(b) the melting point must be the same at all points of the solid-liquid interface, and therefore the sum of the principal curvatures of the interface must be constant

(c) the interface must be stable against small displacements

(d) of alternative configurations all satisfying (a), (b) and (c), the one with the lowest melting point is preferred

Nye and Frank (1973) established Table 4.1. Measurements by Ketcham and Hobbs (1969) indicate that $\varphi = 20^\circ \pm 10^\circ$ which implies that the stable form in ice should be three-grain intersection channels coupled together by non-spherical-faced concave tetrahedra (Table 4.1; Figure 4.2). Thus temperate ice can be considered permeable contrary to Steineman's conclusions.

The studies by Ketcham and Hobbs (1969) and Nye and Frank (1973) are based on calculations for pure water. Glacier ice contains impurities which may affect these results although observations by the authors corroborate theory. To estimate the flow through a vein system we follow Nye and Frank (1973) and assume that water pressure in he veins is close to the hydrostatic pressure in the surrounding ice. We can then approximate the water pressure by $\rho_i g d$, where ρ_i is the density of ice including the liquid water content, g is the gravitational acceleration, and

Table 4.1.
Summary of liquid inclusions as a function of relative surface energy and dihedral angle.

γ_{ss}/γ_{sl}	φ	position of liquid
∞	—	Films, veins and tetrahedra
2	0°	Veins and non-spherical-faced concave tetrahedra
$\sqrt{3}$	60°	Spherical-faced concave tetrahedra, flat-faced tetrahedra
$\sqrt{8/3}$	70° 32′	Spherical-faced convex tetrahedra, spheres anywhere
0	180°	

d is the depth from the ice surface. This pressure is less than $\rho_w g d$ which would give hydrostatic equilibrium and hence there will be a pressure gradient $dP/dx = (\rho_w - \rho_i)\, g$ which drives water downwards. Frank (1968) used a model in which crystals are defined as semi-regular truncated octahedra with sides equal to $\sqrt{2}a/4$. The liquid water content f can be related to the mean radius of the capillary channels R and the mean grain diameter a as $f = 6\pi\sqrt{2}\,(R/a)^2$. Four channels, inclined 45 degree, cross an area a^2 parallel to the square faces. The water flux q under the effect of the pressure gradient can then be expressed as

$$q = \frac{\pi R^4}{2^{3/2} a^2}\,(\rho_w - \rho_i)\, g = \frac{(\rho_w - \rho_i)\, g f^2 a^2}{\chi \eta} \tag{4.11}$$

(Frank, 1968) where f is the fractional volume occupied by water, a is the grain diameter, η is the viscosity of water and χ is a number that characterizes vein cross-section. Frank (1968) assigned a value of 640 for a circular cross-section but values of 1500–2000 would be more appropriate for the concave triangular cross-sections of the veins (Nye and Frank, 1973). Inserting values into Equation (5.3) yields fluxes of 0.009–90 cm year^{-1} for a range of f-values of 10^{-5}–10^{-3}. Assuming that $f < 10^{-3}$, which seems justifiable, this can be translated into a contribution to the base of the glacier of about 1 m of water per year. The transfer time for water to reach the bed from the surface will be O(10–100) years.

However, Lliboutry (1971) argued that Nye and Frank's (1973) calculation leads to inconsistencies. First, Lliboutry argued that with the flow rates given by $f = 10^{-3}$–10^{-2}, the heat dissipated from the water would be $\rho_w g Q dt$ and would increase the radius by dR as

$$\rho_i L 2\pi R dR = \rho_w\,(\rho_w - \rho_i)\, g^2 \pi R^2 dt/8\eta \tag{4.12}$$

or by rearranging

$$\frac{dR}{dt} = \frac{R^3}{\alpha} \tag{4.13}$$

where

$$\alpha = \frac{16\rho_i \eta L}{\rho_w \left(\rho_w - \rho_i\right) g^2} \tag{4.14}$$

Integrating Equation (4.13) with respect to t and assuming an initial radius R_0 yields

$$\frac{1}{2R_0^2} - \frac{1}{2R^2} = \frac{t}{\alpha} \tag{4.15}$$

which shows that $R \to \infty$ and the glacier would be melted after $t = \alpha/2R_0^2$; for $R_0 = 60$ µm, $t = 4$ years. For this process to remain negligible on a real glacier $\alpha/R_0^2 > 500$ years or $R_0 < 5$ µm and $f < 7 \times 10^{-6}$. Lliboutry (1971) therefore argued that some factor must be missing in Nye and Frank's (1973) theory. He identified the role of air bubbles as a likely contributor since glacier ice contains ∼1–2% air by volume and that bubbles because of the recrystallization processes during deformation would migrate towards crystal boundaries. The capillary forces at the air-water interface can suspend the column of water since it is larger than $\left(\rho_w - \rho_i\right) g\Delta z$, where Δz is the vertical height between the upper and lower meniscus of a bubble in a conduit. However, if one passage is blocked, water could find some other way to circumvent the blockage. Bubbles hence reduce the permeability but do not necessarily render the ice impermeable.

The deformation of ice causes constant recrystallization of the ice also at the grain boundaries. The processes at the grain boundaries involve melting and refreezing in response to locally very high stresses. Lliboutry (1971) thus argue that the water at the grain boundary is not a film with Poiseuille flow characteristics but rather a liquid-like transition layer (*e.g.* Drost-Hansen, 1967; Jellinek, 1967). The effect is that although liquid, the layer may in places be too thin to support flow. The recrystallization can also convert passages to inclusions, further reducing the permeability of the ice. Lliboutry thus concludes that ice may be permeable on the scale of a few grains but will when considering the bulk be practically impermeable and cannot be modeled as a Darcian flow type medium. With $R = 5$ µm the water percolating through the glacier is 0.012 cm year^{-1}. The deformational processes at the scale of individual grains thus determine the flow by causing opening and closure of conduits.

Raymond and Harrison (1975) studied ice samples from Blue Glacier, USA, and found conduits with diameter of millimeter scale. In one sample they also observed upward branching. the conduits were irregular from the bounding crystals. They also argue that the density of such conduits may be several per square meter near the surface of the glacier. Observations of centimeter-size conduits spouting water into crevasses are common (*e.g.* Schneider, 2001). Since water flow tends to concentrate into larger conduits (Röthlisberger, 1972; Shreve, 1972), Raymond and Harrison (1975) therefore argue that there may be an upwards branching system that can transport water from the surface to the bed in temperate glaciers.

The permeability of the glacier ice is thus very small and can be neglected when comparing to water fluxes transmitted through crevasses and moulins and to water

production from melting in other locations, *e.g.* subglacial melting from geothermal heat. Since most ice sheets, and the past ice sheets are no exceptions, consist of ice at sub-freezing temperature, we will not consider this process further. Whereas the processes may be important on temperate glaciers for establishing a connection between the surface and basal systems, the cold ice prevents establishment of such slow-flow systems to be established. We need to look at larger scale systems.

4.3 The coupling between surface runoff and en- and sub-glacial drainage

The englacial drainage system consists of tunnels and other water passage ways that transmit water from the surface to the bed or the glacier margin.

Water enters glaciers through crevasses and moulins. Moulins are formed when surface streams are intersected by crevasses. As the crevasses close, the frictional heat from the running water maintains open channels. As new crevasses form up-stream of older crevasses, new moulins continuously form in new locations (Figure 4.5). Although the process of formation of the moulin itself is clear, it is not clear how water entering new crevasses connect to already existing englacial conduits down-stream. With the exception of Holmlund and Hooke (1983); Reynaud (1987) and Holmlund (1988), very little research has been made to investigate the shape and complexity of the englacial drainage.

Holmlund (1988) used repeated mapping of ice structures on the surface of Storglaciären to create a layered model of the upper part of the englacial drainage system (Figure 4.6). This layered model clearly shows how a system of moulins are interconnected along the former crevasse plane. Holmlund and Hooke (1983); Holmlund (1988) also descended into moulins and found that the 30–40 m vertical shaft ended in a plunge pool with a highly sinuous channel descending at 45° from the vertical. This angle slightly disagrees with the $90° - 11\alpha = 33°$ angle of the local equipotential surfaces predicted by Shreve's 1972 theory. It thus seems that moulins are maintained down to a level roughly corresponding to the maximum depth of crevasses (the boundary where ice becomes plastic due to the overburden pressure) and that water flow continues in conduits sloping in the direction of maximum potential gradient through the ice to reach the bottom somewhere down-stream of the moulin. The discrepancy in angle of the descending channel between theory and observation may be the result between an imbalance between creep closure and melting due to viscous dissipation of heat. Based on subglacial water pressure measurements made in the area (*e.g.* Jansson, 1996), the englacial channels must harbor open channel flow along at least part of their length during low water pressure.

The issue of how connections between the surface and the bed are established has not been resolved. The situation is perhaps worse when considering moulins and englacial draiange to the bed formed in cold ice, a situation which commonly seems to be the case on the Greenland ice sheet (Thomsen *et al.*, 1989). Establishing

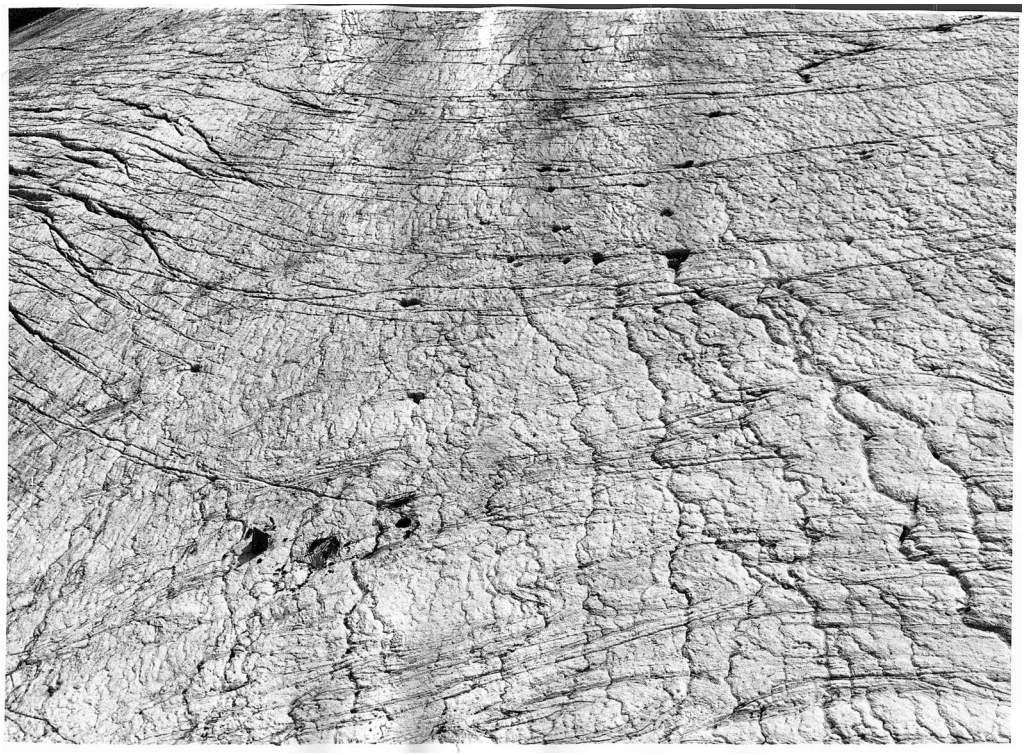

Figure 4.5. View over an area of moulins on Storglaciären. Open crevasses and crevasse traces are clearly visible and dark lines or bands on the ice surface. The dark semi-circular features at the end of the tortous surface streams are moulins. Several moulins have been formed along the same crevasse (trace). Photo: Johan Kleman, 19 Aug. 1981.

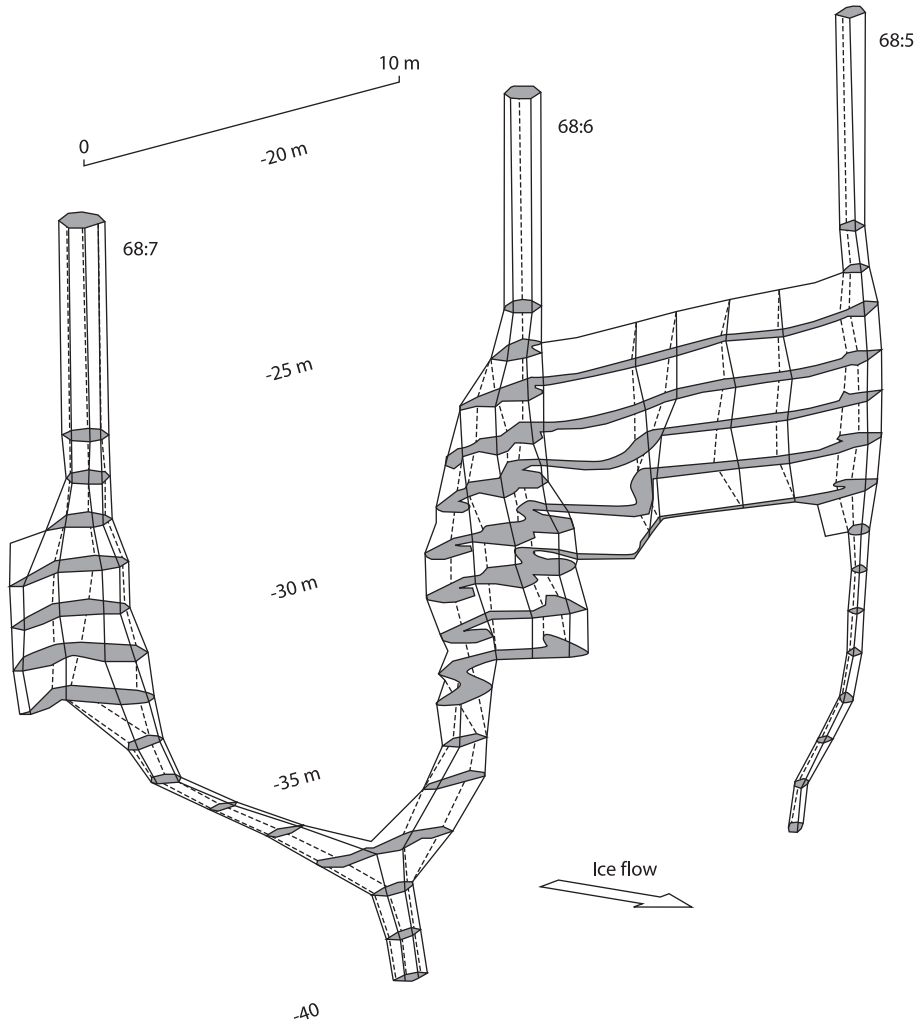

Figure 4.6. A moulin system on Storglaciären modeled by consecutive (1-year interval) surface mapping of ice structures. After Holmlund (1988).

processes that can establish a connection between surface and bed through thick ice and also operate under cold conditions are thus necessary

Alley *et al.* (2005) used an approach by Rubin (1995) considering magma-filled cracks through brittle crustal rocks to investigate the possibility for propagation of water-filled crevasses through cold ice. Weertman (1973), van der Veen (1998a), and Scambos *et al.* (2000) have shown that glacial deviatoric stresses were not sufficient to overcome hydrostatic stresses. Crevasses could hence not propagate to greater depths without being water-filled. If the crevasse was not filled to the surface, it would eventually be pinched off and propagate away as was described by Weertman (1973) and thus lose its surface connection. In such instances no connection can be established between surface and bed. Alley *et al.* (2005) argue that the sustained high water level in supraglacial lakes such as those seen in Figures 3.3 and 3.5 are key to providing the necessary over-pressure for the system to work.

We start by considering a water filled crack that extends down-wards (x-direction) from the ice surface a distance d. The opening of the crack is $2w$ in response to an internal pressure $\Delta P(x)$ perpendicular (y-direction) to the crack direction (z)

$$\Delta P(x) = P(x) - \sigma'_y(x) - P_{ct} \tag{4.16}$$

where P_{ct} is the dynamic drop in water pressure associated with crack propagation, σ'_y is the far-field deviatoric stress (negative if tensile), and $P(x)$ is the difference between the fluid pressure in the crack and the hydrostatic pressure in the ice. $P(x) = \Delta\rho g x$, where the density difference $\Delta\rho = \rho_{water} - \rho_{ice}$. We can approximate the half-width w of the crack at $x = 0$ by

$$w(x = 0) = \frac{\Delta P}{M} d \tag{4.17}$$

(Rubin, 1995) where $M = \mu/(1 - \nu')$ is the elastic stiffness, μ is the elastic shear modulus, and ν' is Poission's ratio. Following (Rubin, 1995) we assume linear elastic fracture mechanics and approximate the stress intensity factor K_I as

$$K_I = \Delta P \sqrt{d} \tag{4.18}$$

This implicitly assumes infinite crack length which obviously is not realistic (Alley *et al.*, 2005). This can be accommodated by applying a shape factor. Alley *et al.* (2005) points out that this factor is of order one or even close to one to be neglected their approach. To further simplify the problem Alley *et al.* (2005), following Rubin (1995), divide the problem into two. They first consider a shallow region where the buoyancy term $P(x)$ can be neglected and a deeper region where it becomes dominant. Alley *et al.* (2005) set the depth of this change to 100 m or more.

By applying a simple criterion for crack propagation, K_I exceeds the fracture toughness $K_I c$, the crack volume will increase, in absence of freezing, as long as the crack propagates. The volume can be approximated by a rectangular parallelopiped (more complex shapes do not significantly improve the results)

$$V = 2wd \tag{4.19}$$

The rate of volume increase due to crack deepening at a rate $u = \partial d/\partial t$ in the shallow region, where the deviatoric stress dominates, is

$$\left(\frac{\partial V}{\partial t}\right) = -\frac{4\sigma'_y du}{M} \tag{4.20}$$

σ'_y is held constant.

We also need to consider the thermal aspect of the problem.If we consider ice at its initial temperature T_0 and water at its pressure dependent freezing temperature T_{pmp} we can estimate the thickness of the frozen on layer $\delta(x)$ during initial stages of crack propagation

$$\delta(x) = 2\lambda\sqrt{\kappa t_f} \tag{4.21}$$

where

$$\lambda = \frac{C(T_{pmp} - T_0)}{\sqrt{\pi}L} \tag{4.22}$$

where κ is the thermal diffusivity, C is the specific heat and L is the latent heat of ice, t_f is the time since the onset of freezing at x. If we simplify by by setting u constant,Alley *et al.* (2005) admits this is an over-simplification, the total freezing rate in the crack can be estimated by integrating the time rate of change of $\delta(x)$ in Equation (4.21) from the surface to the depth d

$$\left(\frac{\partial V}{\partial t}\right)_{\text{freezing}} = -2\lambda\sqrt{\kappa u d} \tag{4.23}$$

For a crack to propagate to depth, it must remain connected to a supply of water. In order for propagation to occur the inflow must offset the freezing and new volume created by the crack propagation. This requires a drop in potential along the crack propagation direction. Most of the potential drop along a crack occurs very close to the crack tip due to the cubic dependence of laminar fluid flow on crack aperture.

To improve this Alley *et al.* (2005) make two simplifying assumptions to asses water inflow: (1) water flow in through the full width $2w$ and not the reduced width $2w - 2\delta$ and (2) the potential drop forcing flow towards the crack tip is distributed along the entire crack and not concentrated to the crack tip. These assumptions lead to quicker crack propagation than real cracks. We also requiring that the crack propagates as quickly as it can, the pressure drop P_{ct} must be such that $K_I = K_{Ic}$ exactly. We now combine Equation (4.16) and Equation (4.18) we get

$$P_{ct} = -\sigma'_y - \frac{K_{Ic}}{\sqrt{d}} \tag{4.24}$$

A limitation of the propagation speed is given by the inflow of fluid, which can be given as a flux per unit length (laminar flow between parallel plates, *e.g.* Rubin, 1995)

$$Q = \frac{G(2w)^3}{12\eta} \tag{4.25}$$

where

$$G = \frac{P_{ct}}{d} \tag{4.26}$$

is the magnitude of the potential driving the fluid flow and η is the viscosity of water.

We can obtain the propagation velocity for which the enlargement of the crack equals the freezing rate by equating Equations (4.20) and (4.23)

$$u = -\left(\frac{\lambda M}{-2\sigma'_y}\right)^2 \frac{\kappa}{d} \tag{4.27}$$

The crack-deepening velocity can be estimated for the situation where fluid inflow is just sufficient to fill the space created by the crack opening. We combine Equations (4.20) and (4.25) and solve for the velocity

$$u = -\frac{G(2w)^3 M}{48\sigma'_y d\eta} \tag{4.28}$$

We can then modify Equation (4.28) by taking w from Equation (4.17) with $\Delta P \approx -\sigma'_y(x)$ and G from Equations (4.26) and (4.24) with $P_{ct} > 0$, which means $-\sigma'_y > K_{Ic}/\sqrt{d}$ so that the crack is propagating,

$$u = {\sigma'_y}^2 \left(-\sigma'_y - \frac{K_{Ic}}{\sqrt{d}}\right) \frac{d}{6\eta M^2} \tag{4.29}$$

Equation (4.29) specifies a curve $u(\sigma'_y)$ for any depth d (Figure 4.7). For stress magnitudes higher than this curve, the crack is wide enough to allow water inflow to balance the volume increase from crack opening, thus maintaining the water-filled condition. Equation (4.27) also defines a curve in Figure 4.7 where higher stresses than the curve yield opening rates that exceed the freezing rate. Because the curves intersect, there is a minimum stress magnitude $-\sigma'_{y\min}$ necessary for propagation. We can solve for this stress by equating Equations (4.27) and (4.29)

$${\sigma'_{y\min}}^4 \left(-\sigma'_{y\min} - \frac{K_{Ic}}{\sqrt{d}}\right) - \frac{3M^4\kappa\eta\lambda^3}{2d^2} = 0 \tag{4.30}$$

or by substituting constants ($K_{Ic} = (1-4) \times 10^5$ Pa m$^{1/2}$ (van der Veen, 1998b), $M = 5 \times 10^9$ Pa, $\kappa = 1.18 \times 10^{-6}$ m^2 s,$^{-1}$ $\eta = 1.8 \times 10^{-3}$ Pa s, $C = 2093$ J kg $^{-1}$K,$^{-1}$ $L = 3.3 \times 10^5$ J kg)$^{-1}$

$${\sigma'_{y\min}}^4 \left(-\sigma'_{y\min} - 1.5 \times \frac{10^5}{\sqrt{d}}\right) = -\frac{2.7 \times 10^{27}}{d^2} \tag{4.31}$$

Alley *et al.* (2005) study thus shows that cracks that form under sufficient tensile stresses and with ample water supply can continue to grow through the ice to reach the bed. Provided the bed is at the melting point, subglacial tunnels can form through the Walder instability (Walder, 1982). Another important aspect of Alley *et al.*'s study is that crevasses can be maintained open at depth in a a glacier provided that the supply of water and the pressure within the water is maintained.

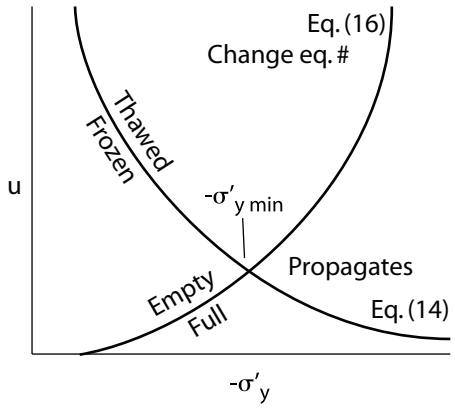

Figure 4.7. Schematic graph of the solution space of crack propagation speed u *vs.* magnityude of the tensile deviatoric stress $-\sigma'_y$ as represented by Equations 4.27 and 4.29.

4.4 Englacial flow in large conduits

Several studies have described englacial drainage based on water pressure measurements in bore holes or bore hole video observations (Hodge, 1976, 1979; Engelhardt, 1978; Hantz and Lliboutry, 1983; Hooke and Pohjola, 1994; Fountain, 1994; Fountain *et al.*, 2005a,b). Englacial drainage in over-deepened basins occurs because of the problems that arise when water is forced to flow uphill at the down-glacier end of the over-deepening. As water flows uphill, it must gain potential energy. The energy used for this is the heat contained in the water. However, subglacial water is at or very near, one or a few tenths of a degree from, the freezing point. As energy is drawn from the water, it must freeze. Basal tunnels on upslope beds will therefore be prone to freeze shut and hence such tunnels are difficult to maintain. This has been taken as a reason for the absence of observations of subglacial channelized drainage systems beneath glaciers in over-deepened basins. Tunnels in the ice sloping down in the direction of flow may instead be stable since they will be maintained with a slope in the down-glacier direction that allows frictional energy released by the running water to counteract closure from the ice pressure in the surrounding ice.

Hooke and Pohjola (1994) used borehole drainage depths to show that bore holes in the over-deepened basin of Storglaciären drained englacially. They further found that 66% of all bore holes drilled drained englacially and used this to estimate the existence of c. 800 channels across the glacier width of 1 km to explain the degree of success in hitting the drainage ways through drilling. Fountain *et al.* (2005a) found even higher success rates during drilling on Storglaciären in 2001–2003, reaching 80% success rate in hitting englacial drainage. Hooke (1991), Hooke and Pohjola (1994), Fountain *et al.* (2005a), Fountain *et al.* (2005b) and Jansson (unpublished data) further found that the drainage characteristics of the overdeepened basin was characterized by water pressures at or near overburden pressure throughout the year and that the hydraulic gradient of the system was very low. Hence flow rates were

also low.

Pohjola (1993) used bore hole video observations in bore holes on Storglaciären to conclude that channels where similar to R-channels. Subsequent studies by Harper and Humphrey (1995) and Copland *et al.* (1997) have shown similar features on other glaciers.

The observations discussed above led Fountain and Walder (1998) to propose a theory for the formation of englacial tunnels in over-deepened basins (Figure 4.8). Their view was that channels start on the surface of the glacier and gradually melt themselves down into the ice. In the initial phase the channels can deepen fast because they can steepen and allow the water to release frictional heat at an accelerating rate. At some stage the stream will be so deeply entrenched that the overlying ice will close above the water level of the channel and form a tunnel. The tunnel can deepen and steepen until it hits the bed at the downglacier end of the over-deepened basin. Once this level has been reached, the frictional energy in the water can only deepen the tunnel upglacier of the lip of the over-deepening, resulting in a gradual decrease in the slope of the tunnel. This lowering can continue until the tunnel reaches a slope where the frictional energy released from the flowing water yields a melt rate on the conduit walls that balances the closure rate from plastic deformation of surrounding ice. Thus, a stable tunnel has been established. Fountain and Walder (1998) suggested that water pressure in englacial conduits should be atmospheric as long as it is above the lowest point of the overdeepening. The conduits cut down into the ice as melting only occurs in the water-filled part of the conduits. Fountain and Walder (1998) theory explains englacial flow through the overdeepening with the consequence of low sediment load in that water. However, water still has the possibility to pick up sediment from the glacier bed at the downstream margin of the overdeepening. Röthlisberger and Lang's (1987) concept on the other hand, shows that englacial conduits might never reach the glacier bed at the downstream margin of overdeepenings. Both theories together might explain water flow through overdeepenings on englacial paths and low sediment load in Nordjåkk.

Fountain *et al.* (2005a,b) also used bore hole video observations on Storglaciären and found that the englacial drainage occurred through englacial crevasses (Figure 4.9). Out of 48 bore holes 76% of the holes intersected a hydraulically connected englacial feature. A total of 36 fracture-like features were observed. The occurrence of such crevasses could explain the high success rates in hitting englacial drainage since a crevasse is a planar feature and R-channels a discrete linear feature. The crevasses all had steep plunges ($\sim 70^{\circ}$), which increases the surface exposed to intersection with a bore hole, and narrow openings (~ 40 mm). The system was found to have be low gradient and thus exhibit low flow velocities $(\sim 10\ \mathrm{mms})^{-1}$. The depth of the crevasses varied substantially, from near the glacier surface (probably surface crevasses) to 96% of local ice depth, the deepest crevasse found at 131 mbelow the surface. They could not explain the origin of the crevasses, some of which seemed very fresh in appearance.

The crevasses observed and described for the first time on Storglaciären by (Foun-

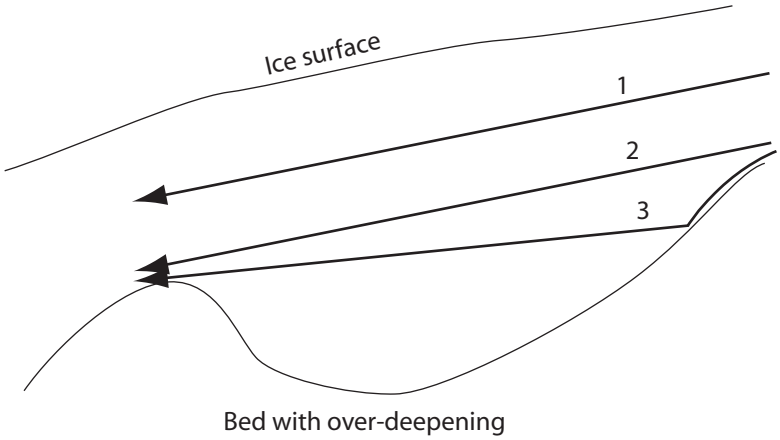

Figure 4.8. Model of the formation of englacial conduits in an over-deepened basin. After Fountain and Walder (1998). A channel (1) melts down into the ice from viscous dissipation of heat. It maintains a certain slope until it encounters the bed at the down-stream end of the over-deepening (2) and that end becomes pinned. Since the down-glacier end is not free to be lowered, the channel can only lower itself upstream of the pinning point, thus lowering its gradient at the same time (3).

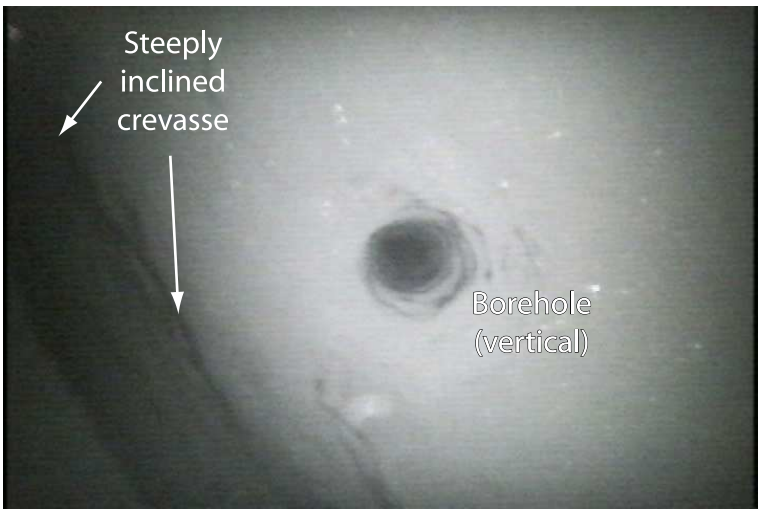

Figure 4.9. Frame capture of an englacial crevasse from a borehole video from within Storglaciären. The vertical borehole is visible as the circular feature at the center of the image. The crack dips steeply towards the lower left corner of the image.

tain *et al.*, 2005a,b) may have been seen in borehole videos from other glaciers but have not been recognized as part of a drainage system. There has also been debated whether crevasses can occur at great depth in glaciers and ice sheets because of the plasticity of ice under high pressure. A crevasse constitutes a brittle failure of ice under either low stress and low pressure or high stress and high pressure. Storglaciären is not a fast flowing glacier. Hence the occurrence of crevasses at depth is puzzling. Furthermore, the lack of observations of englacial crevasses in borehole videos taken by Pohjola (1993) in 1990 and 1991 remains unanswered. Jansson *et al.* (in prep.) have identified that ice velocity on Storglaciären has increased between 1982–84 and 2001. It is possible that the crevassing observed in 2001–2003 is a result of this acceleration although the increased velocity is till small by comparison to most glaciers in the world. Hence no satisfactory conclusion can yet be drawn on the origin of the englacial crevasse system.

In summary, the englacial drainage system can consist of a combination of tunnels and crevasses. It seems likely that crevasse systems are specific to over-deepened basins in the glacier topography. In other parts of the glacier, water is transmitted from the surface drainage system through straight or winding tunnels to the subglacial system.

5. The subglacial hydrological system

5.1 The general flow of water in glaciers

Traces of subglacial drainage paths, such as eskers and erosional features, can often be found at unexpected locations in the landscape, *e.g.* on valley sides rather than valley floors. The reason for this is the effects of the combination of bed topography and the equipotential field which drives the water. Shreve's (1972) approach to glacier drainage can also be applied at the base of the glacier, *i.e.* for the drainage along the bed of the glacier. In absence of ice, the potential field, determined by Equation (4.4) reduces to $\Phi = \Phi_0 + \rho_w g z$ since the water pressure in surface flowing water can be neglected. Hence the potential energy drives water flow across the landscape.

In a landscape covered by ice the "topography" forcing the water will be determined by the intersection between equipotential field and the topography and flow will occur on the bed topography in the direction perpendicular to line of intersection of the equipotential planes and the bed topography. As an example Schneider (2001) has calculated the potential field for Storglaciären given the existing surface and bed topographies (Figure 5.1). In Figure 5.2 we can see the trajectory (A→B) originating in the upper part of the glacier and emerging at the terminus both as it would flow in the basal topography (dashed line) and as it would flow under a potential field (solid line). It is clear from this figure that water flow paths will deviate from the path forced by topography alone.A dotted line also shows a back calculation of where water exiting the glacier in the north river would originate.It is also clear that water pathways could cling to the valley sides (cf. Figure 5.2).

The question of whether water flows en- or subglacially through overdeepenings is still unsolved. The areal distribution of zones in which critical adverse slope is reached is difficult to determine because the conduit slope does not necessarily equal the bed slope. If we knew the location and direction of such conduits, we could use bed slope to calculate conduit slope. The theoretical flow path normal to the maximum potential gradient up-glacier from Nordjåkk is shown in Figure 5.2a (bold line). Schneider calculated the ratio of surface slope to bed slope along this line and found one major zone in which adverse bed slope is more than 1.3 times surface slope (Figure 5.3b). The direction of englacial and subglacial conduits may be estimated

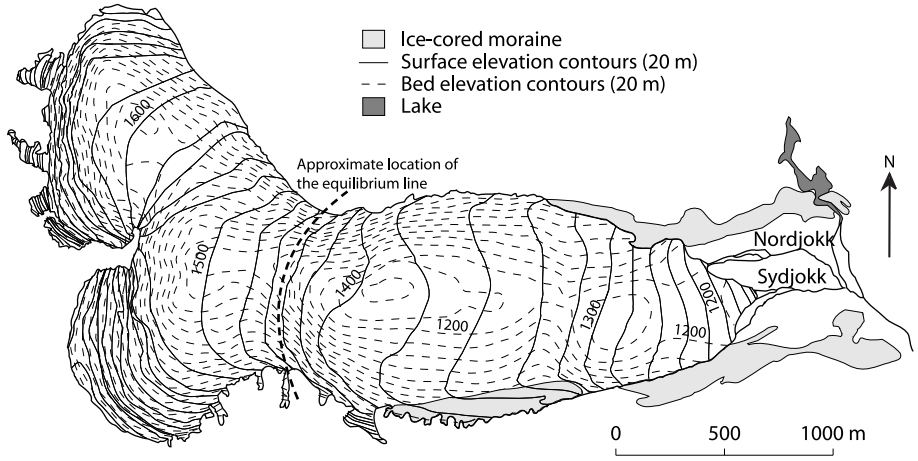

Figure 5.1. The surface and bed topography of Storglaciären. The map also shows the 2 major streams draining the glacier.

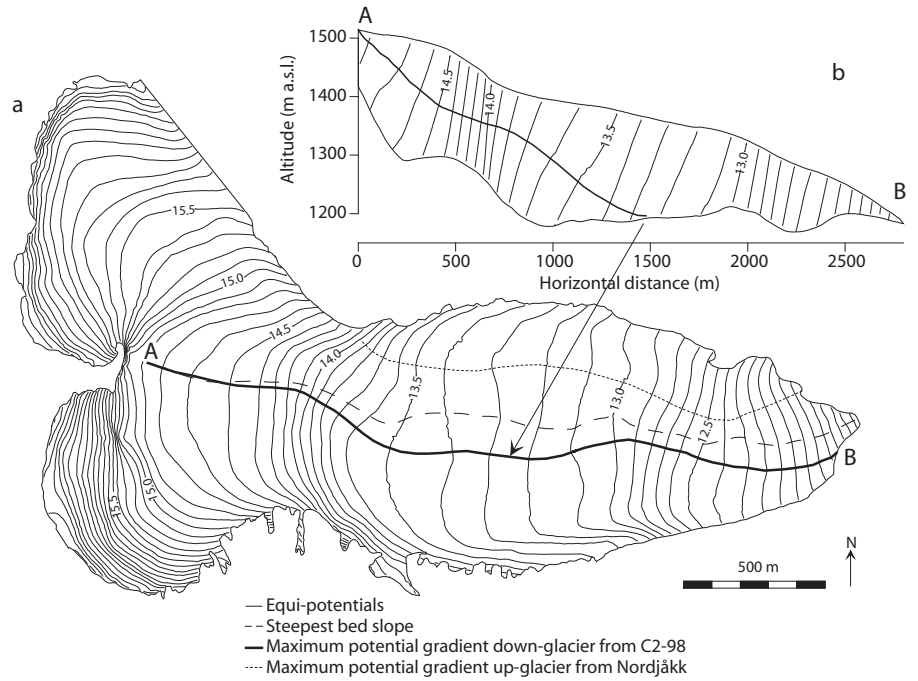

Figure 5.2. Equipotential lines on Storglaciären. Potential was calculated according to Equation (4.4), the potential is given in 10^6 N m^{-2}. Surface elevation is from Holmlund (1996) and bottom topography from Eriksson *et al.* (1993). The bold lines show theoretical flow path along maximum potential gradient from the injection point (A) to the terminal stream (B). The vertical profile shows surface and bottom elevation and potential lines along the bold line in the horizontal view of Storglaciären. The dashed line shows the gradient of steepest slope along the glacier bed, and the dotted line is theoretical flow path along maximum potential gradient up-glacier from Nordjåkk. Potential was calculated by Equation (4.4). From Schneider (2001).

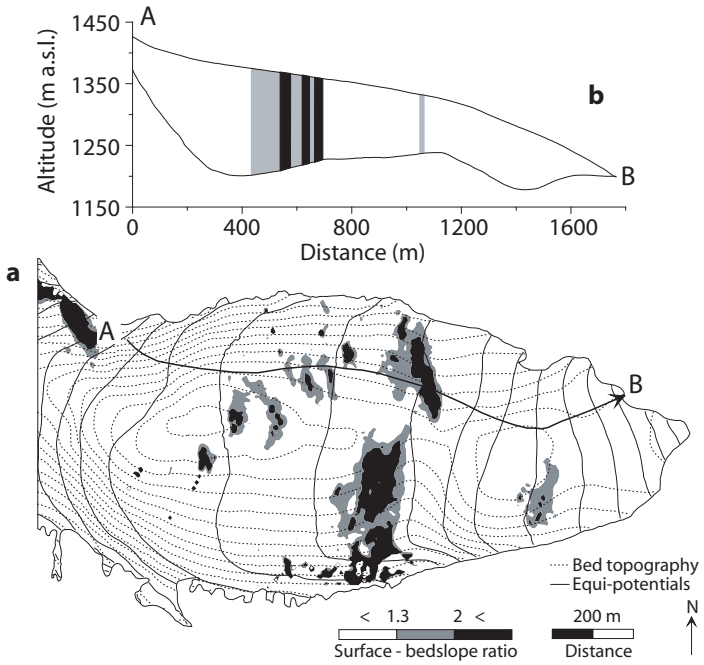

Figure 5.3. Areas of steep adverse bed slope in overdeepenings of Storglaciären. The ratio of surface slope to bed slope was calculated according to Röthlisberger and Lang (1987), critical values are 1.3 and 2.0 depending on air saturation in water. Thin lines are potential contours at the glacier bed (same values as in Figure 5.2) and dotted lines show bed topography. The bold line indicates maximum potential gradient up-glacier from Nordjåkk. From Schneider (2001).

by potential gradient in the glacier. From equipotential lines (Figure 5.3a), we can infer that the main direction of englacial and subglacial channels on Storglaciären is from west to east, the main direction of surface slope and hence ice flow, except within a narrow zone along the glacier margin. Accordingly, areal distribution of zones with critical slope ratio may be roughly estimated by calculating the ratio of surface slope to bed slope in west-east direction (Figure 5.3a). Critical surface-bed-slope ratio is most pronounced up-glacier of the riegel due to steep adverse bed slope. In the northern part of the glacier, areas with large bed-surface slope ratio are more frequent than in the southern part. Hooke *et al.* (1988) and Hooke and Pohjola (1994) report on water up-welling from subglacial sources into a borehole in the same area, which indicates an upward directed pressure gradient. The above analysis may explain englacial flow out of overdeepenings. However, the theory does not explain why water flow should occur along englacial paths in the center of the overdeepenings.

5.2 The subglacial water film

The importance of subglacial water on the dynamics of glaciers has been recognized since the studies of Müller and Iken (1973); Hodge (1974); Iken (1977, 1981); Iken *et al.* (1983); Iken and Bindscahdler (1986); Jansson (1995) who identified that glacier velocity relates to glacier sliding. Weertman (1962) proposed the existence of a thin water film at the interface between ice and bedrock. The role of the film was threefold

(a) water needs to flow from high pressure locations to low pressure locations in the regelation process (Tyndall and Huxley, 1857; Deeley and Parr, 1914)

(b) water prohibits molecular forces to act between the glacier ice and the bedrock and thus reduces drag

(c) water can be transported beneath the glacier on a wide scale

Nye (1973) estimated the thickness of this layer by studying the requirements for regelation. First we define the bed as smoothly undulating according to

$$z_0 = A \sin kx \tag{5.1}$$

where A is the amplitude of the bedrock undulations, assumed small compared with the wavelength $2\pi/k$. The volume of new ice formed from regelation in a portion of the bed ds is $w_n(x)ds$, where $w_n(x)$ is the ice velocity normal to the bed surface. The volume of water extracted from the water film is then given by $(\rho_i/\rho_w)\, w_n(x)ds$. Because of the small amplitude $ds \approx dx$ so that

$$dq = -\left(\frac{\rho_i}{\rho_w}\right) w_n(x)dx \tag{5.2}$$

where q is the water flux.By applying the formula for viscous flow between parallel plates we get

$$q = -\frac{t^3(x)}{12\eta_w}\frac{dp}{dx} \tag{5.3}$$

where $t(x)$ is the water layer thickness, η_w is the viscosity of water and $p(x)$ is the pressure. By applying Equations (26) and (32) in Nye (1969), where Nye derived a solution for ice flow over a wavy bed,

$$w_n(x) = -UA\frac{k^3}{k_*^2 + k^2}\cos kx \tag{5.4}$$

where$U$ is the general flow velocity of the glacier ice, $k_*^2 = \rho_i L_0/4CK\eta_i$ where L_0 is the latent heat of fusion for ice, C is the depression of the melting point by pressure ($= 0.074$ K MPa^{-1} for air free water) K is the mean thermal conductivity of ice and

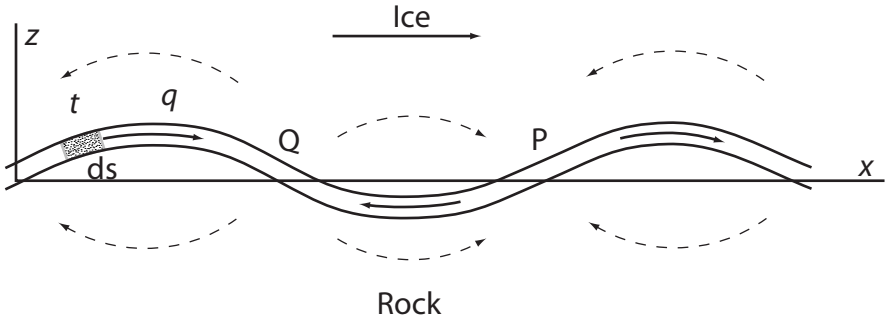

Figure 5.4. Basal water film. See text for discussion. After Nye (1973).

rock and η_i is a linear ice viscosity (Nye approximates ice by a Newtonian fluid), and

$$p(x) = 2UA\frac{k_*^2 k^2}{k_*^2 + k^2}\cos kx \tag{5.5}$$

By inserting Equation (5.4) into Equation (5.2) and integrating to obtain q and differentiating Equation (5.5) with respect to x to obtain an expression for dp/dx and inserting into Equation (5.3), allows us to equate the integrated Equation (5.2) and Equation (5.3) to yield

$$UA\frac{k^2}{k_*^2 + k^2}\sin kx\left(\frac{\rho_i}{\rho_w} - \frac{t^3(x)\eta_i k_*^2 k}{6\eta_w}\right) = 0 \tag{5.6}$$

From this we see that $t(x)$ is a constant and independent from x, U, and A and given by

$$t^3 = \frac{6\rho_i\eta_w}{\rho_w\eta_i k_*^2 k} \tag{5.7}$$

or, by substituting for k_* and setting $k = 2\pi/\lambda$, where λ is the wavelength of the sinusoidal rock,

$$t = \left(\frac{12\eta_w CK\lambda}{\pi\rho_w L_0}\right)^{1/3} \tag{5.8}$$

This result shows several interesting points. The the layer thickness is independent of dx and hence the water film should not have any spatial variation in thickness. The thickness is also independent of the ice viscosity η_i, the ice velocity U, and of the bed rock amplitude A. Since the relevant wavelengths λ found on the glacier bed is from cm to m-scale, the layer thickness is ~ 1 μm.

Weertman (1962) argues for a melt water film 1 mm thick or possibly larger. This film would then be able to act as a means for transporting water downglacier, (c). Nye (1973) discussed qualitatively the effects of increasing the layer thickness derived above by some small increment (see Figure 5.4).

If we increase the thickness of the melt water film by some small amount and also introduce sinks and sources for heat to be able to produce a new steady state.

The applied stress will remain constant and hence also he water pressure and the temperature; the latter because the water will remain at the pressure melting point everywhere. Since the pressure gradients are also the same but the thickness is increased, the water flow will be faster. The water flow depends on the melting at locations such as P and freezing at locations such as Q in Figure 5.4. The melt and refreezing rates must be larger to accommodate this increased flow of water and as a result the heat supplied at P and extracted at Q must also increase. If the source and sink is turned off we will get freezing at P and melting at Q. As a result, the water film will become tinner at P and thicker at Q. Nye (1973) points out that to continue the discussion, small perturbation theory no longer applies. He argues that the water film should regain its former thickness in both places, at Q by either forming a water inclusion (which has also been observed in regelation under high stresses (Nye, 1967)) or by flow of water out from the location in a different direction than downglacier (which would be the case in an open system). It is also possible to argue in the opposite direction for a decrease in film thickness. The effect is for the film to stabilize at P and become instable at Q. Steady state regelation demands a definite film thickness and according to the calculation this should be 1 μm. Nye (1973) concludes that the water film does not support water flow and argues for flow of water to be supported by other systems. The function of the basal melt water film is thus primarily to support the regelation process and should not be considered part of the basal hydrological system.

The theory of a basal water film has received observational support from Hallet (1976) who studied particle sizes of rock fragments cemented into carbonate precipitates generated in subglacial pockets. The maximum fragment size was 20 μm and Hallet inferred this to reflect the maximum thickness of the subglacial water film. Mapping of such subglacial precipitates also revealed complex networks of conduits and cavities (Walder and Hallet, 1979; Hallet and Anderson, 1980). It is obvious that free water exists at the interface between a temperate glacier and the subsurface on which it rests. It is not clear how uniform such a layer would be or if it consists of some microscopic drainage network, amplified by channels at ice crystal intersections. However, since melting occurs at the bed as a result of a combination of geothermal heat, frictional heating from sliding and deformational heat as ice deforms, a process most pronounced near the bed, water is generated across the entire ice-bed interface and is transmitted along the interface to probably gradually larger channels.

Walder (1982) investigated the stability of subglacial sheet flow of water. In this approach we will assume steady, one-dimensional water flow parallel to ice flow. The bed is planar with a slope α. The ice provides a constant pressure gradient to drive the flow of water. The water pressure is equal to the ice overburden pressure. The x-direction is parallel to flow, y is transverse to the flow, and z is perpendicular to the bed (Figure 5.5). The glacier bed is assumed to be impermeable. The ice-water interface is described by

$$z = z_0(y) = h\,(1 + \varepsilon \sin kx) \tag{5.9}$$

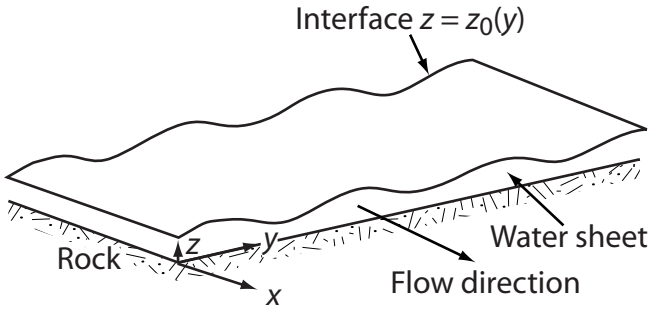

Figure 5.5. The geometry of a basal water sheet. See text for discussion. After Walder (1982).

where h is the average thickness of the sheet and $\varepsilon \ll 1$. The perturbation amplitude $A = \varepsilon h$. The Navier-Stokes equation for steady flow reduces to

$$\frac{\partial^2 u}{\partial y^2} + \frac{\partial^2 u}{\partial z^2} = -\frac{P_g}{\eta_w} \tag{5.10}$$

where u is the flow velocity, $P_g = -\partial p/\partial x$ is the pressure gradient driving the flow, and η_w is the viscosity of water.

The flow can be approximated by an perturbation in flow superimposed on a mean flow

$$u(x, y) = u_0(z) + \varepsilon u_1(y, z) \tag{5.11}$$

By substituting Equation (5.11) into Equation (5.10), separating terms of $O(1)$ and $O(\varepsilon)$ yields

$$\frac{d^2 u_0}{dz^2} = -\frac{P_g}{\eta_w} \tag{5.12}$$

$$\frac{\partial^2 u_1}{\partial y^2} + \frac{\partial^2 u_1}{\partial z^2} = 0 \tag{5.13}$$

with the boundary conditions

$$u = 0 \quad \text{and} \quad \text{on } z = 0, z = z_0(y) \tag{5.14}$$

which should be satisfied to O(ε). The velocity distribution in the water sheet is given by

$$u(y, z) = \frac{P_g h^2}{2\eta_w}\left(-\frac{z^2}{h^2} + \frac{z}{h} + \varepsilon \frac{\sinh kz \sin ky}{\sinh kh}\right) \tag{5.15}$$

Walder (1982, Appendix B, p. 286) provides a full derivation. This expression is used to calculate the temperature field in the water sheet. The thermal energy equation for steady state, incompressible, one-dimensional flow is

$$\rho_w c_w u \frac{\partial T}{\partial x} = k_w \nabla^2 T + \eta_w \left[\left(\frac{\partial u}{\partial y}\right)^2 + \left(\frac{\partial u}{\partial z}\right)^2\right] \tag{5.16}$$

(Bird *et al.*, 1960) where T is the water temperature, ∇^2 is the three-dimensional Laplace operator in Cartesian coordinates, ρ_w is the water density, c_w is the constant volume specific heat of water, and k_w is the thermal conductivity. All constants concern water at the pressure melting point. Through dimensional analysis, Walder (1982) showed that the down-stream and lateral heat conduction components, $k_w \partial^2 T/\partial x^2$ and $k_w \partial^2 T/\partial y^2$, respectively, were negligible in the overall heat balances for most cases. The lateral component was found to be small but finite in terms of perturbation growth rates and was retained in the thermal energy balance.

To facilitate an analytical solution, Walder (1982) also assumed that the temperature in a melt film would not differ much from the pressure melting point T_{pmp},

$$T \approx T_{pmp} \,, \quad \frac{\partial T}{\partial x} \approx c_t P_g \tag{5.17}$$

where $c_t = -\partial T/\partial P$. $\partial T/\partial x$ is constant in this approximation because of the assumption of a constant pressure gradient. Substituting the approximations in Equation (5.17) in Equation (5.16), neglecting down-stream conduction reduces the thermal energy equation to

$$\gamma P_g u = k_w \left(\frac{\partial^2 T}{\partial y^2} + \frac{\partial^2 T}{\partial z^2} \right) + \eta_w \left[\left(\frac{\partial u}{\partial y} \right)^2 + \left(\frac{\partial u}{\partial z} \right)^2 \right] \tag{5.18}$$

where $\gamma = \rho_w c_w c_t = 0.316$ is a dimensionless constant that comes from the pressure melting behavior of ice (Röthlisberger, 1972).

The temperature field can now be described as a composite of a mean value and a perturbation

$$T(x, y, t) = T_0(x, z) + \varepsilon T_1(y, z) \tag{5.19}$$

with boundary conditions

$$T|_{(z=z_0)} = T_{pmp}(x) = -c_t p(x) \,, \quad -k_w \left. \frac{\partial T}{\partial z} \right|_{(z=0)} = q_G \tag{5.20}$$

where q_G is the geothermal heat flux at the bed. T_0 and T_1 can be solved by transforming Equation (5.18) into two separate equations and applying the boundary conditions in Equation (5.20). For the stability analysis we are mostly concerned with $-k\partial T/\partial n$, where n is the local upward vector from the ice-water interface, which describes the heat flux from the water sheet into the ice. By applying the chain rule and noting that the slope $\partial z_0/\partial y$ of the interface is $\mathrm{O}(\varepsilon)$, we get

$$\frac{\partial T}{\partial n} = \frac{\partial T}{\partial z} \tag{5.21}$$

The heat flux into the basal ice can be written

$$\begin{aligned} Q_{Z_0} = \left[q_G + \frac{P_g^2 h^3 (1-\gamma)}{12 \eta_w} \right] + \left[\frac{P_g^2 h^3 (1-\gamma)}{4 \eta_w} \varepsilon \sin kx \right] - \\ + \left[\left(\frac{P_g^2 h^3 (1-\gamma)}{6 \eta_w} + q_G \right) k^2 h^2 \varepsilon \sin ky \right] \end{aligned} \tag{5.22}$$

in which the thickness of the wave length of the perturbation $2\pi/k$ is much larger than the the water sheet thickness, $kh \ll 1$. In Equation (5.22) the first bracketed term is the mean heat flux which includes a geothermal component and the heat from viscous dissipation. $(1-\gamma)$ is a factor that maintains the water at the pressure melting point by correcting for down-stream advection of heat. The second bracketed term is a locally enhanced heat production from viscous dissipation. The dependency on $\sin ky$ varies the melting of ice from heat flow into the ice so that it is larger in thick parts of the sheet ($\sin ky > 0$) and smaller in thin parts ($\sin ky < 0$). This is also the source for the instability. The third bracketed term describes the lateral heat conduction from thick to thin parts of the water sheet due to warping of the isotherms relative to the unperturbed case. This quantity is of $\mathrm{O}(k^2h^2)$ and hence negligible for $kh \ll 1$.

The rate of perturbation growth from melting can be examined through the following. Melt rates in the basal ice is determined by $q_{z_0}/\rho_i L$ where ρ_i is the density of ice and L is the latent heat of fusion. Because the mean heat flux causes a mean melt rate, we can concentrate on the perturbed portion of the melt speed w_m with which the interface moves

$$w_m = \left[\frac{P_g^2 h^3 (1-\gamma)}{4\eta_w \rho_i L} - \left(\frac{P_g^2 h^3 (1-\gamma)}{6\eta_w \rho_i L} + \frac{q_G}{\rho_i L}\right) k^2 h^2\right] \varepsilon \sin ky \tag{5.23}$$

To analyze the relaxation of the perturbed ice-water interface Walder (1982), following Fletcher (1977), used the analogy of an interface between two quasi-static, incompressible fluids with different density and linear viscosity. The linear viscosity for ice is justified because the pressure difference between ice and water in incipient channels at the glacier bed will be small, linearizing the flow law (Weertman, 1972, p. 299–306). The stresses and velocities can be decomposed into a mean (= hydrostatic for stresses and = 0 for mean velocity). The effective viscosity of ice is much larger than that for water so that the analysis reduces to a determination of the perturbation relaxation speed on a free surface. The speed with which the interface moves due to viscous sagging is

$$w_p = -\frac{(\rho_w - \rho_i)\, gA}{2\eta_i k} \sin ky \tag{5.24}$$

where g is the gravitational acceleration and η_i is the effective viscosity of ice.

The water sheet maintains an average thickness h from the mean melt rate. Local variations in melt and sagging rates changes the thickness locally resulting in a quasi-static change in amplitude. This means that points on the interface $z = z_0$ are considered remaining on the interface,

$$\frac{D}{Dt}\left(z - z_0(y,t)\right) = 0 \tag{5.25}$$

where $D/Dt = (\partial/\partial t) + v\,(\partial/\partial y) + w\,(\partial/\partial z)$ is the total time derivative. Equation (5.25) can be expanded to

$$\frac{\partial z_0}{\partial t} = w_p + w_m - v(z_0)\frac{\partial z_0}{\partial y} \tag{5.26}$$

Substituting Equation (5.9), Equation (5.23), and Equation (5.24) and noting that v is of O(kA) yields

$$\frac{1}{A}\frac{dA}{dt} = \frac{1}{\tau_1}\left(1 - 2/3k^2h^2\right) - \frac{1}{\tau_2} - \frac{1}{\tau_3}\left(k^2h^2\right) \tag{5.27}$$

where $A = h\varepsilon$, and

$$\frac{1}{\tau_1} = \frac{P_g^2 h^2\,(1-\gamma)}{4\eta_w \rho_i L}\,, \quad \frac{1}{\tau_2} = \frac{(\rho_w - \rho_i)\,g}{2\eta_i k}\,, \quad \frac{1}{\tau_3} = \frac{q_G}{\rho_i L h}\,, \tag{5.28}$$

$kh \ll 1$. By inserting values into Equation (5.27) Walder (1982) could show that the factor $1/\tau_3$ is negligible and that $1/\tau_2 \ll 1/\tau_1$ given that h and k are not small. Equation (5.27) can thus be approximated by

$$\frac{1}{A}\frac{dA}{dt} = \frac{1}{\tau_1} \tag{5.29}$$

if $kh \ll 1$. This indicates that small perturbations in the water sheet grows exponentially with a time constant τ_1 (Figure 5.6)and that this instability increases with P_g and h.

This analysis shows that perturbations in water sheet thickness would make sheet flow on a planar bed would be unstable. However, the analysis assumes a planar bed and so the effects of roughness must be taken into consideration. Nye (1973) noted that incipient channels, which is one way of viewing the thicker parts of a film may be destroyed when the ice flows over bedrock undulations. Walder and Hallet (1979) and Hallet and Anderson (1980) also discusses the possibility that subglacial cavities on the lee-side of the bedrock bumps may capture melt water and hence limit the thickness of the water sheets. The rate at which incipient channels encounter bedrock bumps is a function of the sliding speed. In Walder's (1982) approach the water sheet will be quasi stable when the characteristic time for sheet perturbation growth is exceeded by the average travel time between bedrock bumps, referred to as a decay time τ_d.

To investigate the effect of bed roughness, Walder (1982) uses the sliding formulation from Lliboutry (1978) in which bed roughness is parameterized as a distribution of hemispherical bumps on a planar bed. The incipient channels will move across the bed and may become destroyed if they encounter a bump which has a size near the *transition obstacle size* $R_\star$ (Lliboutry, 1978). If the bumps are much smaller they do not perturb the water film significantly and if the bumps are much larger than the ice would move around the bumps by enhanced plastic deformation rather than by regelation (Weertman, 1964).

To implement Lliboutry's (1978) formulation, we need to assume a non-dimensional bed where the fraction of bed covered by hemispherical bumps with a radius in the range $(R, R + dR)$ equals $\mu dR/R$ where μ is a constant describing the bed roughness. This means that the total fraction of the bed covered by bumps in the range

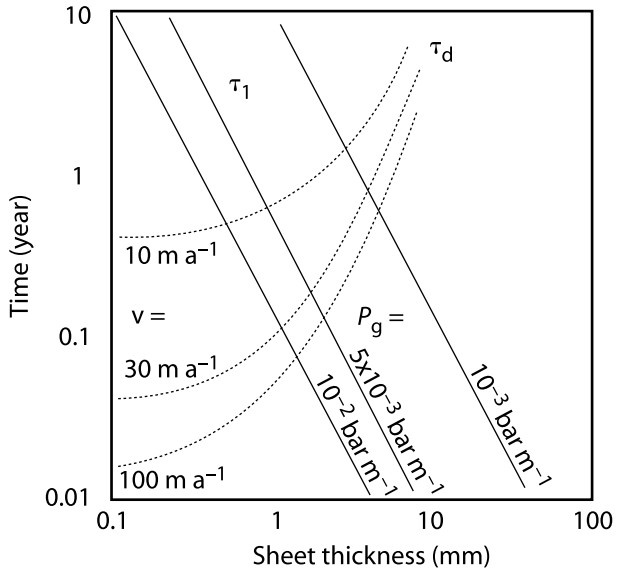

Figure 5.6. Curves for characteristic growth τ_1 and decay τ_d times for water sheet perturbations. After Walder (1982).

$R_{min} \geq R \geq R_{max}$ is $\mu \ln(R_{max}/R_{min})$, assumed to be $\ll 1$. Lliboutry (1978) suggests $R_{min} = 1$ μm and $R_{min} = 10$ m (an approximate size of roche moutonnés) which leads to $\mu \ll 1/16$.

Walder (1982) uses a formulation similar to that for drag on a sphere moving through temperate ice to express the *relative efficiency*

$$E = \frac{2RR_\star}{R^2 + R_\star^2} \tag{5.30}$$

which has the property that $E(R_\star) = 1$ and that $E \to 0$ as $R \to \infty$.

The number of bumps in the range $R_{min} \geq R \geq R_{max}$ per unit area is given by

$$d\nu = \frac{\mu dR}{\pi R^3} \tag{5.31}$$

and hence the *effective* number of bumps per unit bed area, ν_e that may destroy incipient channels is given by.

$$\nu_e = \frac{2\mu R_\star}{\pi} \int_{W/2}^{\infty} \frac{dR}{R^2 \left(R^2 + R_\star^2\right)} \tag{5.32}$$

The lower limit of integration reflects the smallest size bump that blocks and incipient channel of width W. Given a bed area of width W and length l the average number of effective bumps is $\nu_e lW$ with an average spacing of $l/\nu_e lW$. The average time between encounters of incipient channels with bumps can be given by

$$\tau_d = \frac{\pi R_\star}{2\mu UW} \left\{ \frac{2}{W} + \frac{1}{R_\star} \left[\tan^{-1} \left(\frac{W}{2R_\star} \right) - \frac{\pi}{2} \right] \right\}^{-1} \tag{5.33}$$

Lliboutry (1978) suggests that $R_\star = 0.16U^{-1/2}$ and although the value of 0.16 may be incorrect (Lliboutry, 1979), the insensitivity of Walder's (1982) results to both increase and decrease in the factor by a factor of two, we can rewrite Equation (5.33)

$$\tau_d = \frac{0.08\pi}{\mu W U^{3/2}} \left\{ \frac{2}{W} + 6.25U^{1/2} \left[\tan^{-1}\left(3.12WU^{1/2}\right) - \frac{\pi}{2} \right] \right\}^{-1} \tag{5.34}$$

The width of an incipient channel W is identified by its wave number k through $W = \pi k^{-1}$. The incipient channel width is constrained by $W \gg \pi h$ because the analysis of growth of perturbations is valid only for $kh \ll 1$. Walder (1982) therefore assigns $\min(W) = 30h$ and rewrites Equation (5.34)

$$\tau_d = \frac{0.084}{hU^{3/2}} \left\{ \frac{0.067}{h} + 6.25U^{1/2} \left[\tan^{-1}\left(93.75hU^{1/2}\right) - \frac{\pi}{2} \right] \right\}^{-1} \tag{5.35}$$

where h is expressed in m, U in m year^{-1}, and $\mu = 0.01$.

For reasonable choices of P_g and U, Walder (1982) calculated that the stability criterion could only be met for $h <\sim$1–4 mm. If the water sheet becomes thicker it also becomes unstable. A water film of large thickness only seems possible in the absence of discrete drainage pathways. Subglacial pathways are typically low pressure, especially relative to the ice overburden pressure and would act as sinks for the water in the film. The role of the melt water film and the thickness of the film therefore seems to be related to the presence of a conduit system. Walder (1982) concludes that large quantities of surface water is necessary to maintain a significant sheet of water. However, it is difficult to see how large input of surface water can affect a system that occurs in absence of discrete basal conduit systems.

Walder's 1982 study shows that sheet flow is nearly always unstable on planar beds. The roughness met on real beds may, however, result in quasi-stable sheet flow for thicknesses < 4 mm although the numerical experiments proved to be sensitive to the choice of roughness model. The prerequisites for the existence of a water sheet at the bed of a glacier seems to be that cavities are absent or at least rare and that water supply is abundant, *i.e.* large quantities of surface water must penetrate to the bed.

5.3 The tunnel system

The existence of tunnel systems beneath glaciers probably originates from observations of tunnel portals at the terminus of glaciers and the existence of eskers, thought to form in tunnels beneath former ice sheets. However, no ocular observations exist of tunnels beneath glaciers except for ones in stagnant ice or very near the terminus in slow moving ice. Tunnels have thus generally been though of as semicircular in cross-section Figure 5.7.

The first model of subglacial drainage in a tunnel was put forward by Röthlisberger (1972) who considered cylindrical conduits in glacier ice to model the drainage of a glacier dammed lake in Switzerland.

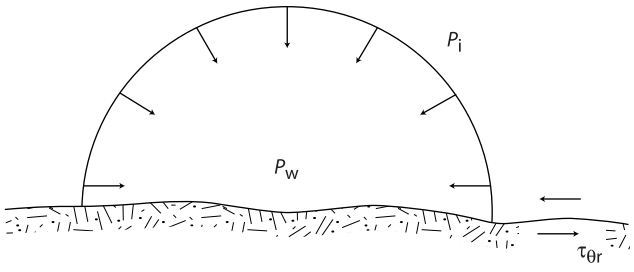

Figure 5.7. Geometry of a classic subglacial tunnel. After Hooke (2005).

Röthlisberger considered a horizontal cylindrical pipe with radius r and water pressure P_w at a location x while the pressure at $x - dx$ is $P_w - dP_w$. Since the conduit is located at some depth beneath the ice surface, the conduit is subjected to an ice pressure P_i, which causes radial ice flow in the direction of the axis of the cylinder proportional to the difference between ice pressure and the water pressure in the conduit, $P_i - P_w$. The melt on the conduit walls is caused by the energy loss from the flowing fluid. Röthlisberger assumes instantaneous energy transfer from the water to the ice which means energy produced within a segment of the conduit is also transferred to the same part of the conduit and that the water will always be at the pressure melting point. Given a discharge, Q, it is thus possible to write the energy loss per unit time as $dE = QdP_w$. Since a pressure change also involves a temperature change, only part of the energy becomes available for melting. This means that the energy available for melt, dE_M, is reduced by an amount corresponding to the energy needed for the change in temperature, dE_T, thus $dE_M = dE - dE_T$. By inserting values for the change in pressure melting point with pressure, c_T, the specific heat capacity of water, c_w, and the density of water at 0°C, ρ_w, we obtain $dE_T = -c_T c_w \rho_w Q dP_w$ which yields $dE_M = 0.684 dE$.

The closure rate of a cylindrical hole in ice is given by

$$\frac{\dot{r}}{r} = \left(\frac{P_i - P_w}{nB}\right)^n \tag{5.36}$$

where r and $\dot{r}$ are the cylinder radius and rate of change of the radius, respectively, n and B are the empirical constants in Glen's flow law for ice. The volume change through creep, per unit time, dV_c, of a cylindrical hole can thus be estimated by

$$dV_c = 2r\pi\dot{r}dx = 2r^2\pi\left(\frac{P_i - P_w}{nB}\right)^n \tag{5.37}$$

At equilibrium, the change in volume from melt is equal to the change in volume from creep, $dV_M = dV_c$. This results in the following differential equation for the change in P_w with distance x

$$\frac{dp}{dx} = \frac{2\pi c_M \rho_i}{0.684Q}\left(\frac{P_i - P_w}{nB}\right)^n r^2 \tag{5.38}$$

In order to relate the radius, r, to Q and dP_w/dx we can use the Gauckler-Manning-Strickler formula (*e.g.* Williams, 1970) to calculate the mean velocity for turbulent flow,

$$\bar{v} = \frac{Q}{r^2\pi} = kR^{2/3}\left(\frac{1}{\rho_w g}\frac{dP_w}{dx}\right)^{1/2} \tag{5.39}$$

where k is the roughness coefficient, R is the hydraulic radius. The radius of the conduit can thus be expressed in terms of Q and dP_w/dx as

$$r^2 = \left(\frac{2^{4/3}\rho_w g}{\pi^2}\right)^{3/8} k^{-3/4} Q^{3/4}\left(\frac{dP_w}{dx}\right)^{-3/8} \tag{5.40}$$

If we insert Equation (5.40) into Equation (5.38) we obtain

$$\frac{dP_w}{dx} = Ck^{-6/11}\left(nB\right)^{-8n/11} Q^{-2/11}\left(P_i - P_w\right)^{8n/11} \tag{5.41}$$

where

$$C = 2^{12/11}\pi^{2/11}\left(\frac{c_m\rho_i}{0.684}\right)^{8/11}\left(\rho_w g\right)^{3/11} \tag{5.42}$$

With this equation in hand we can see that the pressure gradient, dP_w/dx, increases with the pressure difference between ice and water pressure $(P_i - P_w)$ and with channel roughness (k). We can also see that the larger the discharge (Q), the smaller the pressure gradient. If the water pressure is integrated from atmospheric pressure at the terminus to some distance x, a channel with higher Q would have lower pressure than one with lower Q. This means that if two parallel channels occur with different discharge, the channel with higher discharge will pirate water from the one with lower Q because of the pressure difference. Put differently, larger channels will tend to grow at the expense of smaller. Hence distributed networks of channels will with time tend to coalesce into less complicated networks of a few larger tunnels. This has also been inferred from dye tracing experiments (Hock and Hooke, 1993) (Figure 5.8).

In the developments of Röthlisberger (1972) and Shreve (1972) conduits were assumed to be filled with water. In reality it is common to have partially filled conduits which was also recognized by Röthlisberger (1972), Shreve (1972) and Lliboutry (1983). Hooke (1984) investigated how such conditions would affect the theories put forward by Röthlisberger, Shreve and Lliboutry.

If we consider a conduit on the glacier bed as seen in Figure 5.9 we can apply turbulent pipe flow theory to analyze conditions in the pipe. Hunsacker and Rightmire (1947) gives

$$\frac{P_1 - P_2}{\rho_w g} + z_2 - z_1 - f\frac{L}{D_c}\frac{V^2}{2g} = 0 \tag{5.43}$$

where P_1 and P_2 and z_1 and z_2 are the water pressures and elevations at locations 1 and 2, respectively, D_c is the diameter of the cylindrical conduit, f is the friction coefficient, ρ_w is the density of water, V is the velocity of water flowing in the

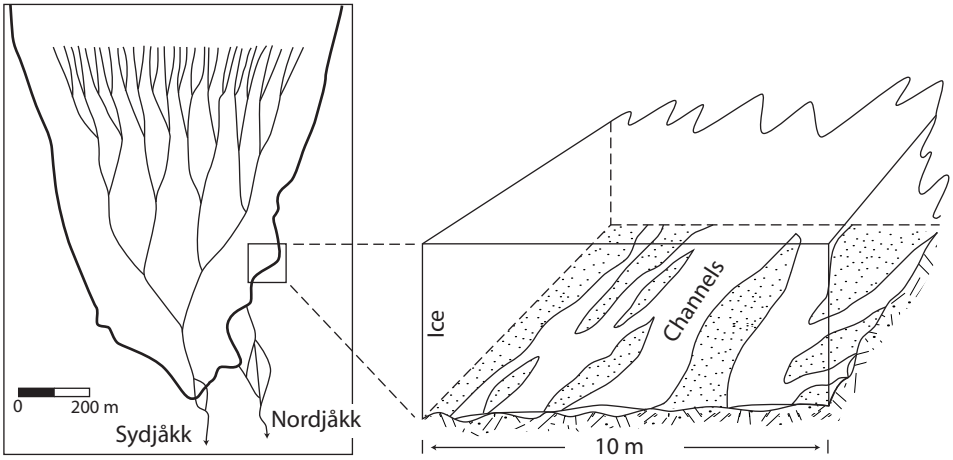

Figure 5.8. Schematic sketch of the multi-branched arborescent conduit system inferred from dye trace experiments on Storglaciären (Hock and Hooke, 1993). Individual streams are inferred to be braided. After Hooke (2005).

conduit, g is the gravitational acceleration, and L is the slope distance between locations 1 and 2. If the conduit is larger than necessary to carry the discharge, the pressure will be atmospheric or from its triple point value to the pressure of air trapped in the ice depending on if the conduit is connected to the atmosphere or not. Under such conditions $P_2 = P_1$ and $P_1 - P_2/\rho_w g$ vanishes. If the air space in the tunnel increases f will decrease and flow will accelerate which will further decrease the cross-sectional area of the conduit occupied by water.

We need to investigate under what conditions a transition from full to open conduit flow in the conduit will occur. Continuity allows us to express the discharge Q as $Q = \pi V D_c^2/4$ and from geometrical considerations the bed slope β, positive if sloping down in the flow direction, can be expressed as $\sin\beta = (z_2 - z_1)/L$. If we substitute these expressions into Equation (5.43) and rearrange to solve for the conduit diameter we obtain

$$D_c = \left(\frac{8fQ^2}{g\pi^2 \sin\beta}\right)^{1/5} \tag{5.44}$$

At the bed, a semicircular cross-section is more reasonable than a circular cross-section. We assume that the hydraulic radius will remain the same an that the friction factor remains constant. This leads to

$$D_s = C_1 Q^{2/5} \sin^{-1/5}\beta \tag{5.45}$$

where the constant $C_1 = 0.55\ \mathrm{s}^{2/5}\,\mathrm{m}^{-1/5}$.

As water flows through the conduit, the potential energy released for a fall in height h is given by $\rho_w Q g h$. Part of this energy may be used to warm the water in

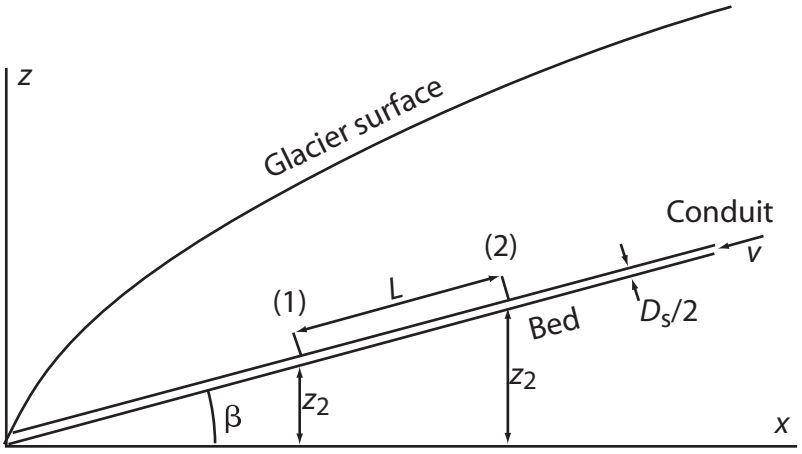

Figure 5.9. Definitions of the conduit system on the glacier bed and symbols used in Equation (5.43). After Hooke (1984).

a full conduit because the pressure melting point temperature T_{pmp} rises as pressure decreases. In a conduit with open channel flow, this does not necessarily hold. Because of the pressure difference between the water and the ice, the walls of the conduit will be colder than the water and some of the energy will be conducted into the walls. The remaining energy will be available for melting at a rate $\dot{m}$ as

$$\frac{1}{2}\rho_i \dot{m} \pi D_s H L = \rho_w Q g h - K \frac{\pi D s L}{2} \frac{dP_i}{dR} \frac{dT_{pmp}}{dP_i} \tag{5.46}$$

where ρ_i is the density of ice, H is the latent heat of fusion, R is the distance into the tunnel wall, K is the thermal conductivity of ice, and P_i is the ice pressure. Through Nye's (1953) relations for closure of a borehole it is possible to show that $dP_i/dR = 8\rho_i Z/9D_s$ for an ice thickness $Z(x)$. Since $\sin\beta = h/L$ we can modify Equation (5.46) to

$$m = \left(\frac{2g}{DsH} \frac{\rho_w Q}{\rho_i} \frac{Q}{\pi} \sin\beta - \frac{4}{9} K Z \frac{dT_{pmp}}{dP_i} \right) \tag{5.47}$$

Harrison (1972) provides values for $K = 2.1$ J m^{-1} s^{-1} and $dT_{pmp}/dP_i = 9.8 \times 10^{-8}$ $^\circ$ Pa^{-1} yielding $KZdT_{pmp}/dP_i = 9.1 \times 10^{-8} Z$. However, the thermal conductivity of ice very near the melting point is 1–10% that of the cold ice values above (Paterson, 1971). Hooke (1984) also identified that a finite temperature rise is necessary across the tunnel wall necessary for finite heat transfer. Hence the second term in Equation (5.47) is of order $5 \times 10^{-9} Z$ or $5 \times 10^{-10} Z$ to be compared with $10^{-2} Q$ for the first term. This indicates that the second term can be neglected for ice thicknesses smaller than a few hundred meters and for discharges exceeding $\sim 10^{-3}$ m^3 s^{-1}. Neglecting the second term and combining Equation (5.45) and Equation (5.47) yields

$$\dot{m} = C_2 Q^{3/5} \sin^{6/5}\beta \tag{5.48}$$

$C_2 = 3.73 \times 10^{-5}$ m$^{-4/5}$ s$^{-2/5}$ for $\rho_i = 916$ kg m^{-3}, $\rho_w = 999.8$ kg m^{-3} at 0°C, and $H = 3.34 \times 10^5$ J kg^{-1}.

From the work of Nye (1953) we can estimate the approximate rate of tunnel closure $\dot{r}$ by

$$\frac{\dot{r}}{D_s/2} = \left(\frac{\rho_i g Z}{nB}\right) \tag{5.49}$$

where B is the viscosity parameter in Glen's flow law for ice (Equation (4.1)). Equation (5.49) is valid only when $\rho_i g Z \approx \tau$, the effective stress, and when no frictional forces exist that prevents sliding of ice over the bed towards the tunnel. The last assumption is not realistic and will be treated in more detail below. Combining Equation (5.45) and Equation (5.49) with $n = 3$ yields

$$\dot{r} = C_3 \frac{Q^{2/5}}{\sin^{1/5}\beta} Z^3 \tag{5.50}$$

where $C_3 = 5.70 \times 10^{-14}$ m$^{-16/5}$ s$^{-3/5}$ for $B = 1.6 \times 10^5$ Pa a$^{1/3}$.

The condition $\dot{m} > \dot{r}$ can be investigated from Equation (5.48) and Equation (5.50)

$$Q > \left(\frac{Z^3}{C_4 \sin^{7/5}\beta}\right)^5 \tag{5.51}$$

where $C_4 = 6.55 \times 10^8$ m$^{12/5}$ s$^{1/5}$. Melt rates will exceed the closure rates when this condition is met resulting in a tunnel that is larger than necessary to carry the existing discharge.

Figure 5.10 shows how bed slope and discharge varies for different values of ice thickness and for the situation when discharge equals the r.h.s. of Equation (5.51). Hooke (1984) points out that because proglacial river discharge typically exceeds 1 m^3 s^{-1} the results indicate that subglacial tunnels on downsloping beds should experience open channel flow. By inserting a value of $5 \times 10^{-10} Z$ in Equation (5.47), Hooke also investigated the field of Q and β values for which second term exceeded 10% of the first term and where thus heat loss to the tunnel walls appreciably reduces the melt rate on the tunnel walls. It is evident from Figure 5.10 that such conditions occurs only at very low Q.

In this analysis we have only considered a constant slope conduit. In reality conduits will be extending over variable bed slopes. Hooke (1984) therefore also considers back pressure effects. We can imagine a situation in which conditions satisfy Equation (5.51) in a conduit downstream of location A and upstream of location B but between A and B in Figure 5.11 because of the differences in bed slope. At B the pressure must be high enough to prevent tunnel closure at a rate faster than the melt rate. In order for this to occur the necessary pressure required must be built up by backing up water upstream of B. Hence, the extent to which a subglacial system is filled or not depends on more than just the local conditions.

Lliboutry (1983) argued that open channel flow was very common beneath glaciers and Hooke's (1984) results corroborate this. In the non-steady state, it is

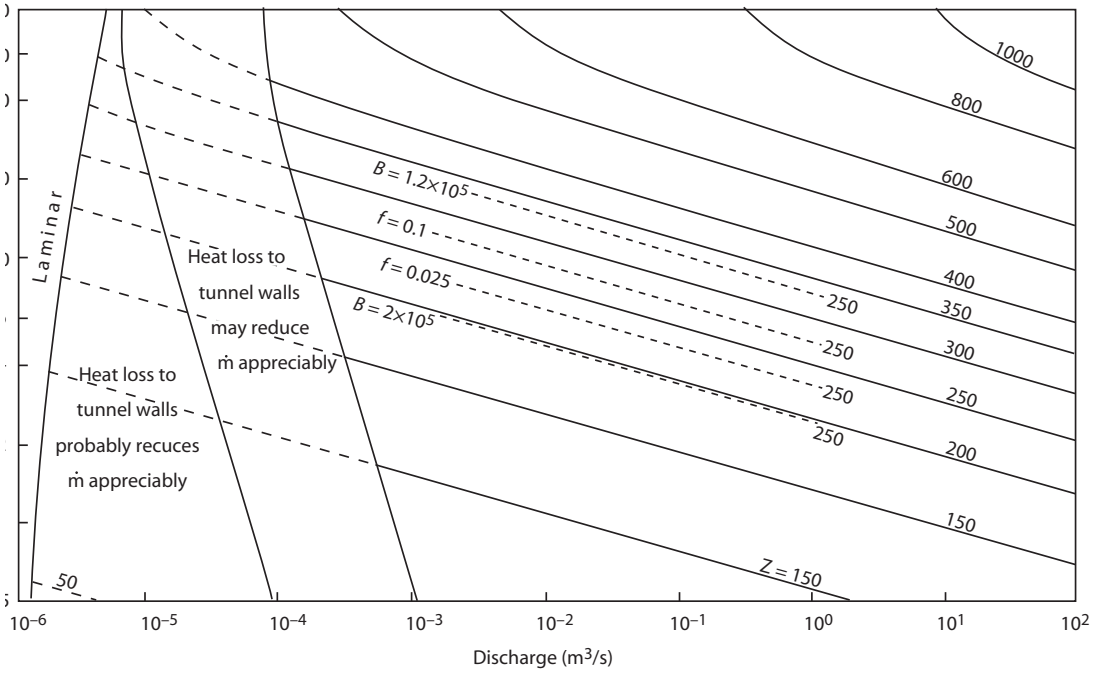

Figure 5.10. Critical values of discharge, bed slope and ice thickness. After Hooke (1984).

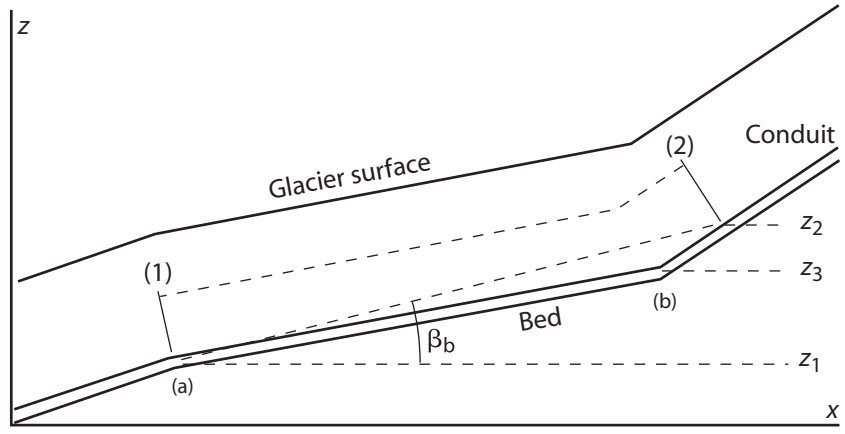

Figure 5.11. A simple model for calculating back pressure effects in basal conduit flow. After Hooke (1984).

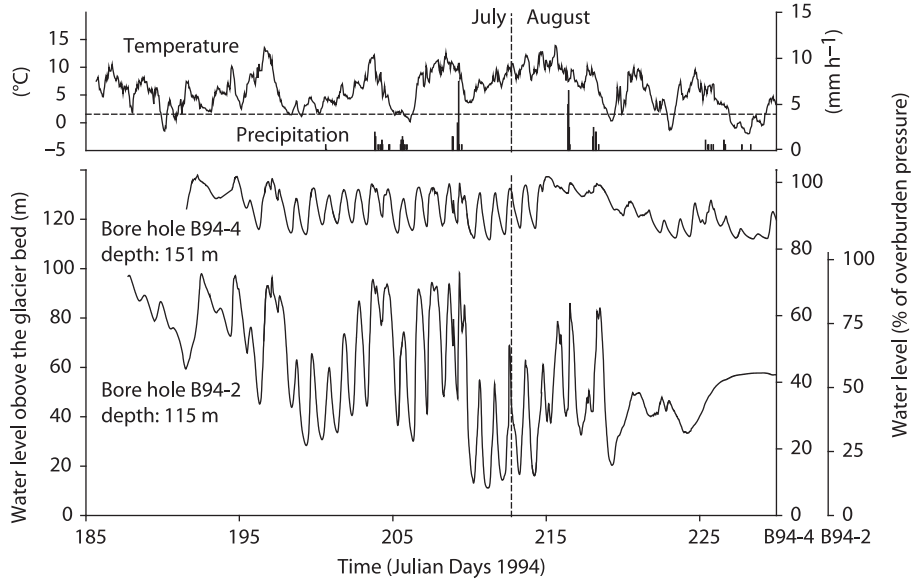

Figure 5.12. Measured subglacial water pressures beneath Storglaciären 1994. After Hooke (1984).

conceivable that diurnal and other short-term variations in water flux may rapidly enlarge the tunnel system while closure from creep is slower. In such a case tunnels might spend more time under open channel flow conditions than under pipe flow conditions. Jansson (1996) also discusses such a scenario based on water pressure observations (Figure 5.12) where water pressures vary on a diurnal basis but are generally lower after high precipitation events only to gradually build during periods with more steady inflow of water.

Kohler (1992, 1995) investigated the extent of pressurized flow beneath Storglaciären by analyzing tracer test results and applying a theoretical model of flow routing through the glacier. The model consisted of a vertical shaft, corresponding to a moulin, and a segment of horizontal semicircular pressurized conduit leading to another segment of channel with open channel flow. Kohler obtained results that indicate that substantial lengths of the subglacial channel was pressurized, in contrast to Hooke's (1984) analysis of Röthlisberger's (1972) results. This may be because the semi-circular tunnel cross-section does not allow fast enough closure or other factors summarized by Hooke *et al.* (1990).

Röthlisberger (1972) applied his model to the conditions beneath Gornergletscher but could not successfully model the water pressure given common values for the constants in the model. To obtain better results, Röthlisberger needed to make the ice softer and also use an unusually high channel roughness. This led Lliboutry (1983) and Iken and Bindschadler (1986) to suggest that perhaps the tunnel geometry used by Röthlisberger was not representative for most of the subglacial system. However, no alternative theory was put forward until Hooke *et al.* (1990) suggested that tunnels could be low and broad.

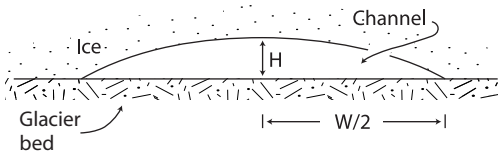

Figure 5.13. Geometry of a Hooke-type subglacial tunnel. After Hooke (2005).

The subglacial tunnels have long been thought of as semi-circular conduits (Figure 5.7). As results from tracer experiments have been analyzed, it has become clear that the traditional tunnel shape does not explain the drainage characteristics of the subglacial system. The observational data implies that tunnel systems may collapse rapidly once water pressure drops in the system and that the cross-sectional area must also be able to adapt quickly. With the traditional shape, the tunnel is kept open by two effects. If the tunnel is to decrease its cross-section, the ice at the bed must slide inwards. Frictional resistance will however be large and prevent this from happening to the extent necessary. Hooke *et al.* (1990) therefore proposed an alternative shape of subglacial tunnels that could better accommodate the observational data (Figure 5.13). Their tunnel was low and broad which allowed it to decrease in size rapidly since closure could be accomplished by simply collapsing the tunnel ceiling downwards.

Hooke *et al.* (1990) found that water pressure beneath Storglaciären, Sweden, and Austdalsbreen, Norway, could be calculated with

$$G^{11/8} - 0.316 G^{3/8} \frac{dP}{dx} = \frac{\Omega D \Delta P^n}{k^{3/4} (nB)^n Q^{0.25} \cos^{11/8} \beta} \tag{5.52}$$

where dP/dx is the pressure gradient along the course of the conduit, D is a constant involving the densities of water and ice, the latent heat of fusion and the gravitational acceleration g, k is the reciprocal of the Manning channel roughness, $n\,(=3)$ and B are the Glen's flow law constants, Q is the water discharge, β is the slope of the bed (positive when sloping down in the direction of flow), ΔP is the pressure difference between the ice overburden pressure at the conduit and the water pressure in the conduit, and $G = (dP/dx + \rho_w g \tan\beta)$, where ρ_w is the acceleration due to gravity. This is identical to Röthlisberger's Equation (5.41) (above) except for the term Ω.

Hooke *et al.* (1990) argued that the shape of low broad tunnels can be approximated by the area between the chord of a circle, constituting the channel bed, and the arc of the circle corresponding to the chord, constituting the tunnel roof (Figure 5.13). The cross-sectional area, A, and wetted perimeter, p, can then be calculated as $A = r^2 (\theta - \sin\theta)/2$ and $p = r(\theta + 2\sin\theta/2)$, respectively. They further argued that closure rates would lie between limiting values obtained by inserting the conduit height H and the conduit half-width $W/2$, respectively, into Nye's 1953 theory. They then used the average of these lengths in place for the radius Röthlisberger

used in Equation (5.36) (above). This leads to Equation (5.52) with

$$\Omega = \frac{\theta\left(1-\cos\theta/2+\sin\theta/2\right)\left(\theta+2\sin\theta/2\right)^{1/2}}{2^{5/2}\pi^{1}/4\left[\left(\theta-\sin\theta\right)/2\right]^{5/4}} \tag{5.53}$$

Numerical simulation made by Hooke *et al.* (1990) show that estimating closure rates with Equation (5.36) and using $r = 1/2\,(H + W/2)$ yields rates that are higher than those modeled by up to 50%. When comparing to field measurements of water pressures, a much closer agreement can be obtain than with Röthlisberger's original formulation. The reason for this is that the angle θ can be varied. Comparisons yielded good results with angles varying from 2° to 36°. Because of the underlying geometrical assumptions, the angles translate into a general shape, low and broad to higher and narrower, but their cross-sectional areas are adjustable to accommodate the discharge. Hence similar discharges can be put through channels of different geometry, whereas in Röthlisberger's version, the geometry was fixed and only cross-sectional areas could be varied.

Analysis of water pressure observations, discharge, and tracer studies, has established that tunnel systems are not stable but change through the course of a melt season. Hock and Hooke (1993) performed numerous dye traces on the lowermost part of Storglaciären where the drainage system is inferred to mostly consist of subglacial tunnels. Tracer dispersion indicated that the tunnel system early in the melt season was highly distributed and that it, as the season progressed, became more focused on fewer and larger, and hence more efficient, tunnels. Transfer times for the tracer clouds were also halved during the course of the season implying a bulk decrease in complexity and lowering of resistance to flow of the system. The tunnel system hence goes through a seasonal variation in terms of its spatial configuration.

Observations of subglacial water pressure variations (Jansson, 1996) indicate that the drainage system can change abruptly on even shorter time scales. Figure 5.12 shows water pressure records from the lowermost part of Storglaciären. Water pressures vary from close to atmospheric pressure to overburden pressure on a diurnal cycle. This variation reflects the variation in water input generated by melting, indicated by the temperature curve in Figure 5.12. On 23 July, precipitation occurs which causes a change in the drainage system so that peak pressures no longer reach overburden. This can be interpreted as an enlargement of the tunnels from the additional water input from the precipitation event so that larger recharge would be required to produce similar pressure peaks as observed before the event. After the precipitation event peak pressures increase day by day, which can be interpreted as an effect of gradual closure of the tunnel back to conditions similar to those before the event. Hence, the system is quickly adapting to changes in input. Enlargement is a quicker process than closure because it involves melting from frictional heating whereas closure depends on the slow creep of the glacier ice.

5.4 The linked cavity system

Tunnel systems are not the only type of system inferred to exist beneath glaciers. During the surge of Variegated Glacier Kamb (1987), Kamb *et al.* (1985) found that the hydraulics of tunnels could not explain the combination of water pressures and discharges measured on the glacier.

The following observations were made:

- fast flow due to high sliding rates.
- water pressure was close to overburden pressure and peaks reach overburden. In contrast, pressures were significantly lower during no-surge conditions.
- Large flood peaks were associated with the termination of the surge indicating that water was released from the glacier as the surge stopped.
- water flow in the basal system was slower during surge than during non-surge conditions
- The drainage system was interconnected over the whole width of the glacier during surge. Dye injected into the glacier emerged in all exiting streams during surge but only in one during non-surge conditions.
- Turbidity was significantly higher during surge than during non-surge conditions.

Dispersivity calculations from dye tracing experiments (Brugman, 1986) indicated that the system could not consist of normal tunnels or R-channels (after Röthlisberger (1972)'s model) during surge, while they exist under non-surge conditions. This is because the observed high water pressure could not be maintained with the small observed flow velocities, where the conduits are of tunnel character. Hence Kamb (1987) developed ideas of a different subglacial drainage system that could maintain a large volume of water at high pressure but discharging only small quantities of water.

Kamb (1987) proposed the *linked cavity system* (Figure 5.14) which is similar to mappings of natural examples (Walder and Hallet, 1979; Hallet and Anderson, 1980). The system is characterized by large *cavities* caused by separation of ice from the bed in the lee of bumps. These cavities are linked by the *separation-gap orifices*. Because of the characteristics of cavity formation, flow tends to occur more in the transverse direction than in the downglacier direction. Also note that cavities are interconnected so that no unique flow path can be established. This will result in the high dispersion observed by dye-tracing Brugman (1986).

Kamb (1987) used a typical cavity and orifice to develop his model (Figure 5.15). Kamb defined typical parameters to describe the system. The average width of the cavity l_c would be measured parallel to ice flow since the width would reflect the separation. The orifice width l_o may be parallel to ice flow but can also have a

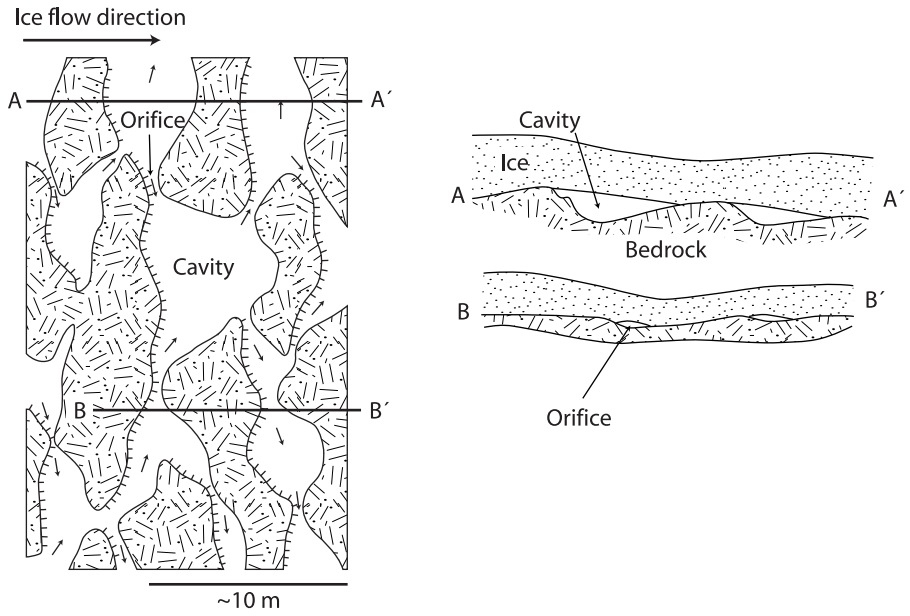

Figure 5.14. Planar (a) and side view (b) of Kamb's (1987) linked cavity system for basal water flow during surge conditions.

significant downglacier component. The length of the orifice L_o is measured in the direction parallel to water flow. The dimension of the cavity is also measured in the direction between two orifices which would represent the direction of water flow. The average height of the cavities is defined as g_c. The height of the orifices $g(x)$ is measured perpendicular to the floor and a function of position across the orifice. The number of independent orifices, *i.e.* orifices not coupled in series, in a cross-section of the glacier is given by N_o which leads to an average lateral spacing of N_o/W, where W is the glacier width.

Figure 5.15 represents a highly simplified picture of the system. The complex natural system of cavities and orifices of different sizes affected by local shear stress τ, water pressure P_w and ice overburden pressure P_i becomes replaced by a typical size reflecting average conditions.

In analyzing the linked cavity system, we need to think of the processes involved. (1) the size and shape of the orifice is determined by the bed roughness and the cavity formed from this roughness given a P_w, P_i, and velocity v. (2) the water flow through the orifice will be determined by the orifice geometry and the hydraulic gradient through the orifice. (3) the water flow through the orifice will dissipate viscous energy that will melt the roof of the orifice. This leads to modifications and a feedback through (1) and (2).

To calculate the flow of water through the linked cavity system, we start by assuming a longitudinal hydraulic gradient α_w along the glacier. We can assume that $\alpha_w = \alpha$ (the ice surface slope) for simplicity. If we assume the flow path has a certain tortuosity ω we obtain a flow path hydraulic gradient as α/ω. Since the

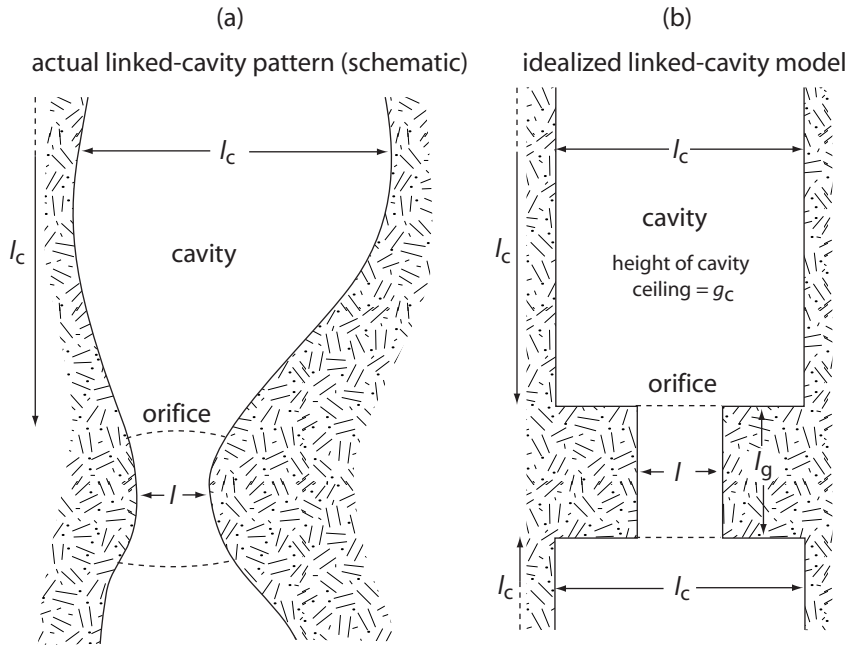

Figure 5.15. Definitions of parameters in Kamb's (1987) linked cavity system model.

model states the role of the orifices is to control the flow, this also means that the hydraulic head loss occur in the orifices and not in the cavities. The head gradient in the orifices is then the average gradient multiplied by the *head gradient concentration factor* $L_c/L_o = \Lambda$. The orifice height is small compared to the width ($\max g(x) \ll l_o$). We can now apply Manning's equation in the same manner as Röthlisberger (1972) (Equation (5.39)) by setting the hydraulic radius $= g(x)/2$,

$$\bar{u}_w(x) = \frac{1}{M}\left(\frac{g}{2}\right)^{2/3}\left(\frac{\alpha\Lambda}{\omega}\right)^{1/2} \tag{5.54}$$

where $\bar{u}_w$ is the mean water velocity averaged across the gap height g, M is the Manning roughness, and $\alpha\Lambda/\omega$ is the local hydraulic gradient in the orifice. The total flux of water carried by the linked cavity system is obtained by multiplying Equation (5.54) by the local gap width $g(x)$, integrating over the width l of the orifice and summing the contribution from all N_o orifices,

$$Q_w = \frac{N_o}{2^{2/3}M}\left(\frac{\alpha\Lambda}{\omega}\right)^{1/2}\int_0^l g(x)^{5/3}dx \tag{5.55}$$

The local heat generation from viscous dissipation of heat is the product of the local water flux $\bar{u}_w g(x)$ and the potential gradient $\rho_w g_r \alpha\lambda/\omega$, where the g_r is the gravitational acceleration and ρ_w is the density of water. The local heat generation rate can be expressed in terms of a equivalent volume rate of melting dividing by

$\rho_i H$, where ρ_i is the density of ice and H is the latent heat of fusion for ice

$$\dot{m} = \frac{(\alpha\Lambda/\omega)^{3/2}}{2^{2/3}DM} g^{5/3} \tag{5.56}$$

where $D = \rho_i H/\rho_w g_r$ is a length constant.

There are two main types of cavity forming situations, separation of the ice from the bed at an *angular step* and at a *sinusoidal bed form*. In the stepped case, the separation point is fixed whereas its has no predetermined location on the sinusoidal bed. The step can also maintain a cavity at lower sliding speed, higher P_e, or lower P_w than that of a sinusoidal bed form. In reality all kinds of mixtures between these forms exist.

We first start by examining the step form with a rectangular step height h (Figure 5.16). The gap height can then be approximated by

$$g(x) = h\left(\frac{1}{2} - \frac{1}{\pi}\sin^{-1}\frac{2x-l}{l} - \frac{2(2x-l)\sqrt{x(l-x)}}{\pi l^2}\right) \tag{5.57}$$

where $0 \leq x \leq l$. The gap width is

$$l = 4\sqrt{\frac{\eta v(h+m)}{\pi P_e}} \tag{5.58}$$

where η is the ice viscosity, v is the sliding velocity, $P_e\,(= P_i - P_w)$ is the effective pressure, and $m = 0$ if there is no melting of the gap roof. The rate of closure of the gap is given in terms of the vertical component of the velocity along the gap roof

$$w(x) = vg'(x) = -\frac{P_e}{2\eta}\sqrt{x(l-x)} \tag{5.59}$$

The closure rate is balanced by the sliding speed to maintain a steady state open gap. Because $l \to 0$ as $P_e \to \infty$ but remains non-zero for small P_e, the step orifices remain open even under large P_i or small P_w. In such cases when $l \ll h$, $g'(x) \ll 1$ breaks down. However, (Kamb, 1987) argues that the system is valid up to the largest values of P_e that occur in reality.

Since actual ice rheology is non-linear, Equation (5.57)–Equation (5.59) are only approximations. We can deal with this by making η shear stress dependent. We can use P_e as a measure of the shear stress level since all stresses would be hydrostatic if $P_e = 0$. We can thus write

$$\eta = \eta_{\text{ref}}\left(\frac{P_{e(\text{ref})}}{P_e}\right)^{n-1} \tag{5.60}$$

where the reference values $P_{e(\text{ref})}$ show the effective viscosity at a reference stress level.

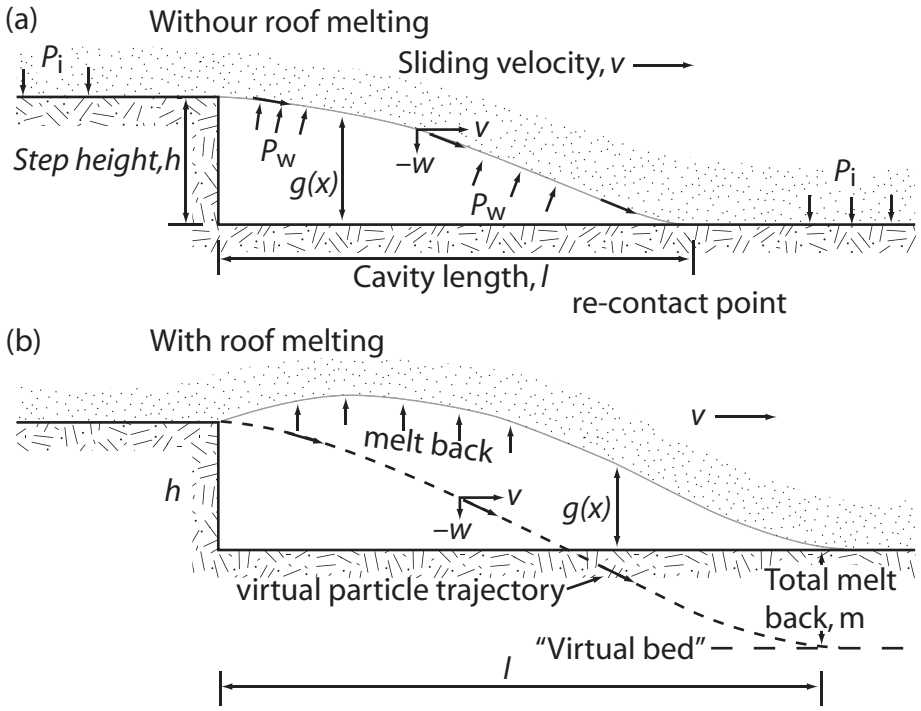

Figure 5.16. Geometry of the step cavity or orifice without (a) and with (b) melting of the ice roof. After Kamb (1987)

In the case of sinusoidal bed separation, we can consider a sinusoidal bed with wave crests perpendicular to ice flow and with wavelength and amplitude λ and a, respectively. As for the angular step, the gap length is l and the gap height is $g(x)$. The origin for x is at the separation point, which is undetermined. If $a \ll \lambda$ the separation problem can be solved in closed form for a linear rheology. This is an appropriate assumption for the orifices. The normal stress on the bedrock undulations is assumed to vary as $(x - x_0)^2$, where x_0 is the inflection point of the le side of the sinusoid. The gap length is

$$l = \frac{4\lambda}{\pi}\left(\frac{2}{5}\right)^{1/2}, \; P_e \leq \Sigma \tag{5.61}$$

where the cavitation parameter Σ

$$\Sigma = 8\pi^2 \eta a v / \lambda^2 \tag{5.62}$$

This is the limiting effective confining pressure for cavitation, if $P_e \geq \Sigma$ there is no cavitation. This indicates that cavities can only form once P_w is sufficiently high $(P_w > P_i - \Sigma)$. The gap height is given by

$$g(x) = \frac{2\pi^4}{3}\frac{a}{\lambda^4} x^{5/2} (l - x)^{3/2} \tag{5.63}$$

for $0 \leq x \leq l$. The separation point lies $3/8l$ upstream of x_0.

Kamb (1970) showed how a non-linear rheology and be introduced to a problem similar to that described above for a sinusoidal bed. The strain rate dependence is written

$$\eta = N\dot{\varepsilon}^{-1+1/n} \tag{5.64}$$

where N and n are constants and where $\dot{\varepsilon}$ is the second strain rate invariant. The value of $\dot{\varepsilon}$ at a height $\lambda/2\pi$ over the sliding interface, which is assumed to govern the effective viscosity, is

$$\dot{\varepsilon} = 4\pi^2 e^{-1} av\lambda^{-2} \tag{5.65}$$

(Kamb, 1970) for small wavelengths. Combining Equation (5.64) and Equation (5.65), with $n = 3$ yields,

$$\eta = N\left(\frac{e\lambda^2}{4\pi^2 av}\right)^{2/3} \tag{5.66}$$

and introducing this into Equation (5.62) yields

$$\Sigma = 2N\left(\frac{4\pi^2 e^2 av}{\lambda^2}\right)^{1/3} \tag{5.67}$$

which shows that $\Sigma \propto v^{1/3}$. This is an approximation where the effect of additional stresses is neglected and one which is reasonable for the sinusoidal wave bed because $P_e < \Sigma$, whereas in the step case η depends on P_e as in tunnel closure.

We now need to introduce roof melting of the orifices into the general theory. This can be done by introducing an adjustment of the contact point equivalent of introducing an imaginary floor lowered from the original floor by an amount corresponding the melt, m. The height of the virtual step thus becomes $h + m$, which was already introduced in Equation (5.58). The steady state gap profile is then obtained by the melt rate and vertical velocity distributions along the gap profile

$$vg'(x) = \dot{m}(x) + w(x) \tag{5.68}$$

By combining Equation (5.56), Equation (5.58), Equation (5.59), and Equation (5.68) and introducing the dimensionless variables

$$\gamma = g/h,\ \xi = x/l,\ \mu = m/h \tag{5.69}$$

we get

$$\frac{d\gamma}{d\xi} = 2\Xi\sqrt{1+\mu}\gamma^{5/3} - \frac{8}{\pi}(1+\mu)\sqrt{\xi(1-\xi)} \tag{5.70}$$

where

$$\Xi = \frac{2^{1/3}}{\pi^{1/2}}\frac{(\alpha\Lambda/\omega)^{3/2}}{DM}\left(\frac{\eta}{vP_e}\right)^{1/2} h^{7/6} \tag{5.71}$$

Ξ is a dimensionless quantity called the *orifice melting-stability parameter* and provides a measure of the importance of roof melting by viscous dissipation of heat in the linked cavity system.

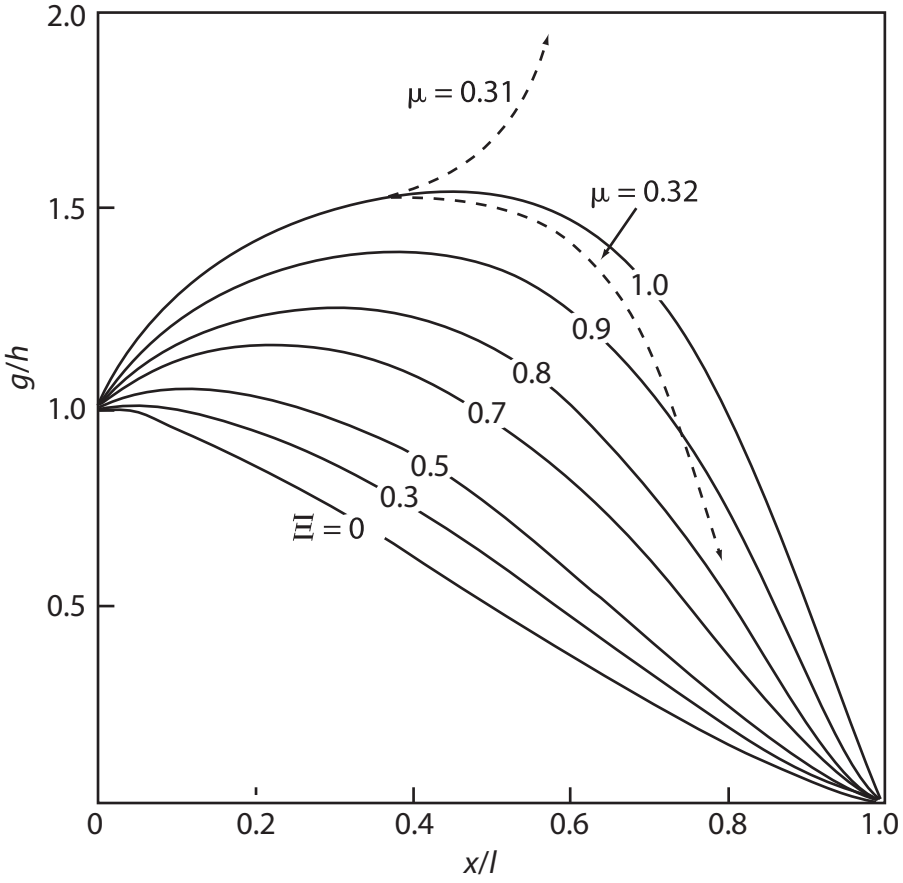

Figure 5.17. Steady state orifice size, in normalized coordinates, for different values of Ξ. After Kamb (1987)

Integrating Equation (5.70) yields the gap profile $\gamma(\xi)$. Figure 5.17 show the effect of melt back of the dimensionless orifice for different values of Ξ. The roof is raised and the peak of the roof is shifted downstream. The length of the gap also increases, which cannot be seen in Figure 5.17 because of the dimensionless length.

When the gap geometry is established we can calculate the discharge as

$$Q_w = \frac{2^{4/3}}{\pi^{1/2}} \frac{N_o}{M} \left(\frac{\alpha\Lambda}{\omega}\right)^{1/2} \left(\frac{\eta v}{P_e}\right)^{1/2} h^{13/6}\Phi \tag{5.72}$$

where the *flux factor* Φ is given by

$$\Phi = \sqrt{1+\mu} \int_0^1 \gamma^{5/3} d\xi \tag{5.73}$$

and is obtained by numerical integration of the results in Figure 5.17.

In the case of a wave orifice (Figure 5.18), the melt back is obtained from Equation (5.62) in the same way as for the step by introducing a virtual floor. A complication arises from the fact that the coordinates for the separation and recontact points

are not constant but are affected by the meltback. The non-dimensionalization is done by $\xi = x/l$ and $\gamma = g/g_o$ where

$$\frac{g_o}{a} = \left(\frac{128}{75}\right)\left(1 - \frac{P_e}{\Sigma}\right)^2 \tag{5.74}$$

We define a meltback parameter

$$\nu = \frac{2^4}{\pi^5}\left(\frac{\lambda}{l}\right)^4 \frac{m}{a} \tag{5.75}$$

and the dimensionless quantity

$$B = \frac{5}{5 - 2\nu + \nu^2} \tag{5.76}$$

We can then write the equation for the gap profile as

$$\frac{d\gamma}{d\xi} = \Xi' (5B)^{1/2} \gamma^{5/3} - B^2 \xi^{3/2} (1 - \xi)(8\xi + 3v - 5) \tag{5.77}$$

with the melting stability parameter Ξ' defined as

$$\Xi' = \frac{2^7}{3^{2/3}5^{7/3}} \frac{(\alpha\Lambda/\omega)^{3/2}}{DM} \left(\frac{\eta}{\nu\Sigma}\right)^{1/2} a^{7/6} \left(1 - \frac{P_e}{\Sigma}\right)^{11/6} \tag{5.78}$$

Σ/η can be removed from Equation (5.78) by Equation (5.62) to yield

$$\Xi' = \frac{2^{11/2}}{3^{2/3}5^{7/3}\pi} \frac{(\alpha\Lambda/\omega)^{3/2}}{DM} \frac{\lambda a^{2/3}}{v} \left(1 - \frac{P_e}{\Sigma}\right)^{11/6} \tag{5.79}$$

which does not contain the effective ice viscosity η. Equation (5.77) can be integrated in the same way as Equation (5.70) for different values of Ξ'.

Wave orifice gap profiles $\gamma(\xi)$ for a succession of Ξ' values are shown in Figure 5.19. The gap height is plotted as a dimensionless ratio g/g_0 where the scaling factor g_0 is the mid-point height of the gap when no melting occurs. One feature of the gap profile is that sagging occurs in the upstream part of the slope cavity. This sagging is linked to the downstream migration of the point of separation when meltback increases.

The discharge carried by the linked cavity model, with wave cavity orifices, can be written

$$Q_w = \frac{2^{25/2}}{75^{5/3}} \frac{N_O}{M} \left(\frac{\alpha\Lambda}{\omega}\right)^{1/2} \lambda a^{5/3} \left(1 - \frac{P_e}{\Sigma}\right)^{23/6} \Psi \tag{5.80}$$

where

$$\Psi = B^{1/2} \int_0^1 \gamma^{5/3} d\xi \tag{5.81}$$

is the flux factor analogous to Φ in Equation (5.73).

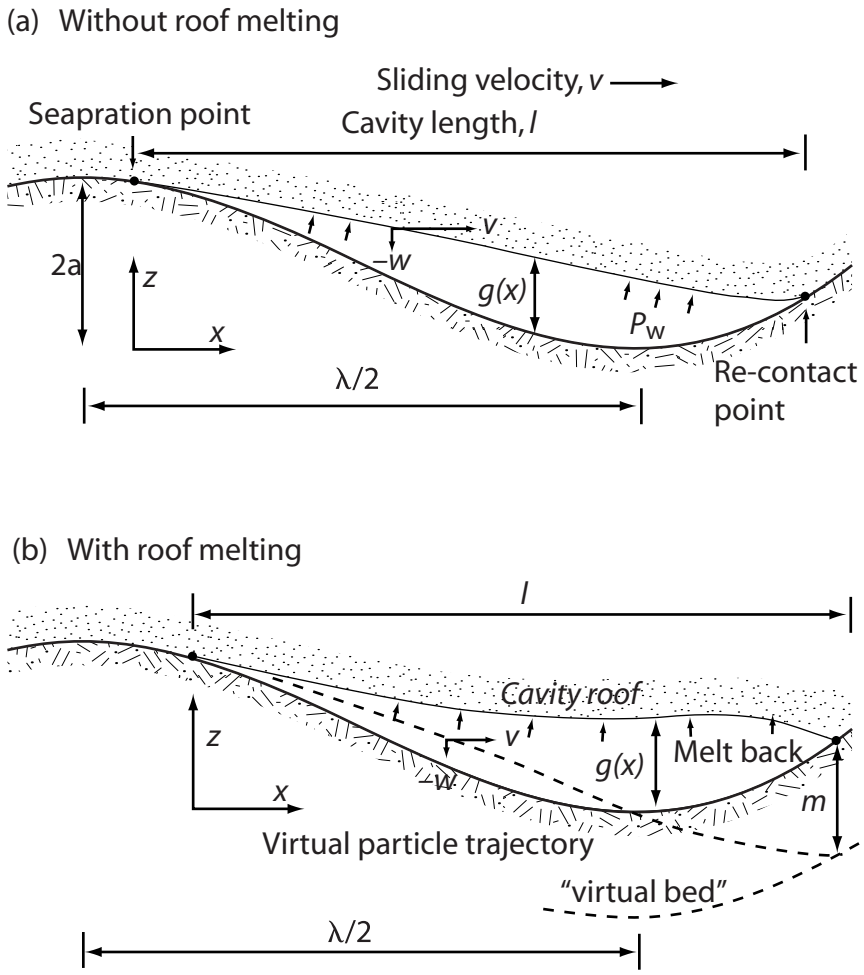

Figure 5.18. Geometry of an ideal wave cavity or orifice without (a) and with (b) melting of the ice roof. After Kamb (1987)

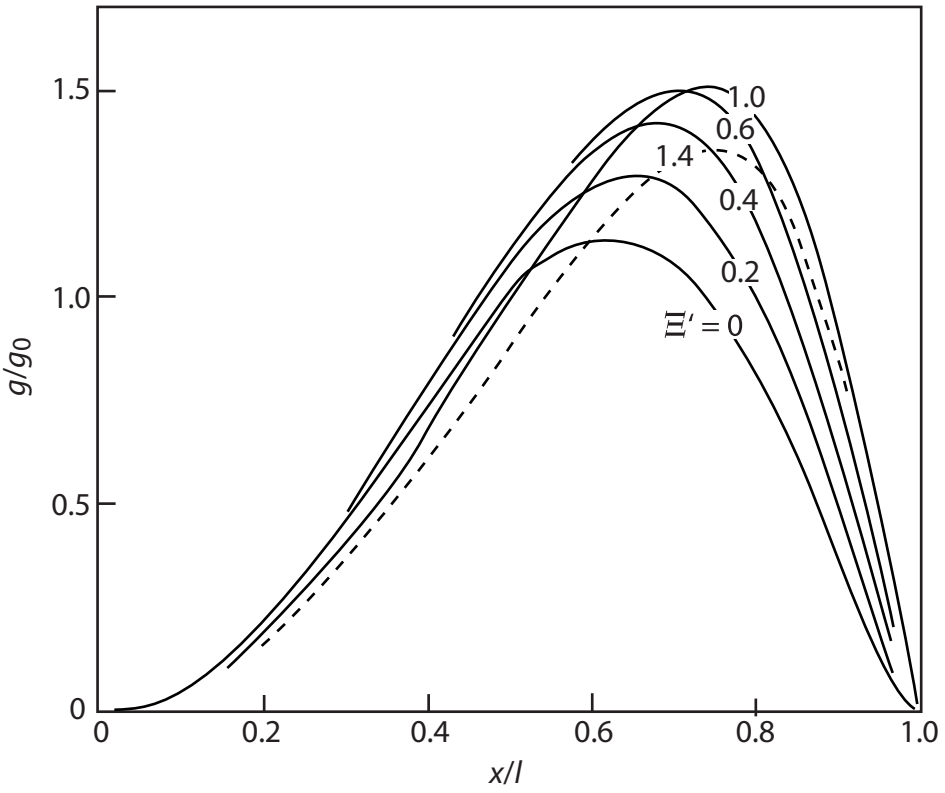

Figure 5.19. Transient cavity growth from different values on the meltback stability parameter Ξ, perturbation in confining pressure P_e/P_{e_0}, and proportionality constant f. After Kamb (1987)

In both the step orifice and wave orifice cases, Kamb (1987) found that the orifice melting stability parameters Ξ and Ξ' indicates instability for certain meltback parameters (μ and ν, respectively). The critical values for this instability are $\Xi \sim 1$ and $\Xi' \sim 1.5$. This can be analyzed by subjecting the system to a perturbation in water pressure. Initially we have an orifice in steady state with a confining pressure P_{e_0}, meltback parameters Ξ_0 and μ_0 and gap length l_0. The confining pressure is then decreased abruptly ($P_e < P_{e_0}$) so that the orifice begins to enlarge. The gap length will be a function of time or equivalently a function of position of the reference point as it moves forward with the ice ($\xi = x/l_0$). The new gap height $\gamma(\xi) = g(\xi)/h$ at the position ξ can be derived from Equation (5.70)

$$\frac{d\gamma}{d\xi} = 2\Xi_0\sqrt{1+\mu_0}\gamma^{5/3} - \frac{8}{\pi}(1+\mu_0)\frac{P_e}{P_{e_0}}\sqrt{\xi\left(\Upsilon(\xi)-\xi\right)} \tag{5.82}$$

where $\Upsilon(\xi) = l/l_0$ derives from l in Equation (5.59). The ratio P_e/P_{e_0} appears because gap closure rates are proportional to P_e. Integrating Equation (5.82) from $\gamma(0) = 1$, $\Upsilon(0) = 1$ we obtain how γ varies with position ξ as the reference point moves along the length of the orifice. To accomplish this, $\Upsilon(\xi)$ needs to be determined. Kamb (1987) does not provide details of this calculation but states that the important results are (1) that the orifice gap immediately starts to lengthen at a rate $\dot{l}(0) = v\,(1 - P_e/P_{e_0})$ in response to the pressure perturbation, and (2) the maximum gap lengthening rate is v. To test the possibility of unstable orifice enlargement, we identify that an increase in water pressure is a prerequisite and the maximum stabilization against enlargement is provided by maximum closure rate which occurs when l is maximized. We make the approximation that the lengthening rate $\dot{l}$ is constant ($\dot{l} = fv$) so that

$$\Upsilon(\xi) = 1 + f\xi \tag{5.83}$$

where f is a proportionality constant. By integrating Equation (5.82) forward from $\xi = 0$, $\gamma(0) = 1$ we obtain a touch-down point ξ_T, corresponding to the chosen $\dot{l}$ value, where the orifice ceiling hits the bed. This requires $\Upsilon(\xi_T) = \xi_T$ which by using Equation (5.83) becomes

$$f = 1 - {\xi_T}^{-1} \tag{5.84}$$

A stable transient response of the orifice is possible if it is possible to find $f < 1$. If $f = 1$, the integration of Equation (5.82) leads to $\gamma(\xi)$ increasing without bound since $f = 1$ yields the maximum closure rate at all stages. Figure 5.20 shows results from calculations of trajectories according to the analysis described above. The magnitude of the perturbations are given by $1 - P_e/P_{e_0}$. The results indicate that step orifices have an unstable response for $\Xi \geq 1$. Kamb (1987) argues that a similar instability arises for wave orifices at $\Xi' \geq 1.5$. The cause of the instability is related to the increase in melt that occurs when the gap height is increased. The stability of the system is probably better than discussed above because the assumption of local heat transfer. Some of the heat will then be transferred to the roofs of the large cavities instead of the orifice roofs.

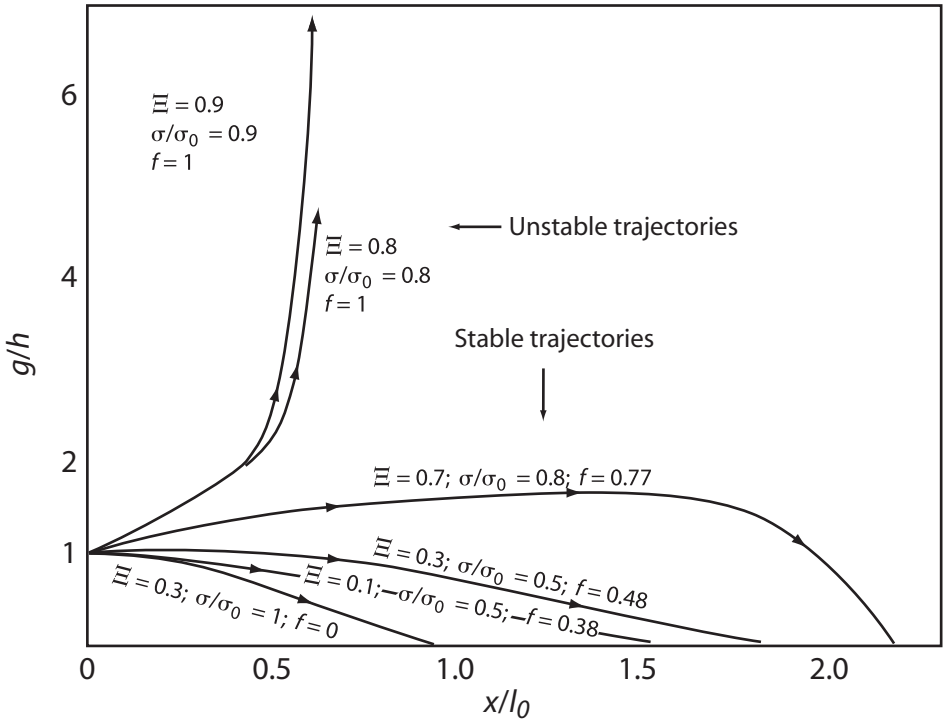

Figure 5.20. Transient cavity growth from different values on the meltback stability parameter Ξ, perturbation in confining pressure P_e/P_{e_0}, and proportionality constant f. After Kamb (1987)

5.5 Transitions between tunnel and linked cavity systems

The tunnel and linked cavity systems are fundamentally different. Discharge in a tunnel system is an inverse function of water pressure. The linked cavity system discharge increases with increasing pressure. This has the effect that the linked cavity system can be maintained as an interconnected system which would be impossible for a tunnel system where large branches will increase at the expense of smaller ones (Röthlisberger, 1972; Shreve, 1972). The linked cavity system also requires much larger basal water pressure than required by a tunnel system. The reason for this is that high pressure is required to keep the orifices open. The cavities present in the system are not a requirement for the flow characteristics but was introduced by Kamb (1987) to account for observed dispersion of tracers injected into Variegated Glacier.

A tunnel system exhibits a strong stability/unstability condition which stems from the inverse water pressure water flux relationship. If a tunnel in steady state experiences a perturbation in pressure the tunnel will increase or decrease in size at ever accelerating rates because wall melting changes faster than tunnel closure rates as the tunnel size changes. This instability is responsible for the jökulhlaup phenomenon (Nye, 1976; Spring and Hutter, 1981; Clarke *et al.*, 1984). The orifices under a fixed hydraulic gradient and steady state conditions, linked cavity system the orifices are stable against infinitesimal perturbations.

The stability of a inked cavity system are set by the melting-stability parameters Ξ and Ξ' since they provide a measure of the viscous dissipation. The stability is maintained as long as $\Xi < 1$ and $\Xi' < 1.5$ or the viscous dissipation is small. At higher values the the viscous dissipation becomes significant and the result is an uncontrollable enlargement of the orifices similar to what happens in tunnel systems. Under steady state hydraulic gradients, tunnels are unstable against even infinitesimal perturbations, whereas linked cavities become unstable for finite perturbations. The response of the tunnels occurs because no steady state condition exists in the absence of of viscous heating. The perturbation size causing instability in a linked cavity system decreases with increasing Ξ and Ξ'. In conclusion, the orifices are unstable only for an increase in size or water pressure whereas the tunnel instability is bilateral. The behaviors of the two systems are thus widely different.

Figure 5.21 shows the relationship between water discharge and water pressure for the linked cavities and tunnel systems. It is clear how the tunnel system experiences an inverse relationship between discharge and water pressure whereas for a linked cavity system there is a direct relationship between the two. The systems are thus fundamentally different. The response functions for step and wave-orifice systems are also different. These relationships imply that a numerous parallel connections can be maintained simultaneously whereas in a tunnel system a smaller tunnel is unstable relative to a larger one, which thus captures the discharge from the smaller one until it closes completely.

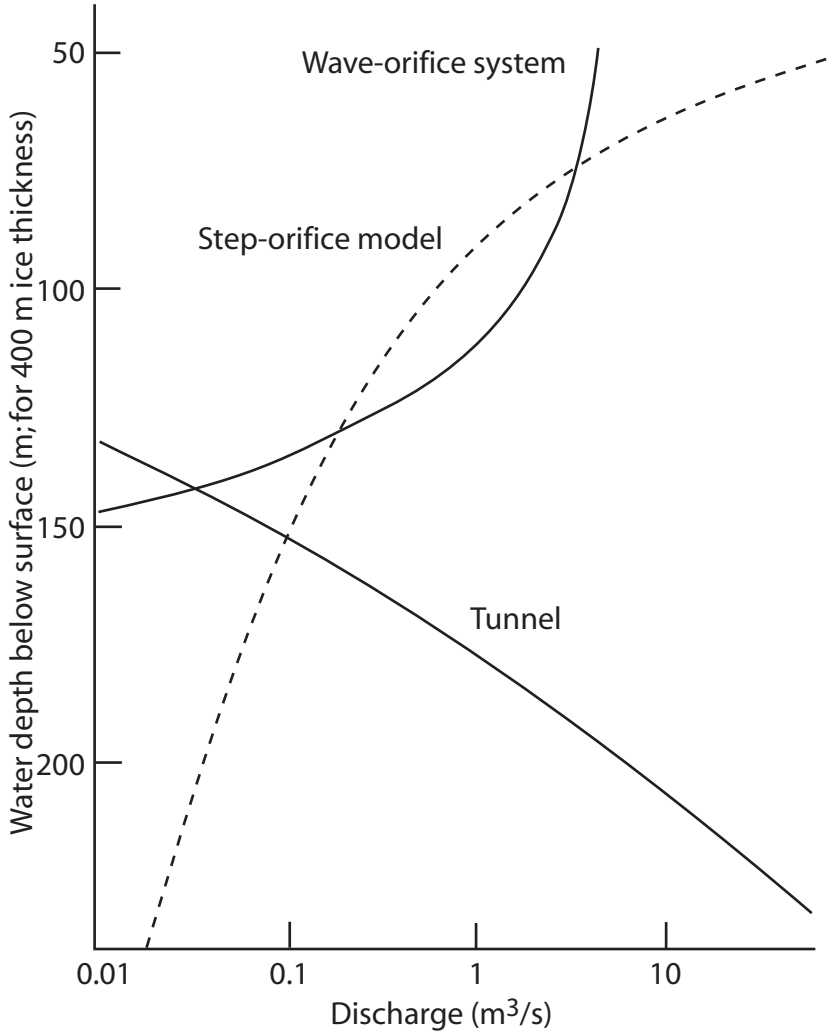

Figure 5.21. Characteristics of tunnel system and linked cavity systems. After Kamb (1987)

Figure 5.22 shows a chain of events initiated by a perturbation of an orifice in the linked cavity system. The orifice grows rapidly and will approach the size of neighboring cavities, it this becomes a tunnel. With time the tunnel is advected downstream by ice flow. Because of the geometry of the upstream part of the tunnel, roof collapse will commence and close off a new orifice from the tunnel. Kamb (1987) argues that simultaneous formation of such tunnel elements from a larger scale perturbation in velocity or water pressure may cause the segments to coalesce into progressively longer tunnel segments until an entire tunnel system is developed. Hence, the linked cavity can irreversibly be converted into a tunnel system. This explains the observations at the end of the surge of Variegated Glacier where large volumes of water were discharged from the glacier while water pressures and velocity dropped.

5.6 Subglacial channels on deformable subglacial sediments

The discussion above on basal melt films, tunnel and linked cavity systems have all dealt with bedrock as the substrate beneath the glacier. This is true for many valley glaciers but is probably not a good general condition to be expected beneath ice sheets where the ice rests on a variety of sediments, the most common of which would be poorly sorted sediments or till. Subglacial sediments can also deform from the shear stresses imposed by the overlying ice. A large number of papers have dealt with the different flow mechanisms of deforming subglacial sediments (Boulton and Hindmarsh, 1987; Kamb, 1991; Iverson *et al.*, 1994, 1995, 1999; Hooke *et al.*, 1997; Fischer *et al.*, 1998).

Shoemaker (1986) was the first to formulate how subglacial channels interacted with the deformable sediments beneath a glacier or ice sheet. He identified three different types of systems:

1. Basal melt water drainage is along the bed. This is the hard bedrock case described in previous chapters.

2. Bed and substrate are fully coupled.

3. Basal meltwater drainage is dominated by ground-water flow.

Shoemaker (1986) developed a model for a temperate ice sheet resting on a deformable bed by applying the following argument. In a radially flowing ice sheet, two conduits A and B (Figure 5.23) separated by a distance d are extended in the flow direction by the advancing ice sheet to A' and B', respectively. He argued that the subglacial channel will occupy a formerly subaerial part of the channel system as the glacier advances over older proglacial areas. To form a new channel C we can apply Darcian flow theory within the substrate to investigate where the steepest hydraulic gradients occur. If we assume that the water flow is radial, symmetrical

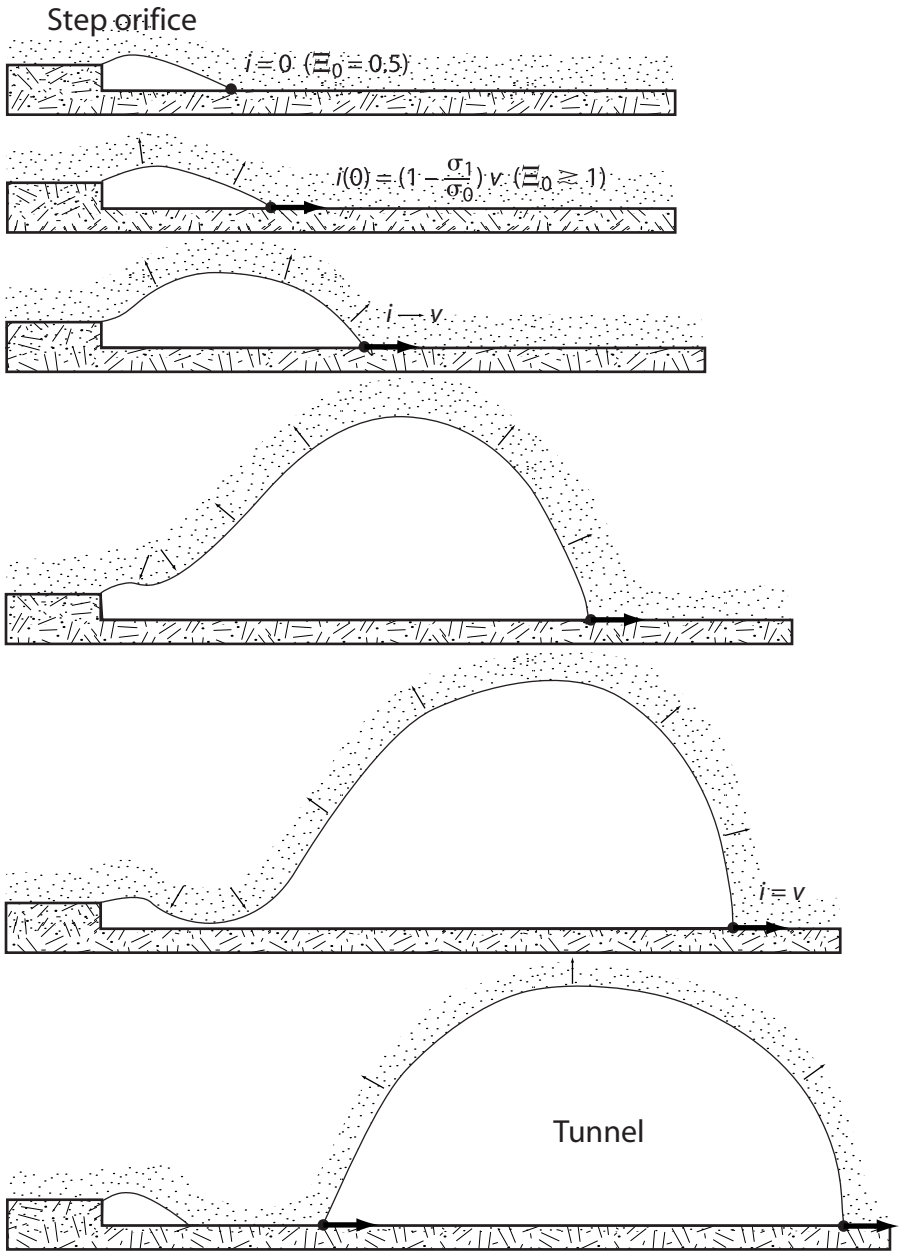

Figure 5.22. Development of tunnel segments from perturbations in orifice size of the linked cavity system. After Kamb (1987).

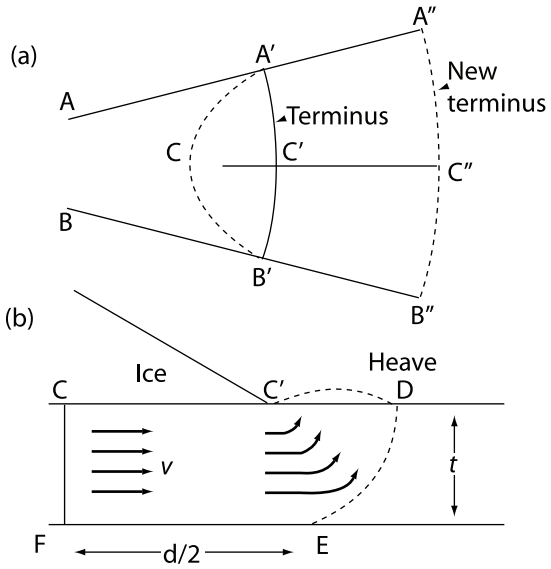

Figure 5.23. Schematic model of subglacial tunnel initiation beneath an ice sheet resting on a deformable bed. After Shoemaker (1986)

around the channel line C–C' and that water is produced in a region described by $A'C'B'CA'$, then the maximum hydraulic gradient must occur at C'.

The flow velocity of water in the substrate along C–C' is given by

$$v = \frac{\dot{m}d}{2t} \tag{5.85}$$

where $\dot{m}$ is the uniform basal melt rate, $d/2$ is the estimated length of the radial flow line for water flow, and t is the thickness of the aquifer. The hydraulic gradient is given by

$$i = \frac{v}{K} \tag{5.86}$$

where K is the hydraulic conductivity. When the ice sheet increases in size, d increases and the hydraulic gradient reaches a critical value i_c where a channelized flow starts. The critical flow length is described by

$$d_c = \frac{2ti_cK}{\dot{m}} \tag{5.87}$$

When the critical value i_c (= 1.2; Terzaghi and Peck (1941) cited by Shoemaker (1986)) is reached, upward flow of water and accompanying soil dilation begins outside of the ice sheet terminus. This condition causes removal of sediment from the "spring" area outside of the glacier and focuses even more water flow to the area. The result will be back-ward erosion in under the ice sheet and formation of a channel incised into the subglacial sediments. Applying Equation (5.87) to values

of K for dilatant tills ($K = 10^{-5}$) yields $d_c = 4 \times 10^4$. because surface water can reach the bed through surface crevasses, the d_c-value must be decreased by perhaps two orders of magnitude. Shoemaker (1986) points out that a similar calculation for non-dilatant till values of K yield unreasonable d_c values (0.04–400 m) which implies that dilatant tills may be commonplace in the terminus area.

In till, a channel will develop until its bed becomes armored by larger particles preventing further removal of fines. These channels resemble N-channels (Nye, 1973).

If we consider steady state flow in a debris-layer system we can use the equations of Röthlisberger (1972) and Weertman (1972) for turbulent steady flow on ice conduits

$$\rho_i g h - P_c = B^\star Q^q \left(\frac{dP_w}{dx} \right)^p \tag{5.88}$$

where x is the distance upstream from the terminus, $\rho_i g h$ is the ice overburden pressure, P_c is the water pressure in the channel, $B^\star$ is the flow law parameter determined by temperature, impurities etc. of the ice. Q is the channel flow rate and dP_w/dx is the pressure gradient in the upstream direction. Weertman (1972) showed that the exponents p and q become $11/24$ and $1/12$, respectively, by assuming $n = 3$ in the flow law for ice (Equation (4.1)). dP_w/dx can be replaced by dP_c/dx since the velocity gradient in general is negligible (Lliboutry, 1983), however, this may not be true near the terminus.

In a steady state situation, the size of a conduit in ice is determined by a balance between ice closure given by

$$u_c = aB \left(\rho_i g h - P_c \right)^3 \tag{5.89}$$

where a is the channel radius, B is a constant different from $B^\star$, and melting from viscous dissipation of heat given by

$$u_m = Q \frac{\frac{dP_c}{dx}}{2\pi a F} \tag{5.90}$$

where F is the heat of fusion modified to account for incomplete heat transfer between water and ice wall (here $2/3$ of the heat is used for melting).

The soil must also be treated in the model. Failure of soils can be modelled by the Coulomb inequality

$$\tau_b \leq c + (\rho_i g h - P_p) \tan \phi \tag{5.91}$$

where τ_b is the basal shear stress, P_p is the pore-water pressure, c is the soil cohesion, and ϕ is the angle of internal friction of the material. Under steady state, neglecting deviatoric stresses, and assuming that the ice thickness h is smoothed over distances of $\mathrm{O}(h)$, the equilibrium equation

$$\tau_b = \rho_i g h \frac{dh}{dx} \tag{5.92}$$

holds.

The pore-water pressure is governed by Darcy's law

$$q = \frac{-Kt}{\rho_w g}\frac{dP_p}{dy} \tag{5.93}$$

where q is the pore-water flow rate, K is the hydraulic conductivity, and y is the direction towards a channel from a point midways between channels. In this model we will assume that the aquifer permeability is uniform and that the vertical pressure drop is negligible.

The pore-water flow rate is given by

$$q = \dot{m}y, \quad 0 \leq y \leq d/2 \tag{5.94}$$

where $\dot{m}$ is a melt rate that can be adjusted for surface water input as long as it reaches the bed uniformly. Shoemaker (1986) points out that surface water is assumed to reach the channels directly in his approach. This seems to be a reasonable assumption. Hence Equation (5.93) and Equation (5.94) describe the motion of water through the aquifer towards the conduits

$$P_p = \frac{\dot{m}\rho_w g}{8Kt}\left(d^2 - 4y^2\right) + P_c \tag{5.95}$$

where the boundary condition $P_p(d/2) = P_c$ was applied during integration. The pressure drop along the conduit is constant

$$\Delta P_p = \frac{\dot{m}\rho_w g d^2}{8Kt} \tag{5.96}$$

By inserting reasonable values for d and K Shoemaker (1986) showed that the resulting pressure difference became high. With melt rates of 1 cm year^{-1} Equation (5.87) yields values of d that are perhaps two order of magnitude too high. Furthermore, if Equation (5.96) is used to evaluate values of d for a specific pressure change, the resulting d-values are $\propto K$, much more reasonable than those obtained from Equation (5.87). For very small K-values, the resulting d-values are still too large. Shoemaker (1986) concludes that it seems reasonable to adopt a fixed dP_p/dx-criterion for establishing channel spacing calculations, although no physical explanation can be given as to why channel spacing should depend on dP_p/dx.

By assuming that the top surface of the aquifer meets the failure failure criterion in Equation (5.91), we can investigate the maximum profiles $h(x)$ of the system. To simplify, we will assume that d is determined by $\Delta P_p/dx = 10^5$ Pa. The average P_p at a specific section x is given by

$$\bar{P}_p = P_c + \frac{\dot{m}\rho_w g d^2}{12Kt} \tag{5.97}$$

which indicates that the bed will either deform uniformly or not at all at a section $x =$ constant. By combining Equation (5.88), Equation (5.91), Equation (5.92), and Equation (5.97) and assuming that $\rho_i = \rho_w$, yields

$$\frac{dP_c}{dx} = \left(\frac{\rho g h - P_c}{B^\star Q^q}\right)^{1/P} \tag{5.98}$$

and

$$\frac{dh}{dx} = \frac{c}{\rho g h} + \left(1 - \frac{P_c}{\rho g h} - \frac{\dot{m} d^2}{12 K t h}\right) \tan\phi \tag{5.99}$$

If we define

$$e = \frac{c}{\rho g H} - \frac{\dot{m} d^2}{12 K t} \tan\phi = \frac{c}{\rho g} - \frac{2 \Delta P_p \tan\phi}{3 \rho g d} \tag{5.100}$$

Equation (5.99) becomes

$$\frac{dh}{dx} = \left(1 - \frac{P_c}{\rho g h}\right) \tan\phi + \frac{e}{h} \tag{5.101}$$

These equations show that there is no solution satisfying $P_c(0) = h(0) = 0$ near $x = 0$ because in general $e < 0$ (Equation (5.103)). At the terminus $\rho g H \to 0$ and $P_p < 0$. Equation (5.91) implies that no stress is sustained if $P_p \tan\phi \geq c$. However, $h' = O(1)$ at the terminus and Equation (5.92) indicates positive shear stresses at the terminus which is inconsistent. In the region of the terminus deviatoric longitudinal stresses t_{xx} must be considered but these were assumed negligible when establishing Equation (5.92). A more general equilibrium equation is

$$\tau_b = \rho g h' - 2 \left(h \tau_{xx}\right)' \tag{5.102}$$

Near the terminus, Equation (5.103) must be replaced by

$$\frac{dh}{dx} = \frac{c + 2 \left(h t_{xx}\right)'}{\rho g h} + \left(1 - \frac{P_c}{\rho g h} - \frac{\dot{m} d^2}{12 K t h}\right) \tan\phi \tag{5.103}$$

and Equation (5.103) by

$$\frac{dh}{dy} = \left(1 - \frac{P_c}{\rho g h}\right) \tan\phi + \frac{e^\star}{h} \tag{5.104}$$

where

$$e^\star = e + \frac{2 \left(h t_{xx}\right)'}{\rho g} \tag{5.105}$$

In order to obtain a simple regular solution at the origin we prescribe

$$e^\star(0) = 0 \tag{5.106}$$

$$h'(0) = \tan\phi \tag{5.107}$$

and

$$t_{xx}(0) = \frac{-\rho g e(0)}{2} \tan\phi \tag{5.108}$$

The prescription of $e^\star(x)$ near the terminus introduces arbitrariness into the solutions but qualitative results are not affected as long as the prescriptions above are satisfied. The function $e^\star(x)$ is arbitrarily defined as

$$e^\star(x) = \frac{e x}{l^\star}, \quad 0 \leq x \leq l^\star \tag{5.109}$$

where $l^\star = 2$ km, but can be assigned other values.

The function $q(x)$ in Equation (5.97) has contributions from both subglacial and surface water and can be written as

$$Q(x) = \begin{cases} md(L-x) & \text{winter} \\ md(L-x)+ & \begin{cases} \frac{Md}{H}\left[H\left(L^\star - x\right) - \int_x^{L^\star} h(x)dx\right], \; h(x) < H \\ 0, \; h(x) > H, \text{ summer} \end{cases} \end{cases} \tag{5.110}$$

The second term in the summer equation concerns elevation dependent surface melting with a cut-off at $h(x) = H$. $L^\star$ is defined by $H = h(L^\star)$. The initial conditions for the maximum profile problem are

$$P_c(0) = h(0) = 0 \tag{5.111}$$

Equation (5.98) and Equation (5.103) can be solved on $0 < x < L$ for $L = 100$ and 1000 km. Using e values from Table 5.1 shows that $t_{xx} < 1$ bar.

Table 5.1: *Standard parameters for four soils used in calculations. After Shoemaker (1986).*

	K	ϕ	c	d	e
	$\mathrm{m\,s^{-1}}$	$^\circ$	kPa	m	m
Silty clay	10^{-7}	5	1	360	∼0.
Silty sand	10^{-6}	20	0	1140	–2.5
Medium sand	10^{-4}	30	0	11400	–3.9
Medium gravel	10^{-2}	50	0	114000	–8.0

Figure 5.24 shows the results of calculations using values from Table 5.2 with $L = 1000$ km, $\Delta P_p = 1$ bar and assuming steady state winter flow. The results indicate that the ice sheet profiles all lie above the first-approximation theoretical surface profile given by $h = 3\sqrt{x}$, indicating that low-relief ice sheet profiles do not result if efficient melt water drainage occurs provided small d values. The surface profiles become very flat some distance away from the divide because $P_c/\rho g h \to 1$ very rapidly. The profiles increase in height with coarser aquifer medium reflecting an increasing ϕ.

Table 5.2: *Ratios of winter h (standard e values)/h (*10× *standard e values) at mid-span and divide for* 100 km *and* 1000 km *ice sheets. Channel spacings are unchanged. After Shoemaker (1986).*

	50 km	100 km	500 km	1000 km
Silty sand	1.09	1.13	1.14	1.23
Medium sand	1.06	1.08	1.10	1.15
Medium gravel	1.03	1.05	1.06	1.08

Alley (1989) developed ideas relevant for understanding the coupling between basal sliding and sediment deformation for the ice streams A–E in Antarctica. The

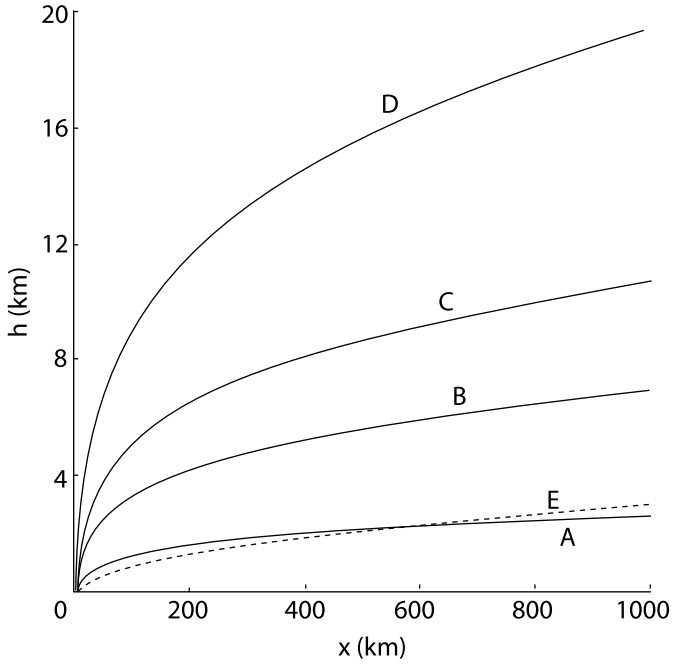

Figure 5.24. Maximum profiles corresponding to data of Table 5.1. After Shoemaker (1986).

presence of subglacial sediments beneath Ice Stream B (currently named Whillans Ice Stream) was determined through seismic reflection investigations (Blankenship and Bentley, 1986; Blankenship *et al.*, 1986, 1987, 1989; Rooney *et al.*, 1987a,b, 1988). In order to understand the processes of till deformation, the hydrology of the ice stream needed a theoretical framework.

Alley (1989) summarizes the sources for water by introducing two types of contributions: *distributed* and *localized* sources. Distributed sources are melting at the bed, downward transport of en- and supraglacial melt and precipitation (through intracrystalline veins), and porous flow from subglacial aquifers; localized sources are downward transport of en- and supraglacial melt and precipitation (through discrete channels), and stream transport from unglaciated areas. Since the most common situation for Antarctica, in absence of surface contribution of water, probably is the distributed contribution from basal melting, Alley (1989) considers only this case. Hence this will be valid for large areas of ice sheets overlain by dry snow or percolation zones (Figure 2.1). The dry snow zone on Greenland is variable with a trend showing a steady decrease (*e.g.* Steffen *et al.*, 2004; ACIA, 2005, fig. 6.18, p. 205). The zonation also show a clear latitudinal trend with larger dry snow zone towards the climatologically colder north. Similar zonation, albeit unknown in extent and configuration probably also existed on the past Fennoscandian ice sheet.

Water generated by at the base of an ice sheet by basal melt will flow downward into the sediment and outward to the edge of the ice sheet through porous flow or sheet flow at the ice-sediment interface or both. The component of porous flow

has been investigated by many (*e.g.* Boulton *et al.*, 1974; Boulton and Jones, 1979; Clarke *et al.*, 1984; Boulton and Hindmarsh, 1987; Clarke, 1987; Lingle and Brown, 1987). However, the porous flow system has a limited capability to transport water and most studies indicate that subglacial aquifers are inefficient for large wet-based ice sheets. (Alley, 1989) shows, as an example, that a 1000 km flow line in a wet based ice sheet produces water that would require a 250 m thick aquifer of unconsolidated sand to evacuate the water (given sliding velocity of 25 m year^{-1}, an average basal shear stress of 10^5 Pa, a surface slope of 0,01, and a hydraulic conductivity of 10^{-4} m s^{-1}). To remedy this situation, it is necessary to invoke a drainage system of some finite thickness at the ice–bed interface such as the film suggested by Weertman (1972) and, including instability, by Walder (1982). Hence depending on the conditions of the basal aquifer, drainage can occur as any combination from 100% porous flow to ∼100% channelized flow in terms of volume rate. Close to ice divides the first situation may be common whereas the importance of discrete channelized flow increases towards the margins of the ice sheet since flow rates increases radially but aquifer, generally does not.

To investigate channel instability on a deformable bed, Alley (1989) assumes that the basal sediment follows a constitutive law of the form

$$\dot{\varepsilon} = \begin{cases} K_b \frac{(\tau - \tau^\star)^a}{N^b} & \tau > \tau^\star \\ 0 & \tau \leq \tau^\star \end{cases} \tag{5.112}$$

where $\dot{\varepsilon}$ is the strain rate, τ is the shear stress, and a, b, and K_b are empirical constants. N is the effective water pressure given by

$$N = P_i - P_w \tag{5.113}$$

and $\tau^\star$ is the sediment yield strength given by the Mohr-Coulomb yield strength criterion

$$\tau^\star = c + N \tan \phi \tag{5.114}$$

where c is the cohesion and ϕ is the angle of internal friction (*e.g.* Lambe and Whitman, 1969). Alley (1989) follows Boulton and Hindmarsh (1987) and uses their experimental results which indicate that $b > a$ in Equation (5.112).

Tunnel closure, in absence of non-hydrostatic fields around the conduit (Boulton and Hindmarsh, 1987), can then be described by the following set of equations

$$\begin{aligned} \xi_c &= \begin{cases} K_b \frac{(N - \tau^\star)^a}{N^b a^a} & N > \tau^\star \\ 0 & N \leq \tau^\star \end{cases} \\ \xi_c &\equiv \frac{\dot{r}}{r} \end{aligned} \tag{5.115}$$

where the subscript c refers to creep closure, the driving stress $\tau = N$, r and $\dot{r}$ are the tunnel radius and change in radius with time, respectively. Equation (5.115) applies to a channel with circular cross-section but Alley (1989) identifies a more realistic case as an channel incised into the till with an ice roof that has collapsed, hence resembling an N-channel in subglacial sediment. The equation above may

reasonably well model this situation although any coupling at the ice-bed interface is ignored. At a steady state the creep closure ξ_c must be balanced by an erosion rate ξ_e. The flow of sediment is crucial. Alley (1989) states that basally derived water will always carry sediments at its carrying capacity since it is always in contact with sediment and hence erosion along some stretch of the conduit will be determined by the added water from melting along that stretch.

The sediment flux in a channel J_s can be approximated by

$$J_s = J_0 \pi r^2 \bar{u}_w^2 \tag{5.116}$$

(*e.g.* Allen, 1985) where J_0 is a constant and $\bar{u}_w$ is the mean flow velocity given by

$$\bar{u}_{w\ell} = \frac{P_g r^2}{8\mu} \tag{5.117}$$

and

$$\bar{u}_{wt} = M P_g^{\,1/2} r^{2/3} \tag{5.118}$$

where subscripts ℓ and t refer to laminar and turbulent flow, respectively, P_g is the magnitude of the volumetric fluid-potential along flow gradient, μ is the water viscosity, and M is the inverse of the Manning roughness coefficient. The transition between laminar and turbulent flow occurs within a narrow range of Reynolds numbers centered on

$$\frac{2r\rho_w \bar{u}_w}{\mu} = 2300 \tag{5.119}$$

(Weertman, 1972) where ρ_w is the density of water. The erosion rate ξ_e in the steady state is

$$\xi_e = \frac{1}{2\pi r^2}\frac{\partial J_s}{\partial x} = \frac{\dot{r}}{r} \tag{5.120}$$

where x is the along-channel distance.

To obtain an expression for ξ_e in terms of water influx into the channel Alley (1989) assumes that J_0, μ, M, and P_g are independent of x and then combine Equation (5.116) and Equation (5.118), differentiate with respect to x to substitute $\partial J_s/\partial x$ in Equation (5.120) to obtain an expression for ξ_c in terms of r and $\partial r/\partial x$. r is related to water flux Q by

$$Q = \pi r^2 \bar{u}_w \tag{5.121}$$

Combining Equation (5.121) and Equation (5.118), differentiating with respect to x, solving for $\partial r/\partial x$ and substituting into Equation (5.120) yields

$$\begin{aligned} \xi_{e\ell} &= \tfrac{J_0 P_g^2 r^2 Q_x}{64\pi\mu^2} \\ \xi_{et} &= \tfrac{3 J_0 M^2 P_g Q_x}{4\pi r^{2/3}} \end{aligned} \tag{5.122}$$

where Q_x is the derivative of Q in the x-direction and corresponds to the water influx to the channel. In the steady state, equations (5.115) and (5.122) equate.

Table 5.3: *Value of constants used in calculating Figure 5.25 and Figure 5.26. Values are gathered to fit data from a variety of cases such as Ice Stream B, Antarctica, and Variegated glacier, Alaska USA. After Alley (1989).*

Parameter	Value	Parameter	Value
a	1	L	3.1×10^8 J m^{-3}
b	2	$\dot{m}$	9.5×10^{-10} m s^{-1}
B	1.8×10^{-25} Pa^{-3} s^{-1}	M	0.58 Pa$^{-1/2}$ m$^{5/6}$ s^{-1}
C	$0, 4, 25$ kPa	P_g	20 Pa m^{-1}
g	9.8 m m^{-2}	$\tan\phi$	$0, 0.2, 0.75$
J_0	1.5×10^{-5} s^2 m^{-2}	μ	1.8×10^{-3} Pa s
K	10^{-6} m s^{-1}	ρ_w	10^3 kg m^{-3}
K_b	0.33 Pa s^{-1}		

The influx of water to the channel depends on the water supply rate at the bed and the collecting area (Shoemaker, 1986). (Alley, 1989) uses two ways to approximate the water supplied to the channel: (1) supply from a porous half-space where water is not drawn down from $N/\rho_w g$ above the center of the tunnel and (2) that water is collected from an area 10^4 times wider than the tunnel width. Approximation (1) leads to

$$Q_x = \frac{2\pi K N}{\rho_w g \ln\left(\frac{2N}{\rho_w g r}\right)} \tag{5.123}$$

where K is the hydraulic gradient in the sediment and g is the gravitational acceleration. With a tunnel radius of 1 m and appropriate constants (Table 5.3), Equations (5.115), (5.122) and (5.123) yields $N = 10^7$ Pa and Q_x equivalent of a basal melt rate of 10 mm year^{-1} over a 2400 km width. Approximation (2) corresponds to

$$Q_x = 10^4 r \dot{m} \tag{5.124}$$

where $\dot{m}$ is the basal melt rate. A 1 m channel would in this case drain a 10 km width of the ice sheet, which becomes the assumed tunnel spacing. Alley (1989) considers Equation (5.124) a restrictive estimate whereas Equation (5.123) constitutes an upper limit.

Figure 5.25 shows estimates of N for steady state N-channels in subglacial sediments calculated using values in Table 5.3. The two cases involve (1) Equation (5.123) which corresponds to a maximum and (2) Equation (5.124) corresponds to a likely case which probably over-estimates Q_x and underestimates N for small values of r. The values used to evaluate the equations are a combination of values from Weertman (1972), Boulton *et al.* (1974), Humphrey *et al.* (1986) and Boulton and Hindmarsh (1987), data fitted to observations from Ice Stream B, Antarctica, and Variegated Glacier, Alaska, USA. The curves in Figure 5.25 represent calculation for two cases, $\tau^\star = 0$ and the upper limit for $\tau^\star$ in a basal sediment, till ($C = 4$ kPa, $\tan\phi = 0.75$; Sladen and Wrigley, 1983). The area between these cases represent likely values, the only exception being the case for low N where an intermediate

curve ($C = 4$ kPa, $\tan\phi = 0.2$; $\tau^{\star}_{\text{likely}}$). Included are also curves for R-channels calculated following Weertman (1972) using the same constants (Table 5.3)

$$\begin{aligned} N_\ell &= \left(\frac{P_g^2 r^2}{16 B \mu L}\right)^{1/3} \\ N_t &= \left(\frac{M P_g^{3/2} r^{2/3}}{2LB}\right)^{1/3} \end{aligned} \tag{5.125}$$

where B is related to the creep hardness of ice, H is the heat of fusion and ice is assumed to obey Glen's flow law for ice (Equation (4.1); Nye, 1953). The difference between the creep closure rate and the melt rate of an R-channel is

$$\begin{aligned} (\xi_\ell)_{\text{net}} &= BN^3 - \tfrac{P_g^2 r^2}{16 \mu L} \\ (\xi_t)_{\text{net}} &= BN^3 - \tfrac{M P_g^{3/2} r^{2/3}}{2L} \end{aligned} \tag{5.126}$$

(Weertman, 1972).

Figure 5.26 shows contours of $(\xi)_{\text{net}})$ for both R-channels and channels in subglacial sediment (assuming $C = 4$kPa, (Boulton and Hindmarsh, 1987), and $\tan\phi = 0.2$, (Alley *et al.*, 1987)). Closure is positive and growth is negative.

Figure 5.25 and Figure 5.26 show that two steady configurations for subglacial channels in sediment. When the driving stress is low, channels are stable at high N and conversely when till viscosity is high. The low values of N occurs near N_c, which is the critical value where driving stress for creep closure equals the yield strength of the subglacial sediment

$$N_c = \frac{C}{1 - \tan\phi} \tag{5.127}$$

The value used for Figure 5.26 is $N_c = 5$ kPa. Because erosion by basal water is slow and is balanced by equally slow creep closure rates, the driving stress is low ($N - \tau^{\star}$) and the effective pressure equilibrium is close to N_c. Furthermore, Figure 5.26 shows that steady state R-channels occur where rapid creep closure of channels in subglacial sediment occurs, which indicates that an R-channel would rapidly fill with sediment through creep. This holds for all but the tills with very high yield strength ($C = 25$ kPa,$\tan\phi = 0.75$; Sladen and Wrigley, 1983). The largest R-channel that can exist over a till bed has an $N \approx N_c$ for that particular bed. A rigid bed is one for which $N_c > N$ in the largest R-channel that can develop over a rigid bed in the glacier in question. Furthermore, till channels at low N occur in a region of R-channel growth, which is a similar situation to that explored by Walder (1982) for rigid beds. Hence perturbations in a distributed water system tends to grow.

In conclusion Alley (1989) hypothesizes that the water system at the ice-sediment interface resembles a thin film but with local mm-sized thickening. The effective pressure should be above N_c but not above the equilibrium value for R-channels of mm radius; this means between 0 and ~ 400 kPa. Any local thickening will be rapidly counteracted by till creep.

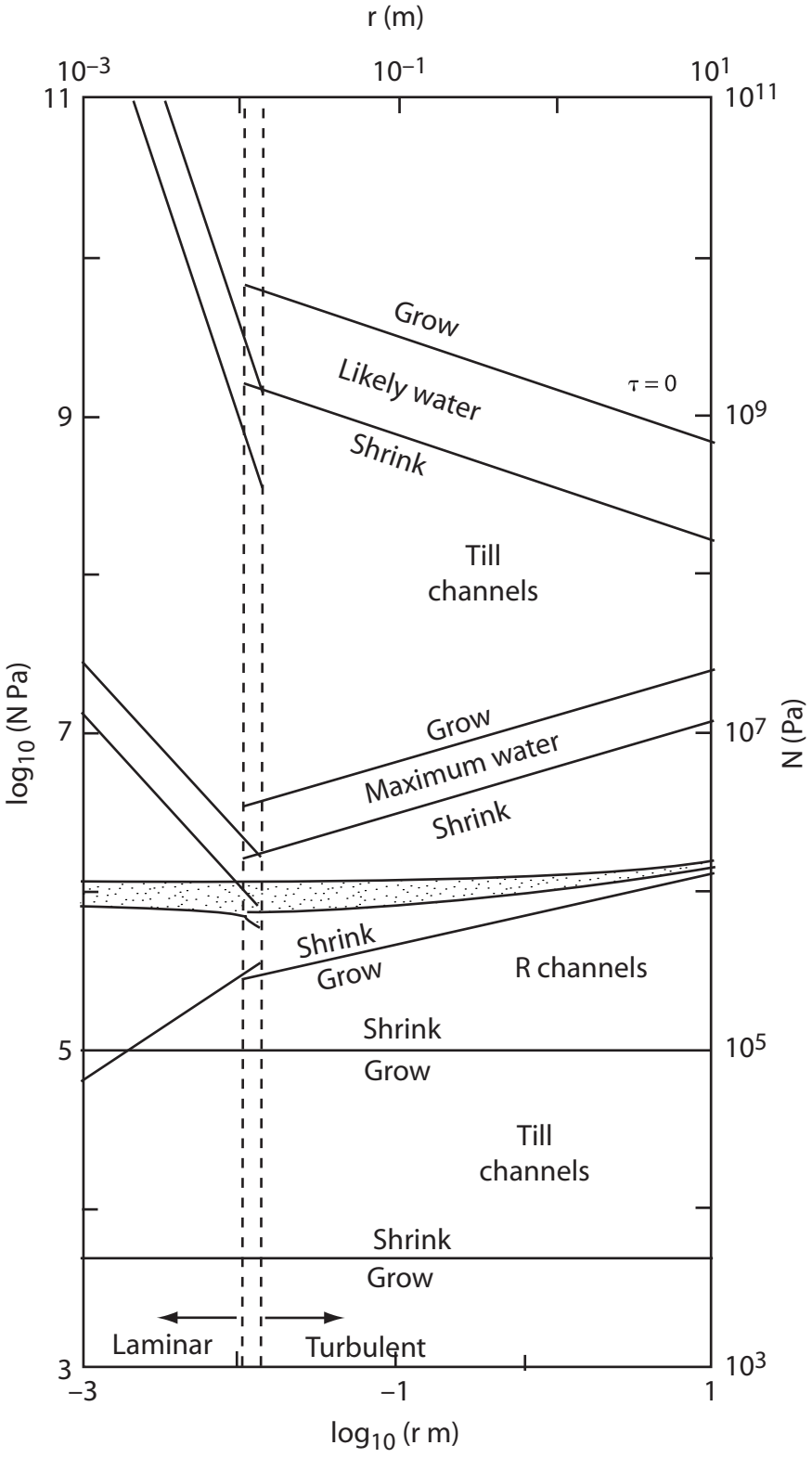

Figure 5.25. Effective pressure (N) as a function of channel radius (r) for Röthlisberger channels and N-channels in subglacial sediment. After Alley (1989).

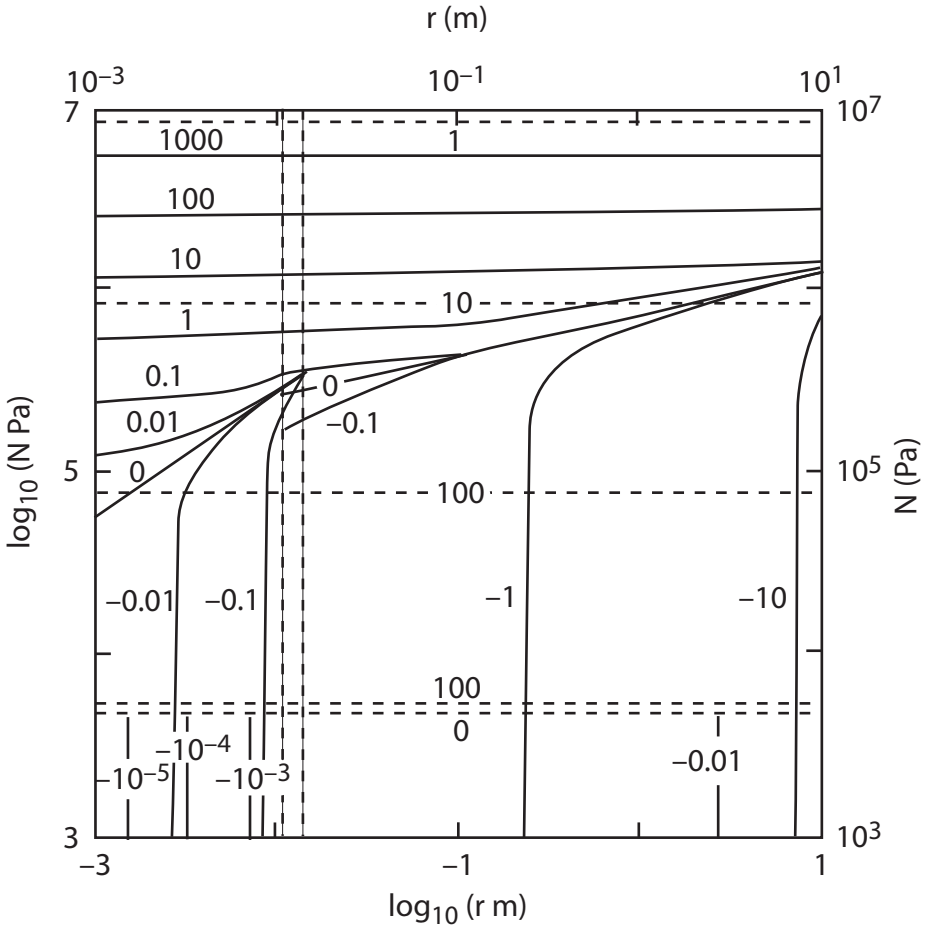

Figure 5.26. Net shrinkage rates ($\dot{r}/r$ in year^{-1}) of R-channels (solid lines) and channels in subglacial sediment (dashed ines) as functions of channel radius r and effective pressure N. The laminar–turbulent transition zone is shown by vertical dashed lines. After Alley (1989).

The water pressure in the water film beneath an ice sheet is of major importance since it affects the sliding speed and hence the dynamics of the ice sheet. Weertman (1972) estimate that an interconnected water film requires an N less than the root-mean-square fluctuation in local ice normal stress on the bed necessary to allow sliding without cavitation. Kamb (1970) provided the following condition for Weertman's estimate

$$N_{max} \leq \frac{\tau_b}{c_1} \tag{5.128}$$

where τ_b is the basal shear stress c_1 is a constant that depends on bed roughness and varies from $1/2$ to $1/9$.

The fraction of the bed f occupied by a water film can expand if the water pressure increases and hence $f \propto 1/N$. Fluctuations in local ice pressure increases with τ_b (Kamb, 1970), which implies that $N \propto \tau_b$. Alley (1989) thus proposes a simple relationship of the form

$$N = \frac{\beta \tau_b}{f} \tag{5.129}$$

where β is a geometric factor as a first approximation to the actual relation.

This relationship can be viewed in the perspective of conditions on an irregular bed. If we consider a unit area of horizontal glacier bed with average normal ice pressure P_i, a single bump occupying a fractional area s and sustaining a vertical stress P_b, and water occupying a fractional area $f = 1 - s$ at pressure P_w. A vertical force balance on the unit area then requires

$$P_b s + P_w(1 - s) = P_i \tag{5.130}$$

or

$$(P_b - P_w)\, s = P_i - P_w \tag{5.131}$$

Since water does not support shear stresses, the average shear stress exerted on the unit area is taken up by the bump with fractional area s, τ_b/s. Thus an excess vertical force acts on the bump which causes ice flow over the bump according to

$$P_b = P_i + \frac{\beta \tau_b}{s} \tag{5.132}$$

where β is the ratio of excess vertical stress to the shear stress on the bump of area s. Combining Equation (5.131) and Equation (5.132) and rearranging yields

$$\beta \tau_b = (P_i - P_w)\,(1 - s) \tag{5.133}$$

and with $N = P_i - P_w$ and $f = 1 - s$ we get Equation (5.129).

Humphrey (1987) showed that the effective pressure becomes constant at $N^\star$ when all low-pressure zones are occupied by water. $N^\star$ is given by

$$N^\star = \beta' \tau_b \tag{5.134}$$

where β' is related to the bed geometry. Humphrey also showed that this is limiting basal shear stress that can be supported by the bed. Depending on the smoothness of the bed, conditions represented by either Equation (5.129) or Equation (5.134) apply. A smooth bed with few irregularities is conducive for producing a linked cavity system as described by Humphrey (1987) through Equation (5.134). A till bed on the other hand will exhibit a wide range of local ice pressures because of the wide range of grain-sizes causing the surface irregularities at the till-ice interface. In such cases Equation (5.129) applies.

Equation (5.129) provides a link between the water system and the velocity from sliding and bed deformation for glaciers with water film drainage. The fractional area covered by water must increase with the average thickness of the water film, $f = f(d)$. Weertman (1972) and Weertman and Birchfield (1982) formulated the water film thickness as

$$d = \left(\frac{12\mu q}{P_g} \right) \tag{5.135}$$

where q is the water flux in $\mathrm{m}^3\,\mathrm{s}^{-1}$ per m width. P_g is measured from conduits or linked cavities, if such are present in other cases

$$P_g = \rho_i g \alpha_s + (\rho_w - \rho_i)\, g \alpha_b \tag{5.136}$$

where α_s and α_b are the surface and bed slopes, respectively.

Alley (1992) extended his 1989 study by investigating co-existence of low-pressure channels and deforming subglacial sediments. Several studies (*e.g.* Engelhardt *et al.*, 1978) have observed deforming sediments in conjunction with low pressure subglacial tunnels. Alley (1992) considers a model as shown in Figure 5.27. Ice with an overburden pressure P_i overlies an h m thick till layer in which a subglacial tunnel with water pressure $P_w < P_i$ is cut down t underlying impermeable bedrock. Alley (1992) models the till layer in three ways: perfectly plastic, linearly viscous, and with a Bingham rheology. The till is characterized by a pseudo-hydrostatic model (Turcotte and Schubert, 1982) in terms of a pressure P and gradients in P. Smaller scale effects such as grain bridging effects and differences between pore-water pressure and clast-contact pressures are thus ignored. Far from the conduit, the subglacial sediment carries the full weight of the overlying ice and $P = P_i$. At the channel $P = P_w$, hence there is a drop in pressure near the channel, $P_i - P_w$ which drives the deformation of the subglacial sediment.

Perfect plasticity. The force causing creep is $F_c = (P_i - P_w)\, h_w$ where h_w is the thickness of the subglacial sediment in contact with the channel. The force acts in the ice flow direction perpendicular to the plane of Figure 5.27. The force resisting creep is $F_r = 2\tau^\star x^\star$ where $\tau^\star$ is the yield strength of the sediment and $x^\star$ is the maximum catchment for sediment creep into the channel. The factor two arises from creep occurring past upper and lower surfaces of the till. By applying a force balance approach and balancing F_r and F_c, we get

$$x^\star = \frac{(P_i - P_w)\, h_w}{2\tau^\star} \tag{5.137}$$

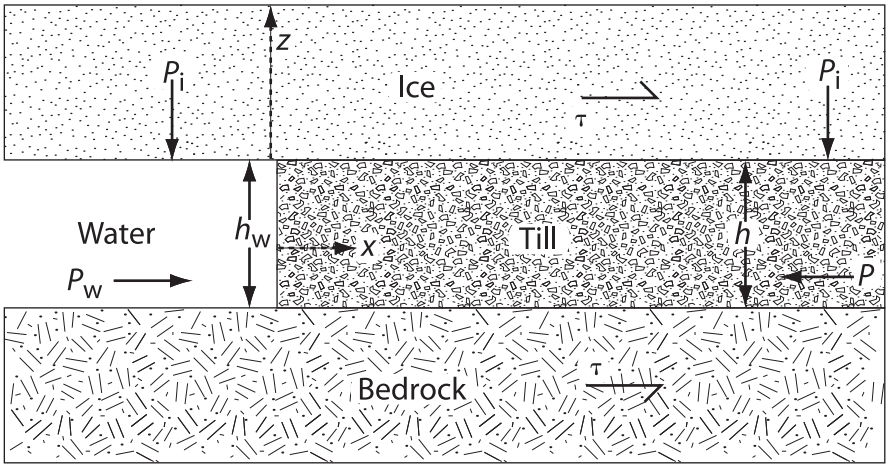

Figure 5.27. The geometry of the model of coexisting low pressure subglacial channels and deforming subglacial sediment. After Alley (1992).

The yield stress can be approximated by a Mohr-Coulomb yield criterion

$$\tau^\star = N \tan\phi + C \tag{5.138}$$

where $\tan\phi$ is the angle of internal friction, C is the cohesion, and N is the difference between the bulk pressure of the sediment and the pore-water in the till, $P - P_p$. In accordance with Boulton *et al.* (1974) and Alley (1989) $C = 4\,\mathrm{kPa}$ and $\tan\phi = 0.2$ for the deforming till.

At the channel ($x = 0$) $N \to 0$ where the boundary condition is $P = P_p = P_w$. Pore water pressures will increase away from the channel to a maximum at the divide between channels but not exceed the Weertman (1972) film value just below P_i. Shoemaker (1986) showed that a low-pressure in typical subglacial sediments will reduce pore-water pressures significantly below the Weertman-film value in a wide zone ($O(10\text{–}100)\,\mathrm{m}$) around the channel and causing $P_p \approx P_w$ near the channel. Alley (1992) shows that this is not necessarily true. P_w probably depends on both ice–water and sediment–water interactions (Walder and Fowler, 1994) but can be approximated by R-channel theory (Röthlisberger, 1972; Weertman, 1972). This assumes that the channel is water-filled and the ice-water interaction controls channel pressure. If channel radius and potential gradients driving channel flow are not too small ($r >\approx 0.1\,\mathrm{m}$, $dP_w/ds >\approx 10\,\mathrm{Pa\,m^{-1}}$) then

$$(P_i - P_w)\tan\phi \gg C \tag{5.139}$$

Combining Equations (5.138) and (5.139) and assuming that N is constant with an average value between the extreme values at $X = 0$ and $x = x^\star$,

$$N = \frac{1}{2}(P_i - P_w) \tag{5.140}$$

we get

$$\tau^\star \approx \frac{1}{2}\left(P_i - P_w\right)\tan\phi \tag{5.141}$$

Inserting Equation (5.141) into Equation (5.137) yields

$$x^\star \approx \frac{h_w}{\tan\phi} \approx 5h_w \tag{5.142}$$

assuming $\tan\phi = 0.2$. This shows that creep cannot occur in a very wide area. Assuming channel heights are of $O(0.1\text{–}1)$ m yields $x^\star \approx 0.05\text{–}5$ m.

The perfectly plastic case assumes the existence of a yield strength but since the till will be deforming pervasively by ice motion the yield strength may be reduced or completely eliminated. This would enlarge the catchment area for creep into the channel significantly to the point of reaching the divide between channels.

Bingham rheology. The Bingham relation for sediment deformation can be written

$$\begin{aligned} \tfrac{\partial u}{\partial z} &= \tfrac{1}{\mu}\left(\tau \pm \tau^\star\right), \quad |\tau| > \tau^\star \\ \tfrac{\partial u}{\partial z} &= 0, \qquad\qquad\quad |\tau| \le \tau^\star \end{aligned} \tag{5.143}$$

where u is the velocity in the x-direction and μ is the Bingham viscosity. The sign in $\tau \pm \tau^\star$ is chosen so that the magnitude of the expression is reduced since sediment deformation slows with increasing yield strength. The pressure gradient in te x-direction must be balanced by a shear stress in the same direction, hence

$$\frac{\partial P}{\partial x} = \frac{\partial \tau}{\partial z} \tag{5.144}$$

Integrating Equation (5.144) with $\tau = 0$ and $z = 0$ yields

$$\tau = z\frac{\partial P}{\partial x} \tag{5.145}$$

Inserting the expression for τ in Equation (5.145) into Equation (5.143) and integrating with a non-slip condition at the upper and lower till boundary ($z = \pm h/2$) yields

$$\begin{aligned} u &= -\tfrac{1}{\mu}\left\{\tfrac{1}{2}\tfrac{\partial P}{\partial x}\left[\left(\tfrac{h}{2}\right)^2 - z^2\right] \pm \tau^\star\left(\tfrac{h}{2} - |z|\right)\right\}, \quad z^\star \le |z| \le \tfrac{h}{2} \\ u &= -\tfrac{1}{\mu}\left\{\tfrac{1}{2}\tfrac{\partial P}{\partial x}\left[\left(\tfrac{h}{2}\right)^2 - z^{\star 2}\right] \pm \tau^\star\left(\tfrac{h}{2} - z^\star\right)\right\}, \quad 0 \le |z| \le z^\star \end{aligned} \tag{5.146}$$

where the sign of $\tau^\star$ is determined by the sign of $\partial P/\partial x$ ($\pm\tau^\star = \mp\partial P/\partial x$). A rigid plug of sediment occurs between $\pm z^\star$

$$z^\star = \left|\tau^\star\left(\frac{\partial P}{\partial x}\right)^{-1}\right| \tag{5.147}$$

The till flux into the channel can be estimated by averaging Equation (5.146)

$$h\bar{u} = -\frac{1}{\mu}\left\{\frac{h^3}{12}\frac{\partial P}{\partial x} \pm \left[\frac{\tau^\star h^2}{4} - \frac{\tau^{\star 3}}{3}\left(\frac{\partial P}{\partial x}\right)^{-2}\right]\right\} \tag{5.148}$$

For an incompressible subglacial sediment, the continuity equation becomes

$$\frac{\partial\left(h\bar{u}\right)}{\partial x} = -\dot{h} \tag{5.149}$$

where $\dot{h}$ is the rate of change in thickness with time. By assuming ice and sediment remain and contact the thinning can be estimated using Walder's (1986) approach of thinning of a cavity containing a low-viscosity fluid

$$-\dot{h} = K_1 h\left(P_i - P\right)^n \tag{5.150}$$

with $n = 3$, the flow law exponent and the constant $K_1 = An^{-n}$ where A is the viscosity factor of the flow law ($A = 1/B$; Equation (4.1)). By differentiating Equation (5.148) with respect to x and combining with Equation (5.149) and solving with $\tau^\star$, μ, K_1, and n assumed independent of x yields

$$\begin{aligned}\left\{h^3 \pm \left[2\tau^\star\left(\frac{\partial P}{\partial x}\right)^{-1}\right]^3\right\}\frac{\partial^2 P}{\partial x^2} &+ \left(3h^2\frac{\partial P}{\partial x} \pm 6\tau^\star h\right)\frac{\partial h}{\partial x} + \\ &+ 12\mu K_1 h\left(P_i - P\right)^n = 0\end{aligned} \tag{5.151}$$

A steady channel with water pressure P_w is introduced to the bed consisting of a deforming sediment of thickness h_0 at $t = 0$ and we require that the sediment is deforming towards the channel while maintaining sediment ice contact. At the sediment creep limit $x^\star$, the sediment pressure must rise to over-burden pressure, the creep must cease at $x^\star$ to maintain ice-sediment contact because the driving stress drops to zero. This leads to the following boundary conditions

$$\begin{aligned} h(x, t=0) &= h_0 \\ P(x=0, t) &= P_w \end{aligned} \tag{5.152}$$

$$\begin{aligned} P(x = x^\star &= P_i \\ \frac{\partial P}{\partial x}\left(x = x^\star, t\right) &= \frac{2\tau^\star}{h} \end{aligned}$$

Here $x^\star$ is time-dependent and determined by the creep and ice-water contact. The system of equations (5.151) and (5.152) can be solved numerically. The second condition in Equation (5.152) enables us to integrate Equation (5.150) to

$$\begin{aligned} h(x=0) &= h_0 \exp\left(-\tfrac{t}{\theta}\right) \\ \tfrac{1}{\theta} &\equiv K_1\left(P_i - P_w\right)^n \end{aligned} \tag{5.153}$$

Table 5.4: *Response times and rates of till supply per unit length of channel for different assumed parameter values. After Alley (1992).*

Channel radius	Potential gradient	Pressure drop	Response time	Sediment thickness	Sediment viscosity	Initial sediment supply
r	Φ	$P_i - P_w$	θ	h_0	μ	
m	Pa m^{-1}	Pa	year	m	Pa s	m^3 year^{-1} m^{-1}
1	20	7.8×10^5	0.33	1	10^{10}	3.7
1	20	7.8×10^5	0.33	1	10^{12}	1.5
1	1000	5.5×10^6	9.5×10^{-4}	1	10^{10}	709
1	1000	5.5×10^6	9.5×10^{-4}	1	10^{12}	90
0.1	20	4.6×10^5	1.6	0.1	10^{10}	0.0077
0.1	20	4.6×10^5	1.6	0.1	10^{12}	0.0043
0.1	1000	3.2×10^6	4.8×10^{-3}	0.1	10^{10}	1.9
0.1	1000	3.2×10^5	4.8×10^{-3}	0.1	10^{12}	0.46

Alley (1992) tested several combinations of realistic values for the variables in the model, results are summarized in Table 5.4, from which the following results are obtained:

1. A decrease in sediment viscosity as well as an increase in sediment thickness increases the initial rate of sediment supply to the channel

2. Sediment thinning is fastest adjacent to the channel

3. The maximum rate of till supply to the channel occurs at $t = 0$

4. Given sediment properties, lowering channel water pressure increases the driving stress for creep and hence the rate of sediment supply

5. The maximum distance $x^\star$ from which creep can occur increases with time because the fastest thinning occurs at the channel. The pressure gradient driving sediment creep must steepen to force sediment through the thinning layer at the channel

6. Results are only weakly sensitive to the assumed sediment yield strength for assumed sediment viscosities

In conclusion the model provided by Alley (1992) shows that low-pressure channels and deforming subglacial sediments can coexist. The key lies in that channels quickly can become isolated from their surrounding through removal and thinning of the sediment layer near the channel. Once the sediment layer is pinched out, the channel is equivalent to a Röthlisberger-channel with ice walls and a stable bed of bedrock or gravel lag. These results seem robust.

Walder and Fowler (1994) developed a model that differs from that of Shoemaker (1986) in that it is located at the ice-till interface and hence have large but not

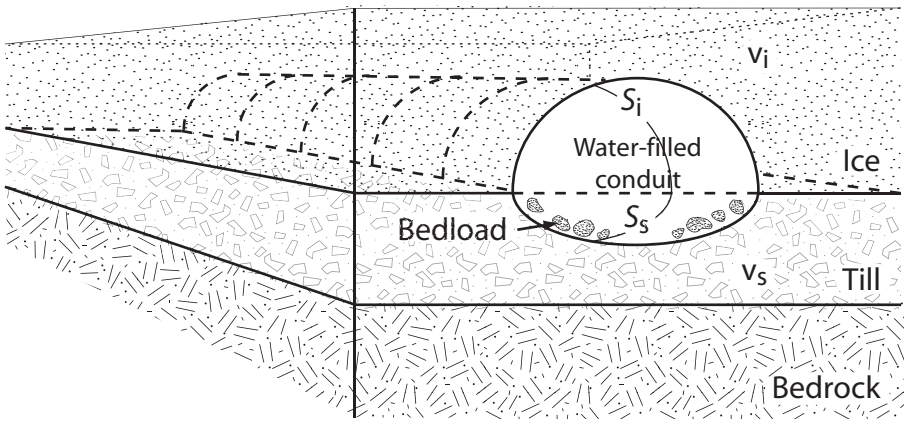

Figure 5.28. A conduit located at the ice-till interface at the bed of a glacier. After Walder and Fowler (1994).

necessarily equal fractions of the cross-sectional circumference in both till and ice (Figure 5.28). In this system $P_i > P_c$, where P_i is the ice overburden pressure and P_c is the water pressure in the conduit. In the channel the effective channel pressure is given by $N_c = P_i - P_c$ and the pore water pressure in the till away from the channel can be described by the effective pressure $N_e = P_i - P_w$. The conduit will remain open by a balance between creep closure and melt-back from viscous dissipation of heat. However, the till will also creep, having a typical yield stress of ~ 50 kPa. Since the basal shear stress typically exceeds this value, creep of till into the conduit is likely to occur in most places beneath the glacier and can only be counteracted by erosion and transport of sediments.

The closure rate of a tunnel is given by

$$\frac{1}{R}\frac{dR}{dt} = -\frac{A_1}{2}\left(\frac{P_i - P_c}{n}\right)^n \tag{5.154}$$

where R is the tunnel radius, and A_i and n are the constants in Glens flow law for ice (Equation (4.1); Nye, 1953). The deformation of till has been investigated by Boulton and Hindmarsh (1987) who suggested a flow law of the form

$$\dot{\varepsilon} = A_s \tau^a {N_e}^{-b} \tag{5.155}$$

where $\dot{\varepsilon}$ is the shear strain rate, τ is the shear stress, N_e is the effective pressure as defined above, and A_s, a, and b are positive empirical constants. Studies by *e.g.* Kamb (1991), Blake (1992) and Iverson *et al.* (1995) have questioned this relationship which is based on only seven measurements. However, lacking a general law for till deformation, Walder and Fowler's approach using Boulton and Hindmarsh's (1987) flow law will continue to apply since it captures the idea that deformation rate is inversely dependent of the effective pressure.

Boulton and Hindmarsh (1987) argued that the creep closure rate of a canal in till can be approximated by

$$\frac{\dot{R}}{R} \sim \frac{-A_s {N_e}^{a-b}}{a^a} \tag{5.156}$$

where $N_c = N_e$ ($P_c = P_w$). By inserting Boulton and Hindmarsh (1987) values for $a = 1.33 < b = 1.8$, Equation (5.156) indicates that sediment creep is most effective at low N_c.

Fowler and Walder (1993) solved the Nye (1953) borehole closure problem for a saturated, deformable till. The closure rate depends on the dimensionless permeability parameter Λ where $10^{-6} < \Lambda < 1$ for a permeability range 10^{-19}–10^{-13} m^2 and an apparent till viscosity of 10^9 Pa s^{-1} (*e.g.* Blake and Clarke, 1989; Blake, 1992; Humphrey *et al.*, 1993). Since for most tills $\Lambda \ll 1$ Equation (5.154) can be generalized to

$$\frac{1}{R}\frac{dR}{dt} = -\frac{1}{2} A_s \left(\frac{N_c}{a}\right)^a {N_e}^{-b} \tag{5.157}$$

under the condition

$$\Delta P_w = P_w - P_c \leq (a-1)\, N_e \tag{5.158}$$

If the condition in Equation (5.158) is not met, conditions near the the hole are probably conducive to piping associated with locally enhanced bulk permeability. This is similar to bank failure which occurs during falling stages following flood events in regular rivers. Fowler and Walder (1993) showed that Equation (5.157) is a reasonable approximation even when considering the failed zone around a bore hole when condition Equation (5.158) is not met. Hence, Walder and Fowler (1994) use Equation (5.157) for their continued analysis.

Walder and Fowler (1994) applied Shoemaker's (1986) analysis of waterway spacing which assumes that $P_w > P_c$ and hence that water generated under the ice is drawn towards conduits. There are several criteria for initiating conduits and Walder and Fowler (1994) suggest that conduit spacing should be self-adjustable so that the edge of the conduits are marginally stable against piping. This means that $N_c = aN_e$ (from Equation (5.158)). If conduits were closer, piping would occur drawing down pore pressure at the drainage divide until the condition was again met. Equation (5.157) then reduces to

$$\frac{1}{R}\frac{dR}{dt} = -\frac{1}{2} A_s \left(\frac{N_c}{a}\right)^{a-b} \tag{5.159}$$

To handle the sediment balance in the channel, Walder and Fowler (1994) resort to applying some rough estimates based on theory from alluvial channels in non-cohesive sediments. Erosion in a channel will only occur if the shear stress τ imposed by the flowing water exceeds a critical threshold τ_c. The value of τ_c is a function of the grain size D_s for sorted sediments. Transport occurs either as bed or suspended load, depending on the size relative to the force of the flowing water. Walder and Fowler (1994) use the Meyer-Peter and Müller (1948) equation to describe the bed

load transport rate Q_b

$$Q_b = \frac{K\rho_s l_s}{{\rho_w}^{1/2} g\Delta\rho}(\tau - \tau_c)_+^{3/2} \tag{5.160}$$

where $(\tau - \tau_c)_+ = \max(\tau - \tau_c, 0)$, K is a constant (≈ 10), ρ_s is the density of the sediment, l_s is the width of the stream bed, g is the gravitational acceleration, ρ_w is the density of water and $\Delta\rho = \rho_s - \rho_w$. In glacial rivers, sediments can be described as a mixture of sand and gravel-sized clasts which enables us to apply an "equal mobility" condition, where all grains starts to move under roughly similar stresses

$$\tau_{\approx}\bar{\mu} g\Delta\rho D_{50} \tag{5.161}$$

(Parker *et al.*, 1982) where $\bar{\mu} \approx 0.05$ is a dimensionless empirical constant and D_{50} is the median grain size. For suspendable sediments erosion rates are harder to estimate because the general theories (*e.g.* Richards, 1982) involve a local steady state where erosion rates $\dot{E}$ equal deposition rates $\dot{D}$. However $\dot{E}$ may be prescribed as a boundary condition on the concentration profile and Parker (1978a) proposed that erosion rates may be given by

$$\dot{E} = K_1 v_s \left(\frac{\tau - \tau_c}{g\Delta\rho D_s}\right)^{3/2} \tag{5.162}$$

and that the deposition rate is given by

$$\dot{D} = K_2 v_s \bar{c} \left(\frac{g\Delta\rho D_s s}{\tau}\right)^{1/2} \tag{5.163}$$

where $\bar{c}$ is the depth averaged suspended sediment concentration and $K_2 \approx 6$. the net erosion rate of suspended sediment is then

$$\dot{m}_s = \rho_{ss}\left(\dot{E} - \dot{D}\right)_+ \tag{5.164}$$

Subglacial channels incised into subglacial sediments differ from alluvial channels in one respect. Alluvial channels maintain their cross-section if there is no net erosion of the banks (Parker, 1978a,b). Subglacial channels maintain such a cross-section only if erosion balances the creep of sediment into the channel. Hence we can write Equation (5.178) for a silt-sand type channel in terms of the cross-sectional averages, denoted by $\langle\ \rangle$

$$\langle\dot{E}\rangle = \langle\dot{D}\rangle + \frac{\langle\dot{m}_s\rangle}{\rho_s l_s} \tag{5.165}$$

For a gravel-type channel $\tau > \tau_c$ on the banks and will be just enough to erode the banks and erode the influx of creeping till at an appropriate rate. Parker's (1978a; 1978b) analysis of equilibrium stream channels does not strictly apply to subglacial channels but the processes described by Parker should apply and hence yield channels with high aspect ratio.

To describe the subglacial channel we first define the total cross-sectional area S as the sum of the areas bounded by either ice S_i or sediment S_s

$$S = S_i + S_s \tag{5.166}$$

The flow in the conduit is based on the equations put forward by Röthlisberger (1972), Nye (1976), Spring and Hutter (1981) and Lliboutry (1983) but must be augmented by a prescription of sediment creep, erosion and transport. Walder and Fowler (1994) assumes homogeneous flow, that sediment and water travel with the same speed. Conservation of mass yields, for water,

$$\frac{\partial}{\partial t}\left[\rho_w\left(1-\alpha_s\right)S\right] + \frac{\partial}{\partial s}\left[\rho_w\left(1-\alpha_s\right)Su\right] = \dot{m}_i + \dot{M}_w \tag{5.167}$$

and for sediment

$$\frac{\partial}{\partial t}\left(\bar{c}S\right) + \frac{\partial}{\partial s}\left(Q_s + Q_b\right) = \dot{m}_S + \dot{M}_s \tag{5.168}$$

where $\dot{m}_i$ is the ice melt, $\dot{M}_w$ and $\dot{M}_s$ are the water supply rate due to flow from tributaries, moulins or veins, $\alpha_s = \bar{c}/\rho_s$ is the volume fraction of suspended sediment and

$$Q_s = \bar{c}uS \tag{5.169}$$

is the suspended sediment flux where u is the mean flow rate.

The kinematics of conduit closure can be described by using Equation (5.154) and Equation (5.159) as

$$\frac{\partial S_i}{\partial t} = \frac{\dot{m}_i}{\rho_i} - K_i {l_i}^2 A_i \left(\frac{N_c}{n}\right)^n \tag{5.170}$$

and

$$\frac{\partial S_s}{\partial t} = \frac{\dot{m}_s}{\rho_s} - K_s {l_s}^2 A_s \left(\frac{N_c}{n}\right)^{a-b} \tag{5.171}$$

where K_i and K_s are $O(1)$ shape factors reflecting the difference between an idealized cylindrical conduit and the general case reflected by Figure 5.28. If conduits are cylindrical $S_i \sim {l_i}^2$ and $S_s \sim {l_s}^2$ and the creep closure rate $dS/dt \sim S$. For a wide flat channel (*c.f.* Hooke *et al.*, 1990) with height h and width $l \gg h$, $dh/dt \sim l$ and $dS/dt \sim l^2$. The approximations are hence reasonable.

The momentum balance for the flow can be replaced by a force balance between pressure forces and drag on the channel walls by neglecting inertial forces

$$S\left(\rho_w g \sin\theta - \frac{\partial P_c}{\partial s}\right) = \tau l \tag{5.172}$$

where $\sin\theta$ is the bed slope and $l_s = l - l_i$ is the channel perimeter. If the flow is turbulent, the average wall shear stress is

$$\tau = \frac{1}{8} f_R \rho_w u^2 \tag{5.173}$$

where the dimensionless friction factor f_R is weakly dependent on the Reynolds number (~ 0.1 for subaerial streams). The average shear stress over the sediment bed τ_s may differ from τ but they are assumed to be the same which is reasonable for pressurized flow but not so for open-channel flow.

The energy equation can be written

$$\rho_w c_p \left[\frac{\partial}{\partial t} (ST) + \frac{\partial}{\partial s} (SuT) \right] = \tau u l - l_i h_T \Delta T \tag{5.174}$$

where c_p is the specific heat, T is temperature, ΔT is the temperature drop across a thermal boundary layer at the ice wall and h_T is the heat transfer coefficient. The temperature is related to the ice at the pressure melting point

$$T = \Delta T - c_t P_c \tag{5.175}$$

where c_t is the change in melting temperature with pressure and ΔT is the temperature drop across the ice water interface. The heat transfer across this boundary, ignoring any temperature gradients in the ice, is given by

$$l_i h_T \Delta T = \dot{m}_i L \tag{5.176}$$

where L is the latent heat.

Equations (5.167), (5.168), (5.170)–(5.172) and (5.174) constitute a system of differential equations for the variables $\bar{c}$, S_i, S_s, u, P_c, and T. (5.160), (5.163), (5.166), (5.169), (5.173), (5.175) and (5.176) are algebraic expressions determining Q_b, $\dot{m}_s$, S, Q_s, τ, ΔT, and $\dot{m}_i$.

The model constituting the list of equations above are used to determine the effective channel pressure defined as $N_e = P_i - P_w$. Walder and Fowler (1994) consider only a steady state situation where the water flux Q is determined by integrating Equation (5.178) and determining the effective pressure from the expression for Q. The steady state situation is probably valid for average conditions but will not be valid for, say diurnal variations in water flow.

At a steady state Equation (5.170) and Equation (5.171) yield

$$\dot{m}_i = \rho_i K_i {l_i}^2 A_i \left(N_c / n \right)^n \tag{5.177}$$

and

$$\dot{m}_s = \rho_s K_s {l_s}^2 A_s \left(N_c / a \right)^{a-b} \tag{5.178}$$

yielding a relative ice to till creep rate of

$$\frac{\dot{m}_i}{\dot{m}_s} = \left(\frac{N_c}{\tilde{P}} \right)^{n+b-a} \tag{5.179}$$

where

$$\tilde{P} = \left(\frac{\rho_s K_s {l_s}^2 A_s n^n}{\rho_i K_i {l_i}^2 A_i a^{a-b}} \right)^{1/(n+b-a)} \tag{5.180}$$

By assuming $K_i \approx K_s$ and $l_i \approx l_s$ and inserting $\rho_i = 900$ kgm^{-3}, $\rho_s = 2650$ kgm^{-3}, $A_i = 7.36 \times 10^{-5}$ Pa^{-3}s^{-1}, $n = 3$, $A_s = 3 \times 10^{-5}$ Pa^{a-b} s^{-1}, $a = 1.33$, and $b = 1.8$ we obtain

$$\tilde{P} \approx 8 \text{ bar} \tag{5.181}$$

This indicates that till creep is larger than ice creep for $N_c < \tilde{P}$ whereas the opposite is true for $N_c > \tilde{P}$ and hence we have two end cases where either process is dominating.

To proceed Walder and Fowler (1994) assumes a non-slip boundary condition between the ice and the till. This implies that as the conduit closes, ice and sediment flow towards the conduit with the same speed. It is thus possible to approximate the creep rates as

$$\dot{m}_k \approx \rho_k V_k l_k \sin\theta_k \tag{5.182}$$

where $k = i, s$ and θ_k is the angle of the ice roof or till floor to the horizontal. We then get

$$\frac{\dot{m}_i}{\dot{m}_s} \approx \frac{\rho_i l_i \sin\theta_i}{\rho_s l_s \sin\theta_s} \tag{5.183}$$

and the two extreme cases $\dot{m}_i/\dot{m}_s \gg 1$ and $\dot{m}_i/\dot{m}_s \ll 1$ corresponding to $\theta_i/\theta_s \gg 1$ and $\theta_i/\theta_s \ll 1$ which correspond to level-floored ice tunnels and level-roofed till channels respectively. This mean that if $N_c > \tilde{P}$ the conduit is essentially a Röthlisberger channel with a stiff till floor and if $N_c < \tilde{P}$ the conduit will be a Nye-type channel cut into the till with a stiff ice roof.

To solve the equation we can make several simplifications. First, $c \ll \rho_s \Rightarrow \alpha_s \ll 1$and the volume flux $Q = Su$ is determined from Equation (5.167). Equation (5.177) shows that melting from frictional dissipation is small and probably negligible in most circumstances and that water fluxes $Q(s)$ will be determined by surface derived fluxes and that $Q(s)$ therefore is a prescribed function. The energy equation (Equation (5.174)) can be rewritten using Equations (5.175) and (5.176) as

$$\frac{\partial}{\partial s}\left[Q\left(\frac{\dot{m}_i}{\kappa_w \text{Nu}} - \gamma\frac{P_c}{L}\right)\right] = -\dot{m}_i + \frac{\tau u l}{L} \tag{5.184}$$

where $\gamma = \rho_w c_p c_t \approx 0.32$ (Röthlisberger, 1972), $\kappa_w = k_w/\rho_w c_p$is the thermal conductivity and $\text{Nu} = h_T l_i/k_w$ is the dimensionless Nusselt number which concerns heat transfer at the ice-water interface.

Equations (5.172), (5.173), (5.177), (5.184), and

$$Su = Q \tag{5.185}$$

allows us to determine S, u, τ, P_c, and $\dot{m}_i$, given l_i and l_s, and can be combined to a single non-linear differential equation for P_c. However, it is possible to simplify the problem by making two approximations. First, $N_c = P_i - P_c$ and $P_i = \rho_i g d$, where d is ice depth, which results in

$$\rho_w g \sin\theta - \frac{\partial P_c}{\partial s} = (\rho_w - \rho_i)\, g \sin\theta + \rho_i g \cos\theta \tan\alpha + \frac{\partial N_c}{\partial s} \tag{5.186}$$

where α is the ice surface slope (Weertman, 1972). For a slowly varying bedrock slope $\partial N_c/\partial s$ will be negligible. As an example, we can study what effects significant bedrock slope changes occur over a length l_f of a flow line of an ice sheet.

$$\frac{\partial N_c/\partial s}{\rho_i g \sin\alpha} \approx \frac{\Delta N_c}{P_i} \frac{d}{l_f \sin\alpha} \tag{5.187}$$

where ΔN_c is the variation of N_c. For an alpine glacier $\delta N_c < P_c$ so that $\partial N_c/\partial s$ can be neglected if $l_f \gg d/\sin\alpha \sim 1$ which corresponds to ~ 10 ice thicknesses. For an ice sheet $l_f \gg d/\sin\alpha \sim 1$. The hydraulic gradient can also be approximated without introducing large errors as

$$\rho_w g \sin\theta - \frac{\partial P_c}{\partial s} = \rho_i g \sin\theta \tag{5.188}$$

A second simplification to solving the system of equations results from Equation (5.184). $Q/\kappa_w \mathrm{Nu}$ is dimensionally a length over which $\dot{m}_i$ relaxes to its equilibrium value. Inserting $Q = 1\ \mathrm{m^3\,s^{-1}}$, $\kappa_w = 10^{-6}\ \mathrm{m^2\,s^{-1}}$, $\mathrm{Nu} \approx 0.1\mathrm{Re}^{0.8}$ (Spring and Hutter, 1981), $\mathrm{Re} \approx 10^6$, assuming $u = 1\ \mathrm{m\,s^{-1}}$and $l = 1$ m, we obtain $Q/\kappa_w \mathrm{Nu} \approx 10^2$ m which implies that the derivative of $\dot{m}_i$ is negligible everywhere. We can thus rewrite the second l.h.s. term in Equation (5.184) as

$$\frac{\partial}{\partial s}\left(-\frac{\gamma P_c Q}{L}\right) = -\frac{\gamma}{L}\left(Q\frac{\partial P_c}{\partial s} + P_c \frac{\partial Q}{\partial s}\right) \tag{5.189}$$

In line with our previous approximation $\partial N_c/\partial s \ll \partial P_i/\partial s$ so that by setting $P_c = P_i - N_c$

$$\frac{\partial}{\partial s}\left(P_c Q\right) \approx \frac{\partial}{\partial s}\left(P_i Q\right) - N_c \frac{\partial Q}{\partial s} \tag{5.190}$$

We can thus rewrite Equation (5.184) as

$$\dot{m}_i \approx \frac{\tau u l}{L} + \frac{\gamma}{L}\left[\frac{\partial}{\partial s}\left(P_i Q\right) - N_c \frac{\partial Q}{\partial s}\right] \tag{5.191}$$

which provides us with a series of algebraic equations to find N_c since both P_i and Q are prescribed functions of s. It is possible to estimate the contribution of the bracketed term in Equation (5.191) to 0.1–0.3 that of $\tau u l/L$ and hence it is possible to neglect it.

In summary the model consists of five algebraic equations

$$\begin{aligned}
\dot{m}_i &= \frac{\tau u l}{L} \\
S\rho_i g \sin\alpha &= \tau l \\
\tau &= \frac{1}{8} f_R \rho_w u^2 \\
\dot{m}_i &= \rho_i K_i {l_i}^2 A_i \left(\frac{N_c}{n}\right)^n \\
Q &= Su
\end{aligned} \tag{5.192}$$

By setting $l_i \approx$ l we get

$$\begin{aligned} l^2 {N_c}^n &= b_2 Q \\ \tau &= B_1 \left(\frac{S}{l}\right)^{1/2} \\ u &= {b_3}^{1/3} \left(\frac{S}{l}\right)^{1/2} \\ \frac{S^3}{l^5} &= \frac{{N_c}^{2n}}{{b_2}^2 b3} \end{aligned} \tag{5.193}$$

where

$$\begin{aligned} b_1 &= \rho_i g \sin\alpha \\ b_2 &= \frac{n^n b_1}{\rho_i L K_i A_i} \\ b_3 &= \frac{8 b_1}{f_R \rho_w} \end{aligned} \tag{5.194}$$

To determine N_c in terms of Q we must prescribe l in terms of S which implies that conduit shape becomes important. We will now look at the two cases $N_c > \tilde{P}$, channel drainage, and $N_c < \tilde{P}$, canal drainage.

Channel drainage. When $N_c > \tilde{P}$ the tunnel resembles a Röthlisberger tunnel and protrudes into the ice. We expect a semicircular cross-section and can prescribe

$$S \approx l^2 \tag{5.195}$$

Equation (5.193) then becomes

$$Q \approx \frac{{N_c}^{5n}}{{b_2}^5 {b_3}^2} \tag{5.196}$$

This equation shows that as Q increases, N_c and thus also P_c decreases which is consistent with an arborescent network of channels. Since the dependence of N_c on Q is weak Q can be approximated by a constant in order to calculate N_c

Canal drainage. When $N_c < \tilde{P}$ then the tunnel resembles a Nye-type canal, incised into the subglacial sediment and hence the processes of erosion and transport of sediment become important. Such canals are expected to be broad and shallow which implies that Equation (5.195) does not apply, instead

$$S \approx hl \tag{5.197}$$

where h is the canal depth, which depends on the nature of the stream bed and thus can be prescribed in different ways. From Equation (5.193) we get

$$Q \approx \frac{b_2 b_3 h^3}{{N_c}^n} \tag{5.198}$$

This result is radically different from that for Röthlisberger channels since N_c increases as Q increases. Such behavior is consistent with a distributed system such as that for linked cavity system (Walder, 1986; Fowler, 1987b; Kamb, 1987).

Based on the Equations (5.192)–(5.194), we can numerically estimate conditions in the channels. Coefficients b_1, b_2, and b_3 depend only on the surface slope and by using $n = 3$ we get

$$\begin{aligned} b_1 &\approx 9 \times 10^3 \sin\alpha \,\mathrm{Pa\,m^{-1}} \\ b_2 &\approx 1.1 \times 10^{20} \sin\alpha \,\mathrm{Pa\,s\,m^{-1}} \\ b_3 &\approx 6 \times 10^2 \mathrm{m\,s^{-2}} \end{aligned} \tag{5.199}$$

When $N_c > \tilde{P}$ Röthlisberger channels exist and Equation (5.196) can be expressed numerically as

$$[Q] \approx 2 \times 10^{-31} \frac{[N_c]^{15}}{\sin^7 \alpha} \tag{5.200}$$

where $Q = [Q]$ $\mathrm{m^3\,s^{-1}}$and $N_c = [N_c]$ bar ($[x]$ denoted the magnitude of x). By inverting Equation (5.200) we obtain

$$[N_c] \approx 1.1 \times 10^2 [Q]^{1/15} (\sin\alpha)^{7/15} \tag{5.201}$$

Inserting $\sin\alpha = 0.1$ and $[Q] = 1$ we obtain $[N_c] \approx 38$, for $\sin\alpha = 0.001$, $[N_c] \approx 4$. This implies that for valley glaciers $N_c > \tilde{P}$ but that this is not generally true for ice sheets. Hence Rötlisberger channels are less likely to exist beneath ice sheets and ice streams where these are underlain by deforming sediments.

If we assume that $N_c < \tilde{P}$ then Equation (5.198) becomes

$$[Q] \approx 6.2 \times 10^7 \frac{^3 \sin^2 \alpha}{[N_c]^3} \tag{5.202}$$

where $h =$ m. Inserting $[Q] = 1$ and $\sin\alpha = 0.1$ we get $[N_c] = 85$; for $\sin\alpha = 0.001$ $[N_c] = 4$. This implies that canals in subglacial sediments can only exist with depths of cm-scale in valley glaciers whereas they can be up to 2 m beneath ice sheets.

No experimental data exist to elucidate how subglacial canals would be configured on a till bed. However, we can gain an appreciation by investigating conditions valid for other materials. Gravel bed rivers are generally wide and shallow and adjust their shape so that the average bed shear stress is roughly equal to the critical shear stress for bed load transport. By combining Equations (5.161) (5.193) (5.197) we obtain

$$h \approx \frac{\tau_c}{b_1} \approx \frac{\bar{\mu} \Delta \rho D_{50}}{\rho_i \sin\alpha} \tag{5.203}$$

Because the subglacial channel also needs to handle a net input of sediment by creep the shear stress needs to be higher than otherwise. Equation (5.203) yields $h/D_{50} = O(1)$ for $\sin\alpha \sim 0.1$ (valley glaciers) and $h/D_{50} = O(10^2)$ for $\sin\alpha \sim 0.001$ (ice sheets).

For sandy silty river beds channels are also expected to be broad and shallow. Parker (1978a) analyzed sand-silt bedded streams and established

$$h = 85 \left(\frac{R_f}{\sin \alpha} \right)^{1/2} D_s \tag{5.204}$$

where $D_s = D_{15}$ is the "characteristic" size of suspended grains, R_f is a dimensionless parameter that depends on grain size and is of $O(10^{-1})$ for sand and silt. This yields $h/D_s \sim 10^2$ for $\sin \alpha = 0.1$ and $h/D_s \sim 10^3$ for $\sin \alpha = 0.001$

Sediments containing clay attain cohesive properties when the clay content exceeds $\sim 10\%$ (Skempton, 1964). Therefore it is likely that clay rich materials can maintain steeper banks and it is thus possible that the dimension of subglacial canals in clay may be similar to Röthlisberger-type channels, *i.e.* $S \approx l^2$.

Typical tills or glacier diamictons are very poorly sorted sediments where the larger clasts are matrix supported. The clay content may vary depending on the parent material but most Swedish tills do typically not have cohesive properties. Hence steep banks could occur if the clay content is favorable. However, the constant flow of poorly sorted material towards the canal and the erosion of primarily finer particles will leave a lag to form the stream bed and hence lead to broad shallow channels. Estimating h for till channels remains difficult and results are ambiguous. For gravelly tills with $D_s \sim 0.01$ m we get $0.01 < h < 1$ m and for sandy-silty till with $D_s \sim 0.0001$ m, $0.01 < h < 0.1$ m.

In all theoretical and field based studies on water flow on or in sediment beds, very little consideration is given to the sediments themselves. This is probably due to that each author bases their study on conditions found at one glacier of particular interest. The studies are therefore sometimes difficult to compare in detail. The picture, however, is clear in that water flow through channels on till beds and their configuration are intimately coupled to the till properties.

6. Melting at the base of a glacier

So far this report has concerned water generated by either melting of the surface ice and snow or by rainfall on the glacier surface and how such water is routed through a drainage system through the glacier. This type of system is gravity driven and characterized by atmospheric pressure both where water is generated and where water exists the glacier. Pressures and pressure gradients are mainly built up by the hydraulic properties of the drainage system. This, however, is not the only type of drainage that occurs in the glacier system. Water can also be generated in and under the glacier. This part of water generation in a glacier or ice sheet is often ignored or assumed negligible for most purposes. Typical melt rates on a glacier surface may be on the order of meters per year, liquid precipitation may be on the order of several decimeters to meters per year. Water generated by melting at the base of glaciers is typically on the order of centimeters or 1/100th or less of that of the surface processes. Melting within a glacier may be even less.

The water supplied by sub- and englacial melting may be negligible in terms of rates when compared to the surface components melt and rain. Whereas the surface components undergo seasonal variations, subglacial melting is more stable through time. Basal melt rates may change if the dynamics of the ice changes since a change in deformation rate also causes an associated change in internal heat production in the ice; frictional heating may also change if the ice is sliding. Furthermore, the subglacial melting may occur over very large areas and the volumes produced are obviously related to the area of such melt. On regular glaciers the volumes are small since glaciers are small. Under ice sheets, however, the sheer magnitude of potentially melting area yields significant volumes of water. There is, hence, reason to also consider the processes responsible for sub- and englacial melt.

6.1 Melting from geothermal heat

Glaciers and ice sheets experience melting of basal ice where the basal ice temperature is at the pressure melting point. Heat for this melting can be added from geothermal heat flow and from the internal deformation of basal ice. The thermodynamic situation at the base of an ice sheet is determined by the thermal properties of ice. Energy can be transferred by diffusion along a temperature gradient in ice as in all materials. However, the solidus of the ice-water vapor phase space has a negative slope, which means that the melting or freezing temperature is depressed

with increasing pressure by 0.09 K Pa^{-1}.

As a general statement, freezing of liquid water occurs when temperature and pressure satisfies the generalized Clapeyron equation (*e.g.* O'Neill and Miller, 1985):

$$\frac{P_w}{\rho_w} - \frac{P_i}{\rho_i} = \frac{L}{273.15}T + \frac{P_O}{\rho_w} \tag{6.1}$$

where P_w is the water pressure, ρ_w is the density of water, P_i is the ice pressure, ρ_i is the density of ice, L is the coefficient of latent heat of fusion, T is the temperature in degrees centigrade, and P_O is the osmotic pressure. Equation (6.1) couples the effect of temperature and pressure. It is a general thermodynamic relationship not specific for the case of ice sheets and glaciers. The phase change of the ice-water system is not only controlled by temperature and pressure as often described. Two other factors may be of importance; 1) the presence of solutes in water, and 2) surface tension arising from interface curvature. Just as in the case with an increasing pressure, an increase in solutes in liquid water also depresses the melting/freezing point. This effect may be referred to as the osmotic pressure (*e.g.* Padilla and Villeneuve, 1992), and it is included in Equation (6.1). If liquid water is present at the base of ice sheet, and it contains solutes, this will together with the pressure modify the melting point.

The second factor constitute an ice/water interfacial effect. It is especially important when ice crystals are growing in within micro-sized pores, such as within different types of subglacial sediments (*e.g.* Tulaczyk, 1999). The finer grains sediment has, the higher the curvature of the ice-water interface becomes, which in turn lowers the melting point (Hohmann, 1997). For example, in clays, liquid water has been observed at temperatures down to −10 °C (O'Neill and Miller, 1985).

If the effect of phase curvature is taken into consideration, the Clapeyron equation may be modified to (Raymond and Harrison, 1975),

$$T = -\frac{273.15}{L}\left(\frac{1}{\rho_i} - \frac{1}{\rho_w}\right)P_w - \frac{273.15\sigma_{I-W}}{L\rho_i R_p} - \frac{273.75}{\rho_w L}P_O \tag{6.2}$$

where σ_{I-W} is the ice-water surface energy, and R_p is the characteristic particle radius. Equation (6.2) is the fundamental equation for the ice water phase transition given by Hooke (2005). In this equation, the first of the three terms describes the effect of water pressure on the ice water phase transition, the second term describes the effect of interfacial pressure, and the third term the effect of osmotic pressure. Equation (6.2) thus give the complete treatment of the ice-water phase transition. Commonly only the first term is used for calculations of the pressure melting point beneath glaciers and ice sheets. Sometimes it is rewritten in glaciological literature to give a simplified expression for calculations of the pressure melting point (*e.g.* Remy and Minster, 1993),

$$T_{pmp} = \frac{H}{1503} \tag{6.3}$$

where T_{pmp} (°C) is the pressure melting point temperature, and H is the ice thickness. The effect of the lowering of the pressure melting point described above is, in

the case of an ice sheet, that the melting point is lowered by ~ 2 K beneath 3 km of ice. This is very important, since the basal conditions change drastically if the bed of an ice sheet becomes melted or frozen. It affects ice sheet flow by turning on and off basal sliding, governs if glacial efficiently can take place or not, and of course have a profound impact on basal hydrology.

In a glacier with either entirely cold ice (frozen to its bed) or just reaching the melting point at the bed, all geothermal heat is transferred through the glacier by the temperature gradient in the ice (Figure 6.2a). The basal temperature of an glacier is determined by the general heat equation (considering incompressible ice)

$$\kappa \left(\frac{\partial^2 \theta}{\partial x^2} + \frac{\partial^2 \theta}{\partial y^2} + \frac{\partial^2 \theta}{\partial z^2} \right) - u \frac{\partial \theta}{\partial x} + v \frac{\partial \theta}{\partial y} + w \frac{\partial \theta}{\partial z} + \frac{Q}{\rho C} = 0 \tag{6.4}$$

where θ is the temperature, κ is the thermal diffusivity, ρ_I is the density of ice, C is the heat capacity of ice, Q is the change in heat from *e.g.* internal deformation, u, v, and w are the velocity components in the x, y, and z-directions, respectively. The temperature in the ice is hence determined by both diffusion and convection, where the diffusion is the transfer of the geothermal heat, heat generated at the base from friction and heat from internal friction during flow deformation along the resulting temperature gradient, and the convection is the flow of ice with different temperature through the general flow of the glacier. A typical temperature profile based on data from the Camp Century drill site (*e.g.* Hooke, 2005) can be seen in Figure 6.1.

If ice at the base is at the pressure melting point, the actual temperature will be increasing upwards in the temperate ice due to the change in pressure melting point (Figure 6.2b). Since heat conduction can only occur from higher to lower temperature, the heat entering the base of the glacier can only be used to melt ice. We will now focus on supply of heat from the ground used for such melt.

The geothermal heat flow has two main components, one originating from the mantle (reduced- or Moho heat flow) and one constituting radiogenic heat produced within the upper part of the Earth's crust (c.f. Furlong and Chapman, 1987). Over typical continental cratons, such as the East European craton hosting Fennoscandia, the Moho heat flow show smooth large-scale spatial trends. The Moho heat flow is lowest in the central part of the Baltic Shield (Čermak, 1989). The crustal part of the geothermal heat flow displays much larger spatial variations, down to a regional scale (Näslund *et al.*, 2004). In the upper part of the crust energy produced by the natural radioactive decay of primarily ^{40}K, ^{238}U, and ^{232}Th is absorbed by the bedrock and stored as heat. There is a close correlation between the distribution of heat produced in the crust and regional geological units, with higher heat flow observed in granitic rocks. As example, over Sweden and Finland the total geothermal heat flow observed at the crustal surface varies with a factor of more than 2 on a regional scale Näslund *et al.* (2004). The geothermal heat flow has a strong control on basal temperatures of ice sheets (*e.g.* Waddington, 1987). Typically, for a 3 km thick ice sheet at steady-state, a 20% error in geothermal heat flux generates a 6 K error in

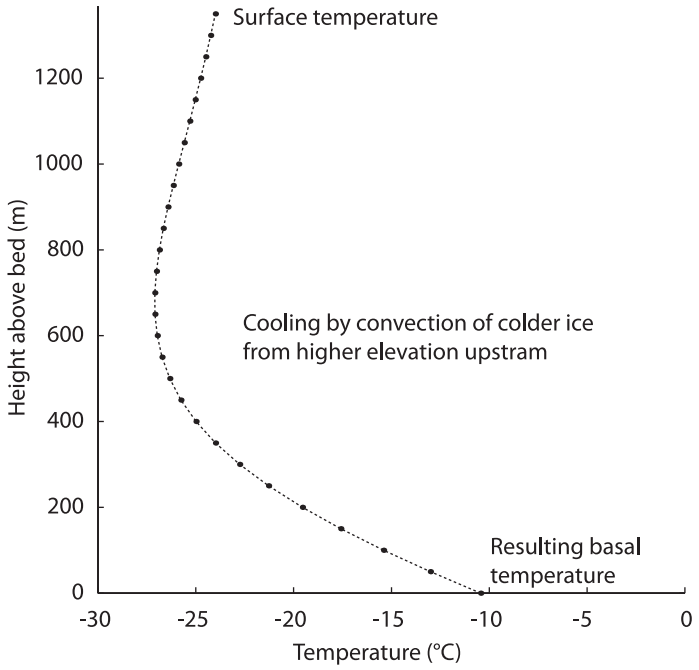

Figure 6.1. Vertical temperature profile through an ice sheet calculated using a simplified Equation 6.4 focussing on vertical components.

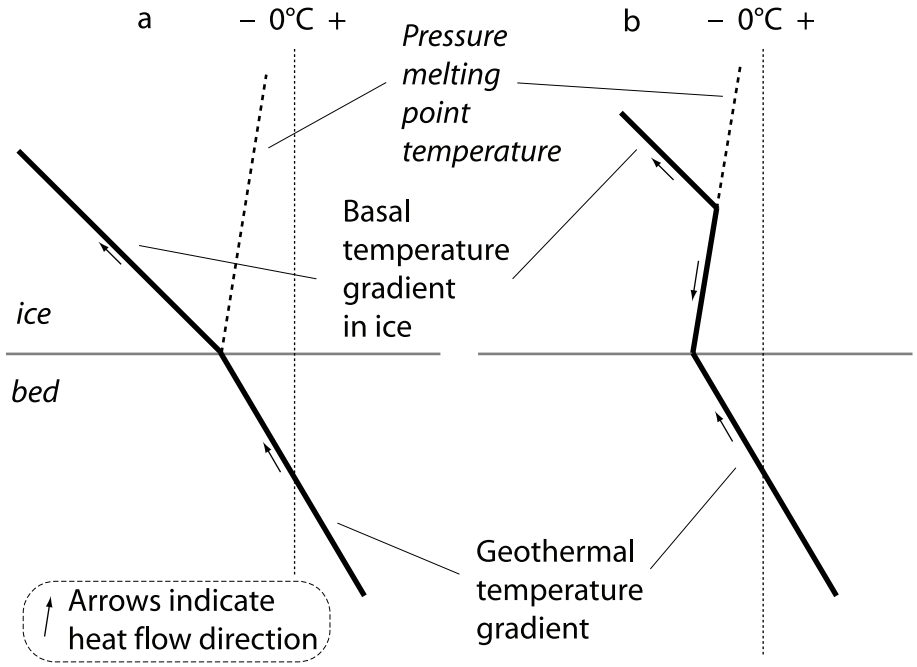

Figure 6.2. Schematic detail of the bed-ice interface of a glacier showing (a) the conduction heat from the glacier base due to a geothermal gradient, and (b) the heat trap produced by the presence of temperate ice at the bed. See text for further discussion.

basal temperature. This has direct implications on for example numerical ice sheet modeling, if the geothermal heat flow is not realistic in the model setup, ice sheet models will not produce useful patterns on basal melting.

The basal melting beneath an ice sheet can not easily be estimated from the geothermal heat flux, although, in a relative sense, melting will be a function of the flux. Since the basal conditions are determined by all components of Equation 6.4, knowledge of the geothermal heat flux will not suffice, typically numerical modeling of the Equation with known and estimated boundary conditions are required.

Qualitatively, the energy available for melting is determined by the flux of heat conducted away from the base through the overlying ice. At the boundary this reduced to the difference between the geothermal heat flux and the conduction of heat through the ice near the boundary. The melt rate is thus determined by

$$\dot{m} = \frac{\tau_b u_b + G - K\beta_0}{K\rho_I} \tag{6.5}$$

(*e.g.* Tulaczyk *et al.*, 2000; Hooke, 2005), where β_G is the geothermal heat flux, $K\beta_0$ is the heat conducted away from the bed interface upwards in the ice (K is the thermal conductivity of ice and β_0 is the local thermal condition in the ice), $\tau_b u_b$ is the frictional heat production, τ_b is the basal shear stress and u_b is the basal sliding speed, L is the latent heat of fusion, and ρ_I is the density of ice.

The geothermal heat flux varies spatially as discussed above. For the Fennoscandian ice sheet the average value from Näslund *et al.* (2005) of 49 $\mathrm{mWm^{-2}}$, can be considered typical. To provide an order of magnitude estimate of basal melting, we can consider data calculated by (Hooke, 1977) from which we can extract a temperature gradient of 0.015°C $\mathrm{m^{-1}}$. If we disregard frictional heating from the bed a typical melt rate would be on the order of millimeters to a centimeter per year. Fahnestock *et al.* (2001) show estimated annual melt rates beneath Greenland to on the order of cms, although much higher values reaching 0.15 m are inferred in areas of rapid ice motion, indicating the typical feedback between basal water and glacier sliding. Modelling results also yield values from a several $\mathrm{mm\,year^{-1}}$ to a few $\mathrm{cm\,year^{-1}}$ (J. Johnson, personal communication, Nov. 10, 2006). Hence, values on the order of $\mathrm{cm\,year^{-1}}$ can be expected and used to estimate the volumes of water produced beneath an ice sheet if the area of melt is considered known.

To roughly estimate the maximum contribution of discharge from basal melt, we will perform a rough calculation using the following assumptions.

1. We consider a straight flow line from the ice divide to the terminus located at the Younger Dryas zone of south central Sweden. The choice of terminus position is mainly that of a well defined position, we do not consider the climate aspects of this stand. The flow line length would be approx. 300 km (this number should be taken for its magnitude, not absolute value).

2. The width of the drainage area would be triangular with an apex at the divide and widening towards the margin, as envision by Shoemaker (*e.g.* 1986). We

consider the esker spacing a measure of drainage area width at the margin which yields a rough width of 30 km (Geological Survey of Finland, 1984).

3. The entire triangular drainage area experiences a uniform 0.01 m year^{-1} basal melt rate.

Performing the simple calculation yields a discharge of 14 m^3 s or 1.2×10^6 m^3 day^{-1}. This corresponds to normal discharge in a medium size natural stream. The importance of this water, however, is that it is highly pressurized through most of its transport in the basal meltwater film.

That basal melting from geothermal heat is important for understanding the stability of ice sheets is gaining more support. (Näslund *et al.*, 2005) provide a first detailed geothermal heat flux distribution of the Fennoscandian ice sheet and show that significant differences occur in response to local variations. The ice sheet average melting and discharge, however, is not severely affected. It should be remembered that the paleo-ice-sheet geothermal heat distributions are more easily obtainable than those for Antarctica and Greenland (Fox Maule *et al.*, 2005). Hence studies introducing large scale variable geothermal heat flux boundaries are emerging (*e.g.* Fahnestock *et al.*, 2001; Pollard *et al.*, 2005; Näslund *et al.*, in prep).

6.2 Melting from internal deformation and basal friction

Heat that can be made available for basal and englacial melting is produced by the deformation processes as ice flows. Such contributions depend strain rates and, hence, larger contributions occur near the bed and where the ice moves faster. In the case of fast flowing ice streams where much movement is by sliding, large strain rates are primarily found in the marginal shear zones of the streams. It is possible that heat can also be produced by subglacial sediment-deformation and friction between the base and the substrate.

In the simplest case, we can consider *simple shear*. The rate of energy dissipated by internal deformation can then be described by

$$\frac{dE}{dt} = \tau_{xz}\dot{\varepsilon}_{xz} \tag{6.6}$$

where τ_{xz} is the basal shear stress (parallel to the bed) and $\dot{\varepsilon}_{xz}$ is the the strain rate parallel to the bed, defined by $\dot{\varepsilon}_{xz} = (\tau_{xz}/B)^n$, where B and n are the constants of Glen's flow law for ice (Equation 4.1). Equation 6.7 can be rewritten as

$$\frac{dE}{dt} = \frac{(\rho g h \sin\alpha)^{n+1})}{B^n} e^{k\theta} \tag{6.7}$$

by using $\tau_{xz} = \rho_I g h \sin\alpha$ and the approximation that the temperature dependence of B can be accommodated by an exponential effect($e^{k\theta}$ Hooke, 2005). Because of

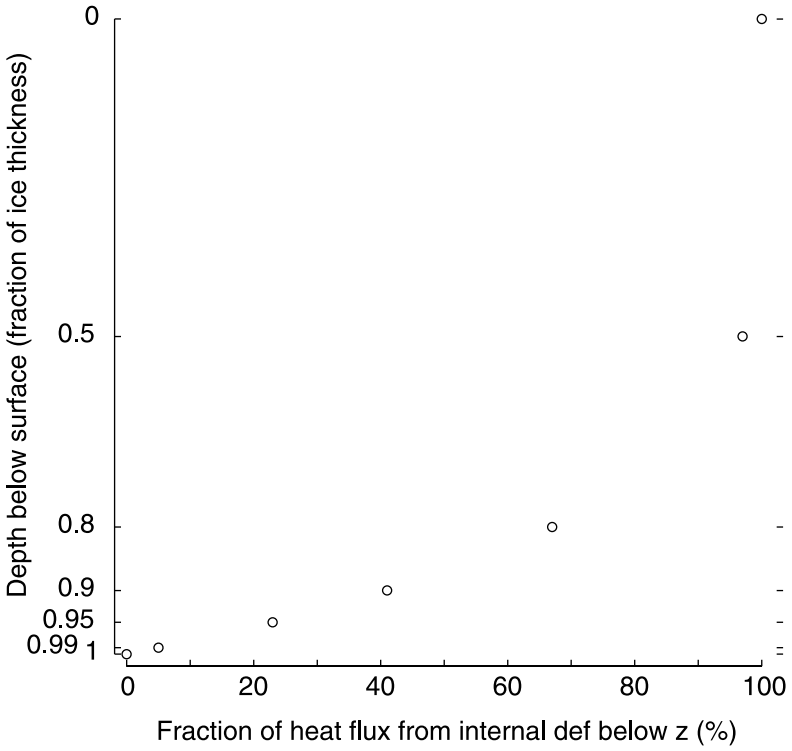

Figure 6.3. Graph of the fraction of heat contributed from ice below a certain depth in a glacier. Data from Budd (1969, table 4.2b, p. 69).

the strong deformation rates, most of the contributed heat is produced near the bed. Figure 6.3 shows how much of the total heat flux is caused by internal friction at a certain level in the ice column. It is evident that only 3% of the heat from internal deformation is produced in the upper half of the ice column. The lower 1/5 contributes 67% and the bottom 10% of the ice contributes over 40% of the heat. Hence much heat is generated near the basal boundary where melting is most likely to occur.

When ice under temperate basal conditions slides over its bed and deforms in response to the basal shear stress, heat is produced. One process involved in sliding is the *regelation*. Regelation was first described by Tyndall and Huxley (1857), Faraday (1859, 1861) and Deeley and Parr (1914) but developed into the sliding theory for glaciers by Weertman (1957, 1964), and Robin (1976). Figure 6.4 shows how regelation in a closed system works where basal ice encounters a small obstacle on the glacier bed. The term *closed* indicates that neither water nor heat are lost from the system in the figure. When ice encounters the obstacle it becomes compressed on the upglacier side of the obstacle. This rise in pressure changes the pressure melting point so that ice is melting from the rise in pressure alone. The melted water can then flow around the obstacle to the downglacier side. The downglacier side experiences a proportionally lowered pressure and hence higher

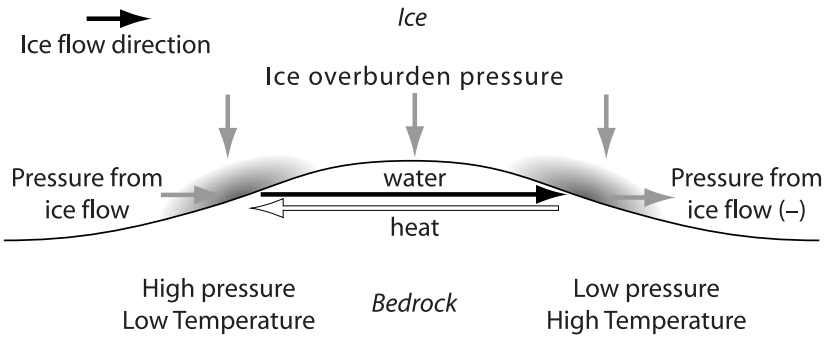

Figure 6.4. Principles for heat the energy circulation around a bedrock obstacle from the process of regelation as ice moves past the obstacle. See text for discussion.

pressure melting point. Water that arrives here will thus freeze because of the lower pressure. The phase change requires energy to either be gained (melting) or lost (freezing) by the ice or water. This means that energy is produced by freezing at the downglacier side and consumed by melting at the upglacier side. This sets up a temperature gradient through the obstacle and a circulation of energy by liquid water flowing in the glacier flow direction and through heat conduction through the obstacle in the reverse direction.

If we consider an open system (in contrast to the closed discussed above) where water or heat or both can escape the system, the result is that a net loss of ice in the form of liquid water can result at the bed. Hence, the sliding mechanism can contribute to the subglacial water production. However, the heat that inevitably must be used to switch phase, is of course taken from other processes and may e.g. cool the basal ice and reduce the amount of basal melting from geothermal heat. The net result may therefore be very little when all processes are considered in conjunction.

7. Ice sheet hydrology

As stated at the beginning of this report, ice sheet and valley glacier hydrology does not differ in terms of the processes involved. However, the scale over which the processes act and the size of the water fluxes are of course much larger on the ice sheet than on the valley glacier. The only modern ice sheet that can be used as an analogue to the past Fennoscandian ice sheet is the Greenland ice sheet. Antarctica is a poorer analog since it largely lacks surface melting and also has vast marine-based portions; Greenland is a land-based ice sheet. Although the analog can be argued not to be perfect, Greenland exhibit the same processes as those found in conjunction with past ice sheets and at similar scales. The Greenland analog is therefore important. We will therefore summarize work done on the Greenland ice sheet and how this fits with general theory.

7.1 Surface hydrology of present ice sheets

The Greenland ice sheet covers 1 640 000 km^2 (*e.g.* ACIA, 2005, p. 205). K. Steffen (reported in ACIA, 2005) has estimated the ablation area to cover 5×10^5km^2 and the area of the dry snow zone to be 1 140 000 km^2. There is however large variability in ablation area extent ranging 3–6$\times10^5$ km^2, and with minimum and maximum values beyond this range. Most of the ablating area is found in southern Greenland because of the large latitudinal range of Greenland.

Since Greenland is sparsely populated, the interest for studying the hydrology of the ice sheet has been mostly for academic reasons. One notable exception is a study for hydroelectric purposes performed by Grønlands Geologiske Undersøgelse (Thomsen *et al.*, 1986, 1993; Braithwaite and Thomsen, 1989; Thomsen *et al.*, 1989). Thomsen *et al.* (1986, 1989) investigated the surface hydrology of the Greenland ice sheet in the Ilulissat/Jakobshavn area for hydro-electric power planning purposes. They found that the surface hydrology of the ice sheet consisted of numerous equidistant drainage areas draining through moulins into the interior of the ice sheet (Figure 7.1).

This study does not cover the entire ablation area but the most peripheral part. The ice sheet topography is also rougher in these parts (see Figure 7.1) than higher up. It is therefore likely that catchments grow in size on the lower slope upstream parts of the ablation area. The map in Figure 7.1 also shows indications of this. The surface drainage, nevertheless, forms a mosaic of smaller catchments that each are

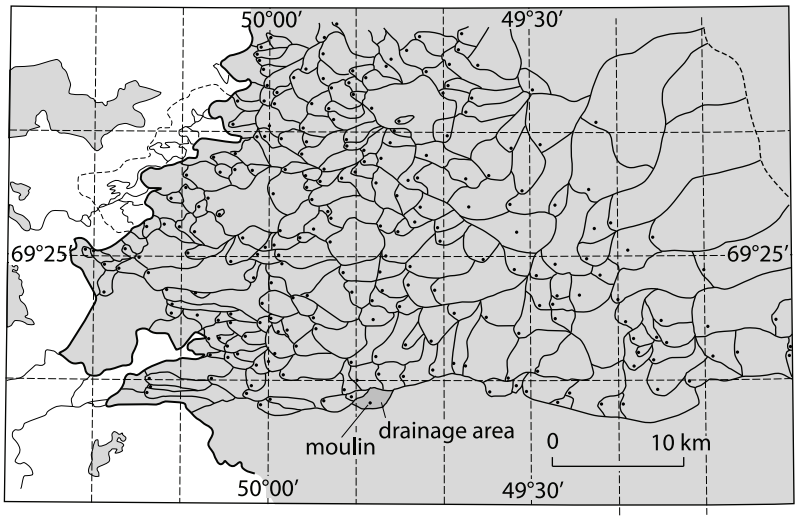

Figure 7.1. Delineation of surface drainage basins on the Greenland Ice Sheet near Ilulissat/Jakobshavn. From Thomsen *et al.* (1989)

associated with moulins. Since moulins, and thereby connections to the bed, can only be established in the presence of crevasses, the size of the drainage systems will be determined by how widely spaced such crevassed areas are. There are currently no such maps available.

Ahlstrøm *et al.* (2002) have built on the earlier studies and introduced space-borne sensors to study the ice-sheet drainage basin. By combining the surface observations with a digital terrain model of the ice sheet bed topography, made from ground penetrating radar surveys, and a energy balance melt-model, they could model and compare results with 25 years of runoff data.

7.2 Subglacial hydrology

Very few publications deal with the subglacial hydrological conditions beneath ice sheets. Water has been found at the base of ice sheets through deep drilling for ice cores (*e.g.* Kapitsa *et al.*, 1996; Dahl-Jensen *et al.*, 2003). Indirect evidence in the form of seismic investigations, ground penetrating radar measurements and inferences from fast flowing ice are, however, abundant. The fast flowing ice streams of the Siple Coast in West Antarctica serve as good examples (*e.g.* Kamb, 1991). Zwally *et al.* (2002) analyzed differential global position system (DGPS) data from a location near the equilibrium line on the Greenland ice sheet and found seasonal variations in flow velocity. Their locality is near ($\sim$ 30 km) the Jakobshavns isbrae, the fastest flowing glacier in the world. Zwally *et al.* (2002) attributes these variations in velocity to variations in water input from the surface presumably affecting the basal hydrological system and causing accelerations. Modeling of the ice in the area suggests sub-freezing basal temperatures. However, such modeling experiments

rely heavily on assumed values of geothermal heat flux which has been shown by Näslund *et al.* (2004) to be highly variable and probably the cause for erroneous basal temperatures. The importance of Zwally *et al.*'s findings are that the entire ablation area of the ice sheet seems to be affected by, at least, seasonal variations in basal hydrology. Hence the ice sheet margins may be subject to significant variations in both water pressure and glacier sliding speed. Furthermore, it seems likely that water routing from the surface to the bed is a common process on ice sheets with ablation areas.

To date no study has been made where processes found on smaller glaciers have been studied in the ice sheet context. The need for such a study is thus of major importance to verify that a coupling similar to that on smaller glaciers occur also on ice sheets.

7.3 Subglacial Lakes

Subglacial lakes have been known to exist since the discovery of Lake Vostok, east Antarctica, in 1996 (Kapitsa *et al.*, 1996). Numerous large lakes have since been identified to exist beneath the Antarctic ice sheet (Siegert *et al.*, 1996, 2005) by *e.g.* satellite based remote sensing methods. The lakes leave a footprint in the surface topography of the ice sheet. Because the ice sheet is locally floating in the water of the lakes, the basal shear stress is locally zero which produce a near horizontal ice surface over the lake. It is reasonable to assume that lakes are identifiable by this method as long as they have larger width and length than the local ice thickness since the effect would otherwise be taken up by the ice mass (*e.g.* Balise and Raymond, 1986).

Lake Vostok is the largest lake found beneath the Antarctic ice sheet and measures 280 km in length and 50–60 km in width and with a maximum depth of in excess of 1000m, Comparable to Lake Ontario in North America. The lake subglacial lake alters the basal ice composition through melting-refreezing and other processes (Petit *et al.*, 1998; Duval *et al.*, 1998; Siegert *et al.*, 2000, 2001). In the case of Lake Vostok hydrothermal activity does not seem to be present for maintaining the water body (Jean-Baptiste *et al.*, 2001). In other cases (Siegert and Glasser, 1997) it is possible that either strain heating or geothermal heat or both produce excess heat that can melt and maintain water bodies at the base of the ice sheet. This issue is of major importance for the stability of the lakes.

If the subglacial lakes are in thermal equilibrium, water is generated through melting and lost through freezing at equal rates, thus maintaining a constant water volume. If the lake water is generated by *e.g.* high anomalies in geothermal heat fluxes and strain heating it is likely that a positive water balance results. Such lakes thus have the possibility to grow until thresholds are reached where they can drain. Such inferences have been made from observation of changes in the East Antarctic Ice sheet surface topography (Wingham *et al.*, 2006). Such re-organization of subglacial water will likely reach the marginal areas through outburst-like phenomena. It is not

certain that outbursts will be similar to the spectacular Jökulhlaups from Icelandic ice caps where subglacial lakes formed by extremely high geothermal heat fluxes from volcanoes generate large quantities of water that catastrophically drains through the overlying ice caps (Björnsson, 1998). The effect of large bodies of water at the base of ice sheets can be sudden outburst floods which yield transient extreme pressure and discharge peaks.

There are several indications that large floods have occurred from ice sheets. In Antarctica, Denton and Sugden (2005) discuss observable melt water generated features originating from larger extents of the ice sheet. Sawagaki and Hirakawa (1997) observed traces of meltwater in coastal areas of Antarctica. There are indications that large quantities of water drained through the Laurentide ice sheet during its waning phase (*e.g.* Josenhans and Zevenhuisen, 1990; Barber *et al.*, 1999; Clarke *et al.*, 2003). Some of the observations from Antarctica have been heavily discussed but the evidence is mounting that large floods do occur. Spectacular floods have been inferred from re-interpretation of landforms typically not thought to be associated with floods (*e.g.* Shaw, 2002). This flood hypothesis has not gained general acceptance (*e.g.* Clarke *et al.*, 2005) but cannot be completely disregarded. Hence, large scale, low frequency drainage phenomena are possible in ice sheets. In the case of the Fennoscandian ice sheet all identified large scale drainage phenomena area associated with subaerial lakes dammed by ice at the margin and not subglacial phenomena.

8. Modeling glacier hydrology

Modeling of the hydrology of glaciers and ice sheets is important for several reasons. There is a need to predict runoff volumes and timing of variations in runoff from glaciers on short-term time scales (*e.g.* Jansson *et al.*, 2003). Because of the strong coupling between glacier dynamics and basal water pressure (*e.g.* Jansson, 1995), it is vital to include basal hydrology in glacier and ice sheet models to correctly model their behavior.

Modeling efforts attempting to replicate the drainage system of a glacier faces several problems. The general flow of water, in the direction of the gradient in potential, does not pose a major problem. The reality, including discrete tunnels or other conduit-like systems, is very hard to implement, especially since the systems are varying both temporally and spatially. The ice sheet models typically use grid cells that are of km scale which means any hydrological model must average or parameterize processes that vary over shorter distances than this (Alley, 1996). Hence, ice sheet models can replicate the general directions of water flow but cannot reproduce the development and changes of discrete pathways in parallel with changes in size of the general ice sheet. We will therefore describe the general modeling of ice sheet hydrology and the attempts that have been made to include specific flow routing through and under the ice sheet.

8.1 General flow of water under ice sheets

To model the general hydrology at the base of an ice sheet, it is common to take an existing thermo-mechanical ice sheet flow model and couple it to a model for the subglacial hydrology (*e.g.* Johnson and Fastook, 2002). The basal melt rate is determined by the ice model and includes geothermal heat, heat from internal deformation, and heat from basal friction. In the example of the Johnson and Fastook (2002) model, the water is handled by a separate flow model for water which is similar to the ice flow part. We will briefly summarize this approach.

Johnson and Fastook's 2002 model for subglacial water uses a water depth w as the variable. This water depth is not a true thickness of basal water or similar concept but a way of describing the flux of water. The flux equation for the system is

$$\frac{\partial w}{\partial t} = -\nabla \cdot \vec{\sigma} + S \tag{8.1}$$

where $\vec{\sigma} = \vec{v}w$, $\vec{v}$ is the velocity vector, S represents external sources of water such as melting or re-freezing of water at the bed. Once the water is generated it is subject to a pressure which is determined from the overburden pressure of the ice and the topography of the subglacial landscape. The pressure is described by

$$\phi = \rho_I g H + \rho_W g z_b - N \tag{8.2}$$

where ρ_I and ρ_W are the densities of ice and water, respectively, g is the gravitational acceleration, H is the ice thickness, z_b is the elevation of the bed and N is the effective pressure (the difference between ice overburden and water pressure, $P_I - P_W$) and calculated by Alley (1989) as

$$N = k_n \frac{\tau_b}{w} \tag{8.3}$$

where k_n is a constant and τ_b is the basal shear stress. Johnson and Fastook (2002) following Alley (1989) argues that the concept of w is such that when higher water pressure will tend to lower w and an increase results in increased t_b. The driving stress can be expressed as

$$\tau_b = \rho_I g H \nabla h \tag{8.4}$$

since $H = h - z_b$, h is the local ice surface elevation and by assuming the driving stress is balanced locally by vertical shear stresses. $\nabla = \partial/\partial x\imath + \partial/\partial x\jmath$, where $\imath, \jmath$ are the cardinal directions in the map plane. This results in

$$\phi = \rho_I g h + \rho_I g \left(\frac{\rho_W}{\rho_I} - 1 \right) z_b - k_n \frac{\rho_I g (h - z_b) |\nabla h|}{w} \tag{8.5}$$

The velocity of the water must then be specified in terms of the pressure gradient. This can be made with the Manning's equation (*e.g.* Freese and Cherry, 1979) which can be rewritten to the form

$$\vec{V} = \frac{R_p}{n} \left(\frac{\nabla \phi}{\rho_I g} \right)^q \tag{8.6}$$

where n is the Manning's n Modified to produce a velocity in ms^{-1}, R is the hydraulic radius, and p and q are exponents which vary depending on the type of flow. The use of Equation (8.6) is not obvious since it represents an averaging of phenomena that take place on much shorter scales than accommodated by the resolution of the ice flow model. Johnson and Fastook (2002) argue that an appropriate parametrization can be reached for a carefully chosen set of p (= 2,laminar; = 1/2, turbulent), q (= 1,laminar; = 2/3, turbulent) and n (= 0.025, gravelly channel, turbulent; 5.7×10^{-7}, laminar).

The concept outlined above allows for detailed flow routing of melt water produced at the base of an ice sheet. Such a model is highly suitable for estimating basal contribution of melt water and to survey how water is generally routed beneath an ice sheet. The concept has also been widely used (*e.g.* Pattyn *et al.*, 2005). When studying smaller scale phenomena, however, the lack of discrete tunnels and input from surface melt, possibly with diurnal variations (*e.g.* Allen, 1971; Lindeberg and Ringberg, 1999) or at least annual variations (*e.g.* Banerjee and McDonald, 1975) is not covered. A few attempts of solving this problem have emerged.

8.2 Discrete routing of flow

The lack of detail in hydrological models of ice sheets regarding small scale phenomena, such as point input of water from the surface and tunnel routing of water at the base of the ice sheet and the variable pressure effects expected in such a system, poses a large problem when trying to estimate how ice sheets affect the subsurface flow of water. The problems are largest when concerning transient effects on diurnal to seasonal time scales. We will therefore review emerging models which attempt at implementing such dynamic processes Arnold *et al.* (1998), Arnold and Sharp (2002) and Flowers and Clarke (2002a,b).

Arnold *et al.* (1998) presents a model for valley glacier hydrology which consists of three main submodel components, a surface energy balance model which calculates meltwater on the glacier surface, a surface routing model which routes generated water across the glacier surface and a subglacial hydrology submodel which predicts flow conditions in the subglacial system. The subglacial system can change between a distributed system and a channelized system depending on flow conditions, governed by the input rates from the surface. The model is semi-empirical in the sense that it relies on site specific experimental data for estimating certain model parameters.

In this model the input points are known since Arnold *et al.* (1998) attempted to model an existing glacier. Hence water routed on the surface was transferred to the base a a fixed number of points. The subglacial routing was accomplished by using parts of the US Department of Transportation Agency Storm Water Management Model (EPA SWMM; Roesner *et al.*, 1988). This model simulates *drains* (moulins) where water can enter and leave the system by *pipes* (tunnels) with individual characteristics. To simulate the distributed, or linked cavity, system (Kamb, 1987), Arnold *et al.* (1998) used *bundles* of eight small rough conduits or by using one very low and broad rectangular rough conduit. Conduits are allowed to increase in size from melting and decrease in response to creep. The melting rate at the conduit wall is calculated using

$$M = \frac{(\pi S)^{1/2} \rho_W (f_t v^3/4)}{L} \tag{8.7}$$

(Spring and Hutter, 1981) where S is the conduit cross-section, f_t is a friction parameter, v is the water velocity in the conduit and L is the latent heat of fusion of water. The rate of conduit closure is calculated using

$$A = -(P_I - P_W)|P_I - P_W|^{n-1} s (1/nb)^n S \tag{8.8}$$

where P_I and P_W are the ice overburden and subglacial water pressure, respectively, n and B are the empirical constant of the Glen flow law for ice (Equation (4.1)).

The resulting physically based semi-distributed model captures the essential features of the glacier Haut d'Arolla in terms of temporal variations and to some extent also spatial variations in the drainage. The spatial variations do not include re-organization in terms of location of conduits, recognized from (*e.g.* Hock and Hooke, 1993).

Arnold and Sharp (2002) developed a model which generates water at the base and at the surface of the ice sheet and routes water down to the bed where the subglacial hydraulic potential gradient (Shreve, 1972) drives the water along the bed. The model then calculates the flow of water at the bed according to two possible configuration, the *linked cavity* system proposed by Kamb (1987) characterized by slow flow speeds, and a fast drainage system consisting of tunnels as suggested by Röthlisberger (1972). The water pressure in these systems is calculated by Fowler's 1987a; 1987b theory. For tunnels the effective pressure is calculated by

$$N_R = [\rho_W g \phi Q_R \rho_I A L S_K]^{1/n} \tag{8.9}$$

where N_R is the effective pressure for a tunnel based system, ρ_W and ρ_I are the densities of water and ice, respectively, g is the gravitational acceleration, Q_R is the tunnel discharge, A is the Arrhenius' parameter, L is the latent heat, S_K is the tunnel cross sectional area, and n is the Glen's flow law exponent (Equation (4.1)). The hydraulic gradient, ϕ, is defined as

$$\phi = \alpha + \left[\frac{\rho_W - \rho_I}{\rho_W}\right] \beta \tag{8.10}$$

where α and β are the ice surface and glacier bed slope,respectively. The tunnel cross-sectional area S_K is calculated as

$$S_R = \left(\frac{f Q_R^2}{\rho_W g \phi}\right)^{3/8} \tag{8.11}$$

where f is an empirical constant related to turbulent channel flow. For cavities, the effective pressure is calculated by

$$N_K = r \left[\frac{\rho_W g \phi}{\rho_I K L} \frac{Q_K}{n_K S_K}\right]^{1/n} \tag{8.12}$$

where N_K is the effective pressure fora cavity based system, r is a shadowing function (Lliboutry, 1978), defined as the probability that a randomly selected area of the bed is in contact with the ice, Q_K $(= Q_R)$ is the discharge through the cavity system, n_K is the number of passageways across the width of the glacier and S_K is the cross-sectional area of a typical passageway. Which of these configurations exist at a specific node point is calculated by a stability criterion provided by Fowler (1987b). At each time step and in each node of the model, this criterion has the form

$$\Lambda = \frac{\nu U_s}{l A N} \tag{8.13}$$

where ν $(= a/l)$, a and l are the characteristic bedrock bump amplitude and length, respectively, and A is the Arrhenius' parameter.The critical value for tunnel stability Λ_c is given by

$$\Lambda_c = \left(\frac{3 n S_R}{A^\star}\right)^{(4-\mu)/\mu} \tag{8.14}$$

where $A^\star$ is the total cavity cross-sectional area, and μ is the power function for self-similar bedrock surfaces (Fowler, 1987a,b)

Water generated by melting and precipitation at the surface of the modeled ice sheet is routed on the surface by an *upstream contributing area* algorithm suggested by Sharp *et al.* (1993). At model nodes where the accumulated water reaches a threshold value it is added to the basal water at that node location. Hence, this model allows water to enter at points that are not pre-determined as in the Arnold *et al.* (1998) model. The same routing routine is used to calculate the discharge at the basal model nodes based on the subglacial hydraulic potential gradient (Shreve, 1972). This model thus encapsulates the idea that the surface and basal hydrology of ice sheets are coupled. The way in which the input points for surface water into the subglacial system are determined is not based on observational knowledge. In fact, this is a key point which, despite its importance, is lacking in our understanding of ice sheet hydrology.

(Flowers and Clarke, 2002a,b) has developed a physically based model for glacier hydrology which couples glacier surface runoff, englacial transport and storage, and flow of water beneath the glacier, including flow within subglacial sediments. This model was developed using the extensively investigated Trapridge Glacier, Yukon, Canada, as a reference but has since been used in other contexts as well. The model consists of communicating two-dimensional, vertically integrated layers, model components.

Figure 8.1 shows the hydrological system handled by the Flowers and Clarke (2002a) model. Surface melt is handled by a *degree-day model* (*e.g.* Hock, 2005), a common approach in all glacier and ice sheet models. The surface runoff, a linear diffusion approach (Marshall and Clarke, 1999) is used where routing is governed by a local runoff depth h^r and spatial gradients in h^r and surface elevation. The water volume is conserved, assuming incompressibility,

$$\frac{\partial h^r}{\partial t} + \frac{\partial Q_j^r}{\partial x_j} = M + R - \phi^{r:e} + \phi^{r:s} + \phi^{r:a} \tag{8.15}$$

where Q_j^r is the discharge per unit width, $j = 1, 2$ are the two horizontal directions, M is the melt generated by the degree day model, R is the rate of liquid precipitation, $\phi^{r:e}$ is a source/sink term connected to exchange of water with the englacial system ((b) in Figure 8.1), $\phi^{r:s}$ is the rate of discharge from the subglacial system to proglacial runoff and $\phi^{r:e}$ is the exchange with the groundwater system in the ice free region.

$$Q_j^r = \frac{K_{jk}^r h^r}{\rho_W g} \frac{\partial \Psi^r}{\partial x_k} \tag{8.16}$$

where $j, k = 1, 2$ are the two horizontal directions, ρ_W is the density of water and g is the gravitational acceleration. The total fluid potential Ψ^r is given by the sum of the water pressure and the elevation potential

$$\Psi^r = p^r + \rho_W g z_s \tag{8.17}$$

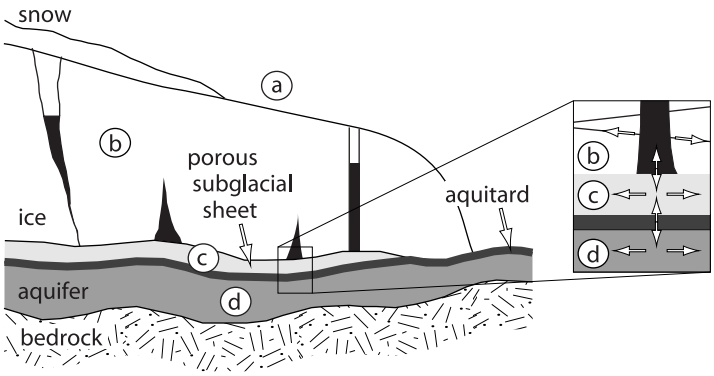

Figure 8.1. The conceptual model for glacier hydrology containing fours coupled model systems: (a) surface hydrology; (b) englacial hydrology; (c) flow in a porous subglacial sheet; and (d) groundwater flow (excluding bedrock flow). After Flowers and Clarke (2002a).

where p^r is the water pressure and z_s is the elevation above a datum $z_s = 0$.

The englacial drainage in the Flowers and Clarke (2002a) model is represented by a combination of storage elements, surface and basal crevasses and vertical pipes (moulins). These elements are given volumes according to

$$\begin{array}{ll} V_1 = \pi r_1^2 h_1 & \text{(moulins)} \\ V_2 = 1/2 w_2 l_2 h_1 (f_2 + 1) & \text{(surface crevasses)} \\ V_3 = 1/4 w_3 l_3 h_1 & \text{(basal crevasses)} \end{array} \tag{8.18}$$

where r_1 is the radius of the moulin, h_1 is the ice thickness (moulins and surface crevasses are thought to extend through the ice, basal crevasses are $h_1/2$ in height), w_2 and w_3 are the surface and bed widths of surface and basal crevasses, respectively, f_1 is geometric factor that scales the area in contact with the bed to the area exposed at the surface. The total englacial void volume is then given by

$$V_T = \int_S N_i(x,y) V_i(x,y) dS \tag{8.19}$$

where $N_i(x,y)$ density of storage element i per unit area, $V_i(x,y)$ is the volume of those storage elements calculated by Equation (8.18). The different storage elements have different hypsometric curves, which yield unique relationships between water volume and pressure. For a vertical pipe, we obtain

$$p_1 = \frac{\rho_W g V_1^W}{\pi r^2} \tag{8.20}$$

for the pressure at the base of a surface crevasse

$$p = \begin{cases} \frac{\rho_W g V_2^W}{w_2 l_2}, & f_2 = 1 \\ \rho_W g \sqrt{\frac{2 V_2^W h_1}{w_2 l_2}}, & f_2 = 0 \\ \frac{\rho_W g h_1 f_2}{(1-f_2)} \left(-1 + \sqrt{1 + \frac{2 V_2^W (1-f_2)}{h_1 w_2 l_2^2}} \right), & f_2 \neq 0, 1 \end{cases} \tag{8.21}$$

For basal crevasses solutions for both underfull conditions and conditions when the uncompressed water volume V_3^W exceeds the void volume V_3 are required. Underfull conditions yield

$$p_3 = \frac{\rho_W g h_1}{2}\left(1 - \sqrt{1 - \frac{4V_3^W}{h_1 w_3 l_3}}\right) V_3^W \leq V_3 \tag{8.22}$$

For $V_3^W > V_3$

$$p_3 = \frac{\rho_W g h_1}{2} + \frac{1}{\beta}\ln\left(\frac{V_3^W}{V_3}\right) \tag{8.23}$$

where β is the compressibility of water. In the model, Flowers and Clarke (2002a) make the assumption that only one type of drainage element occurs in each grid cell of the model and that water pressures in all elements are equilibrated such that $p^e = p_1 = p_2 = p_3$.

Horizontal transport is achieved by applying a fractured medium approach. The areally average englacial water volume is defined as

$$V^e = \int_S h^e(x, y, t) dS \tag{8.24}$$

The water balance equation analogous to Equation (8.15) is

$$\frac{\partial h^e}{\partial t} + \frac{\partial Q_j^e}{\partial x_j} = M + R - \phi^{r:e} + \phi^{r:s} \tag{8.25}$$

where the source/sink terms involve exchange with the surface runoff system and the underlying subglacial sheet system. The horizontal flux is determined by a Darcy-type equation

$$Q_j^e = -\frac{T_{jk}^e}{\rho_W g}\frac{\partial \Psi^e}{\partial x_k} \tag{8.26}$$

where the fluid potential $\psi^e = p^e + \rho_W g z_B$, z_B is the glacier bed elevation. $T_{jk}^e = K_{jk}^e h_1$, where K_{jk}^e is the hydraulic conductivity and h_1 is the local ice thickness. The hydraulic conductivity of a fractured aquifer with uniform planar joints is

$$K = \frac{\rho_W g}{\mu}\frac{N_L b^3}{12} \tag{8.27}$$

(Snow, 1968) where μ is the dynamic viscosity of water, N_L is a line-density of cracks, and b is crack aperture. Rearranging Equation (8.27) yields an expression for the effective porosity

$$n^e = N_L b = \frac{\mu}{\rho_W g}\frac{12K}{b^2} \tag{8.28}$$

The volume of englacial joints is calculated by

$$V_{joint} = \int_S \int_{z_B}^{z_S} n^e dz dS \tag{8.29}$$

$V_{joint} <<\ll V_T$ in general but where bulk storage is absent $V_{joint} = V_T$. The englacial water pressure in such situations is given by

$$p^e = \rho_I g h_1 (v^e / V_T) \tag{8.30}$$

where ρ_I is the density of ice.

The subglacial drainage in the Flowers and Clarke (2002a) model is treated as a porous sheet composed of water and sediment. The thickness of the subglacial water sheet is defined as an areally averaged water volume

$$h^s(x, y, t) = \frac{1}{S} \int_S n^s(x, y, t) H^s(x, y, t) dS \tag{8.31}$$

where S is the area, n^s is the porosity and H^s is the combined thickness of the binary sediment-water mixture. The water balance of the system is

$$\frac{\partial h^s}{\partial t} + \frac{\partial Q_j^s}{\partial x_j} = b^s - \phi^{r:s} + \phi^{e:s} + \phi^{r:a} \tag{8.32}$$

where b^s is a source term that includes basal melting dur to geothermal heat and glacier sliding friction, $\phi^{r:s}$ is discharge from the glacier margin, $\phi^{e:s}$ is the exchange with englacial storage and $\phi^{s:a}$ is the exchange with the underlying aquifer.

The basal melt rate is determined by

$$b^s = \frac{Q_G + Q_F}{\rho_I L} \tag{8.33}$$

where Q_G and Q_F are the heat fluxes from geothermal and frictional sources, respectively, L is the latent heat of fusion for ice. The frictional heat flux is estimated in terms of the basal velocity and the basal shear stress

$$Q_F = \tau_{bj} v_{bj} \tag{8.34}$$

where the shear stress is given by

$$\tau_{bj} = \rho_I g h_1 \sin \alpha_{sj} \tag{8.35}$$

where α_{sj} is the local surface slope. In cases where surface water dominates basal melting b^s is negligible.

The flux of water in te subglacial water sheet is determined by Darcian-type flow

$$Q_j^s = -\frac{K_{jk}^s h^s}{\rho_W g} \frac{\partial \Psi^s}{\partial x_k} \tag{8.36}$$

where $\Psi^s = p`s + \rho_W g z_B$. For mathematical closure, a relationship is required between h^s and p^s which Flowers and Clarke (2002a) achieves by implementing the empirical relationship derived by Flowers (2000, derived for Trapridge Glacier)

$$p^s = p_I \left(\frac{h^s}{h_c^s} \right)^{7/2} \tag{8.37}$$

where $p_I = \rho_I g h_1$ and h_c^s is the critical water thickness such that $p^s = p_I$. The hydraulic conductivity is allowed to fluctuate in space and time as a function of h^s as

$$\log(K^s) = \frac{1}{\pi}\left[\log(K^s_{max}) - \log(K^s_{min})\right] \arctan\left[k_a\left(\frac{h^s}{h^s_c} - k_b\right)\right] + \\ + \frac{1}{2}\left[\log(K^s_{max}) + \log(K^s_{min})\right] \tag{8.38}$$

(Flowers, 2000) where k_a modulates abrupt transitions from K^s_{min} to K^s_m and k_b determines it position.

Flowers and Clarke's 2002a model, finally, has a subsurface groundwater submodel, envisioned as an aquifer, subparallel to the glacier bed and capped by a low-permeability till. The mass of water in the aquifer can be estimated by

$$m^a(x,y,t) = \int_S \int_{z_L}^{z_W} n^a(x,y,t)\rho^a(x,y,t)dzdS \tag{8.39}$$

where the second integral is calculated between the lower boundary of the aquifer $z_L(x,y)$ and the upper boundary of the saturated layer $z_W(x,y,t)$, n^a is the porosity and p^a is the water density. By assuming no variations in z and that the water thickness in the aquifer $h^a(x,y,t) = n^a(z_w - z_L)$ Equation (8.39) becomes

$$m^a = \int_S \rho^a h^a dS \tag{8.40}$$

All exchange in mass is thought to occur either with the overlying subglacial water sheet or with the runoff system depending on what overlies the aquifer. Hence the mass balance is described by

$$\frac{dm^a}{dt} = \int_S \rho^a(\phi^{s:a} + \phi^{r:a})dS \tag{8.41}$$

By applying Reynold's transport theorem, Flowers and Clarke (2002a) compute dm^a/dt as

$$\frac{dm^a}{dt} = \frac{d}{dt}\int_S \rho^a h^a dS = \int_S \left[\frac{\partial}{\partial t}(\rho^a h^a) + \frac{\partial}{\partial x_j}(v^a_j \rho^a h^a)\right] dS \tag{8.42}$$

or by combining Equation (8.41) and Equation (8.42)

$$\int_S \left[\frac{\partial}{\partial t}(\rho^a h^a) + \frac{\partial}{\partial x_j}(v^a_j \rho^a h^a)\right] dS = \int_S \rho^a(\phi^{s:a} + \phi^{r:a})dS \tag{8.43}$$

which becomes

$$\frac{\partial}{\partial t}(\rho^a h^a) + \frac{\partial}{\partial x_j}(v^a_j \rho^a h^a) = \rho^a(\phi^{s:a} + \phi^{r:a}) \tag{8.44}$$

in its local form. Since v_j^a is equivalent to q_j, the Darcy flux (Freese and Cherry, 1979), $Q_j^a = v_j^a h^a = q_j^a h^a$ where

$$q_j^a = \frac{K_{jk}}{\rho_W g} \frac{\partial \Psi^a}{\partial x_k} \tag{8.45}$$

where the fluid potential is determined by $\Psi^a = p^a + \rho_W g z_L$. With the assumption $v_j^a(\partial \rho^a / \partial x_j) \ll (\partial \rho^a / \partial t)$ Equation (8.44) becomes

$$\frac{\partial}{\partial t}(\rho^a h^a) + \rho^a \frac{\partial Q_j^a}{\partial x_j} = \phi^{s:a} + \phi^{r:a} \tag{8.46}$$

The final balance equation may then be obtained by dividing Equation (8.46) by ρ^a and differentiating the first term

$$\left(\frac{h^a}{\rho^a}\right) \frac{\partial \rho^a}{\partial t} + \frac{\partial h^a}{\partial t} + \frac{\partial Q_j^a}{x_j} = \phi^{s:a} + \phi^{r:a} \tag{8.47}$$

which governs both saturated and unsaturated flow in the aquifer. The transition between saturated and unsaturated conditions is handled by choosing a rule $p^a(h^a)$, for unsaturated conditions,

$$p^a = \rho_W g h`a,\ h^a \leq n^a d^a \tag{8.48}$$

and for saturated conditions

$$p^a = \rho_W g h^a + \frac{h^a - n^a d^a}{\alpha^a d^a} \tag{8.49}$$

where $\alpha^a = 1/(1 - n^a)\partial n^a / \partial p^a$ is an aquifer compressibility and $d^a = z_U - z_L$ is the aquifer thickness.

The exchange between the different models is determined by a series of rules.

$$\phi^{r:e} = \begin{cases} \frac{\Xi^{r:e} h^r}{\tau^{r:e}} & V^e \leq V_T \\ \frac{\Xi^{r:e} h^r}{\tau^{r:e}} \left(\frac{V_T}{S} - h^e\right) & V^e > V_T \end{cases} \tag{8.50}$$

where $\tau^{r:e}$ is a time constant, $\Xi^{r:e}$ represents the coupling strength of the two systems. Subglacial discharge to the proglacial runoff is written

$$\phi^{r:s} = \frac{1}{S} \int_S Q_j^s \hat{n}_j dl \tag{8.51}$$

where the line integral follows the margin, $\hat{n}_j$ is the unit outward flow normal to dl and S is the area over which water is deposited. The exchange between the englacial and subglacial models is formulated as

$$\phi^{e:s} = \frac{\chi^{e:s}}{\rho_W g \tau^{e:s}} (p^e - p^s) \tag{8.52}$$

where $p^e - p^s$ is a pressure differential, $\chi^{e:s}$ is a coupling strength and $\tau^{e:s}$. The saturation level of the aquifer is written for two cases

$$\phi^{s:a} = \begin{cases} \frac{\chi^{s:a} K_t}{\rho_W g d_t} \left[(p^s - p^a) + \rho_W g d_t \right], & h^a \geq n^a d^a \\ \frac{\chi^{s:a} K_t}{\rho_W g d_t} \left[p^s + \rho_W g d_t \right], & h^a < n^a d^a \end{cases} \tag{8.53}$$

where $\rho_W g d_t$ represents the driving potential arising from the elevation difference between the two systems. The exchange between surface runoff and the groundwater system is described by

$$\phi^{r:a} = \begin{cases} \frac{\chi^{r:a} K_t}{\rho_a g d_t} \left[(p^r - p^a) + \rho_a g d_t \right], & h^a \geq n^a d^a \\ \frac{\chi^{r:a} K_t}{\rho_W g d_t} \left[p^r + \rho_W g d_t \right], & h^a < n^a d^a \end{cases} \tag{8.54}$$

This model has been successfully used to model the hydrological system of Trapridge Glacier, Canada (Flowers and Clarke, 2002b). Flowers *et al.* (2003) used a simplification of the the Flowers and Clarke (2002a) model and applied it to Vatnajökull, Iceland, to study the contribution of water from the ice cap to Icelandic rivers. Flowers *et al.* (2005) continued to also model the future development of Vatnajökull by further coupling the hydrological model to an ice flow model.

To include discrete water carrying features, Flowers *et al.* (2004) employed one-dimensional flow line model that account for both sheet-like and ice-walled conduit water flow. This development is based on Clarke (2003) revision of the Spring and Hutter (1981, 1982) work. The balance equation for the subglacial water sheet is written as

$$\frac{\partial h^s}{\partial t} = -\nabla Q^s - \phi^{s:c} \tag{8.55}$$

where h^s is the water sheet thickness, Q^s is the water flux and $\phi^{s:c}$ concerns water leakage into conduits from the water sheet. The water sheet is treated as a macroporous horizon that accommodates turbulent flow at the ice contact (Stone and Clarke, 1993)

$$Q^s = -\frac{2_s^K h^s \nabla \psi^s}{\rho_w g} \left(1 + (1 + C \left| \nabla \psi^s \right|)^{1/2} \right)^{-1} \tag{8.56}$$

where K_s is the hydraulic conductivity, ρ_W is the density of water, $\psi^s = p^s + \rho_w g z_L$ is the fluid potential, z_L is the drainage path elevation, p^s is the water pressure. $C = (2880 K_s^3 (1-m)^2 / \mathrm{Re}^2 \mu m^3 \rho_W g^3)^{1/2}$ where m is the porosity, $\mathrm{Re} = Q^s \rho_W / \mu$ is the Reynolds number, and μ is the viscosity. The exchange of water between the sheet and the conduits is written as a function of pressure

$$\phi^{s:c} = \chi^{s:c} \frac{K_s h^{s:c}}{\rho_W g d_c^2} (p^s - p^c) \tag{8.57}$$

where $\chi^{s:c} \in 0, 1$ controls the coupling between sheet and conduit. The evolution of conduit cross-sectional area depends on the balance between conduit closure by

creep and melting due to viscous dissipation of heat. The rate of change in conduit cross-sectional area $\partial S/\partial t$ thus becomes

$$\frac{\partial S}{\partial t} = -\frac{Q^c}{\rho_I L}\left(\nabla\psi^c - D\nabla p^c\right) - 2S\left(\frac{p_I - p^c}{nB}\right)^n \tag{8.58}$$

where Q^s is the conduit discharge, L is the latent heat of fusion for water and $\psi^c = p^c\rho_W g z_L$ is the fluid potential. n and B are the empirical constants of the Glen's flow law for ice (Equation (4.1)). $D = c_t\rho_W c_W$ where c_t is the change in melting point temperature with pressure, c_W is the heat capacity of water. The water mass balance for a system of conduits is thus expressed as

$$\frac{\partial p^c}{\partial t} = -\frac{1}{\beta S}\left(\frac{\partial S}{\partial t} + \nabla Q^c + \frac{Q^c}{\rho_W L}\left(\nabla\psi^c - D\nabla p^c\right) - d_c\phi^{s:c}\right) \tag{8.59}$$

where β is a numerical compressibility parameter (Clarke, 2003). The conduit discharge can be expressed by

$$Q^c = -\left(\frac{2S^3}{P_W\rho_W f_R}\right)^{1/2}\frac{\nabla\psi^c}{|\nabla\psi^c|^{1/2}} \tag{8.60}$$

where P_W i sthe wetted perimeter, $f_R = 8gn'^2/R_H^{1/3}$ is the Darcy-Weisbach roughness with a Manning roughness n', and hydraulic radius R_H. Using this model, Flowers *et al.* (2004) modeled the discharge through Jökulhlaup from Grimsvötn, Iceland. Such drainage is a special case but the approach is the first where spatially discretized conduits occur.

8.3 Conclusions on glacier hydrology modeling

The state of physically-based models that simulates glacier hydrology remains fairly crude although promising work is emerging. The model efforts have been made to gain insights into specific glaciers or glacier-types and are not necessarily easily and generally applicable. The well investigated melt water production at the glacier surface can be handled comparatively well. It is also the most easily observable part and hence simplest part to model by surface energy balance models and temperature index melt models. The internal and subglacial system is characterized by large variability in possible drainage system configurations. Much uncertainty remains as to the exact geometry of drainage systems and how these systems can co-exist or switch from one state to the other. A crevasse-like englacial network, as adopted in the Flowers and Clarke (2002a) model, has been observed on Storglaciären, Sweden (Fountain *et al.*, 2005a,b), countering previous notions of englacial water flow through few melt-enlarged conduits. If subglacial sediments are present, groundwater flow may be a significant part of the system, as in the Flowers and Clarke (2002a) model, or flow may occur in channels eroded into the subglacial sediments.

On harder beds or beds of less permeable sediments such as tills, water flow may occur in conduit systems melted into the ice or in linked cavity systems. Hence, a general physically-based model would have to accommodate all these possibilities and even coupled different types of systems beneath different parts of a glacier. Such a model would be inherently complex.

Another issue which at present is not satisfactorily met is the time-transgressive development of subglacial systems. In the Flowers and Clarke (2002a) model, this is not necessary since flow through porous sediments does not involve significant time-dependent changes, except possible changes such as development of piping or siltation of the porous media from fines produced through sediment deformation. In the case of the Arnold and Sharp (2002) model, it is widely reported (*e.g.* Nienow *et al.*, 1998) that the subglacial drainage system changes both in sizes of conduits and in complexity of the network of channels through the course of a season. The subglacial system is very dynamic and it seems as if a complete and accurate model description of this system may be distant. However, most changes in such a system occur in response to rapid changes, both increases or decreases in water inputs, so a first-order approximation may be to switch between a series of systems prompted by key events in the forcing.

9. Concluding statement

The hydrological systems of glaciers and ice sheets have attracted much attention in the glaciological research literature. Detailed theories have been developed for the drainage of water through and beneath the glaciers that detail the processes in tunnels, distributed systems as well as water films. Flow of water beneath glaciers in the presence of a subglacial diamicton is also well understood. As with all process studies, these theories describe variations on time scales where problem geometries, such as conduit location (but not change in size of conduits) are constant. Hence, changes in routing of water is not handled in process theories and their modeling. Modeling of general water flow through glaciers has its origin at the other end of the time spectrum and models, hence, handle changes in large scale flow routing well but do not implicitly include processes. A few attempts have been made to include discrete tunnels or other physically-based characteristics into models and this direction in model development will obviously develop further.

The main problem with our understanding of the hydrology of glaciers and ice sheets, hence, lie in that processes and large scale flow characteristics are not coupled in models. The main reason for this is of course the complexity of the highly, especially spatially, transient behavior of the glacier hydrological system. A tunnel system with conduits of meter-width may change location over areas of a factor 10–100 larger, whereas the model resolution may be at one order of magnitude larger still. Furthermore, most process studies have been made on small glaciers whereas most modeling attempts concern ice sheets. This division comes from the scale issues discussed earlier but also from the fact that no glacier hydrological process studies have been made on ice sheets. In order to significantly improve our understanding of glacier hydrology on ice sheet scales and couple the processes into numerical schemes, we need to perform detailed process studies on present day ice sheets, preferably the Greenland ice sheet. Since the dynamic response of ice sheets to global warming is becoming a key issue in, *e.g.* sea-level change studies, the problems of the coupling between the hydrology of an ice sheet and its dynamics is steadily gaining interest.

10. Acknowledgement

Thanks are due to Prof. Gwenn Flowers for carefully reviewing the manuscript and suggesting many valuable improvements and to Prof. Jesse V. Johnson for providing much input on the modeling section. Any remaining ambiguities or inadequacies are, as always, the responsibility of the authors. Dr. Rickard Pettersson provided invaluable help with LaTeX formatting.

References

ACIA, 2005. *Arctic Climate Impact Assessment*. Cambridge University Press, Cambridge.1042 p.

Agassiz, L., 1847. Système glaciaire. Nouvelles études et expériences sur les glaciers actuel, leur structure, leur progression et leur action physique sur le sol. Paris: V. Masson.

Ahlstrøm, A.P., 2003. *Ice sheet ablation assessed by observation, remote sensing and modelling*. PhD diss. Danmarks og Grønlands Geologiske Undersøgelse. rapport 2003/49.

Ahlstrøm, A.P., Egede Bøggild, C., Mohr, J.J., Reeh, N., Lintz Christensen, E., Olesen, O.B., and Keller, K., 2002. Mapping of a hydrological ice-sheet drainage basin on the West Greenland ice-sheet margin from ERS-1/-2 SAR interferometry, ice-radar measurements and modelling. *Ann. Glaciol.*, 34, 309–314.

Allen, J.R.L., 1971. A theoretical and experimental study of climbing-ripple cross-lamination, with a field application to the Uppsala esker. *Geogr. Ann.*, 53A (3–4), 157–187.

Allen, J.R.L., 1985. *Principles of physical sedimentology*. George Allen and Unwin, London.

Alley, R.B., 1989. Water-pressure coupling of sliding and bed deformation: I. Water system. *J. Glaciol.*, 35 (119), 108–118.

Alley, R.B., 1992. How can low-pressure channels and deforming tills coexist subglacially? *J. Glaciol.*, 38 (128), 200–207.

Alley, R.B., Blankenship, D.D., Bentley, C.R., and Rooney, S.T., 1987. Till beneath ice stream B. 3. Till deformation: evidence and implications. *J. Geophys. Res.*, 92 (B9), 8921–8929.

Alley, R.B., 1996. Towards a hydrological model for computerized ice-sheet simulations. *Hydr. Proc.*, 10 (4), 649–660.

Alley, R.B., Dupont, T.K., Parizek, B.R., and Anandakrishnan, S., 2005. Access of surface meltwater to beds of subfreezing glaciers: Preliminary insights. *Ann. Glaciol.*, 42, 8–14.

Arnold, N., and Sharp, M., 2002. Flow variability in the Scandinavian ice sheet: modelling the coupling between ice sheet flow and hydrology. *Quat. Sci. Rev.*, 21 (4–6), 485–502.

Arnold, N., Richards, K., Willis, I., and Sharp, M., 1998. Initial results from a distributed, physically based model of glacier hydrology. *Hydrol. Proc.*, 12 (2), 191–219.

Banerjee, I., and McDonald, B.C., 1975. Nature of esker sedimentation. In: *Jopling, A.V., and McDonald, B.C., (eds.), Glaciolofluvial and glaciolacustrine sedimentation. Society of Paleontologists and Mineralogists, Tulsa OK, Special Publ.*, 23, 132–154.

Balise, M.J., and Raymond, C.F., 1986. Transfer of basal sliding variations to the surface of a linearly viscous glacier. *J. Glaciol.*, 31 (109), 308–318.

Barber, D.C., Dyke, A., Hillaire-Marcel, C., Jennings, A.E., Andrews, J.T., Kerwin, M.W., Bilodeau, G., McNeely, R., Southon, J., Morehead M.D., and Gagnon, J.-M., 1999. Forcing of the cold event of 8,200 years ago by catastrophic drainage of Laurentide lakes. *Nature*, 400 (6742), 344–348.

Benson, C.S., 1961. Stratigraphic studies in the snow and firn of the Greenland Ice Sheet. *Folia Geographica Danica.*, 9, 13–37.

Bird, R.B., Stewart, W.E., and Lightfoot, E.N., 1960. *Transport phenomena.* John Wiley & Sons, New York.

Björnsson, H., 1998. Hydrological characteristics of the drainage system beneath a surging glacier. *Nature*, 395 (6704), 771–774.

Blake, E.W., 1992. *The deforming bed beneath a surge-type glacier: measurement of mechanical and electrical properties.* PhD diss. University of British Columbia, Canada.

Blake, E.W., and Clarke, G.K.C., 1989. In situ bed strain measurements beneath a surge-type glacier. *Eos*, 70 (43), 1084.

Blankenship, D.D., and Bentley, C.R., 1986. Seismic mapping of a till at the base of Ice Stream B. (Abstract) *Eidgenössische Technische Hochschule (ETH) Zürich, Versuchsanstalt für Wasserbau und Hydrologie. Glaziologische Mitteilungen*, 90, 29–30.

Blankenship, D.D., Bentley, C.R., Rooney, S.T., and Alley, R.B., 1986. Seismic measurements reveal a saturated porous layer beneath an active Antarctic ice stream. *Nature*, 322 (6074), 54–57.

Blankenship, D.D., Bentley, C.R., Rooney, S.T., and Alley, R.B., 1987. Till beneath Ice Stream B. a. Properties derived from seismic travel times. *J. Geophys. Res.*, 92 (B9), 8903–8911.

Blankenship, D.D., Rooney, S.T., Alley, R.B., and Bentley, C.R., 1989. Seismic evidence for a thin basal layer at a second location on Ice Stream B. (Abstract) *Ann. Glaciol.*, 12, 200.

Boulton, G.S., and Jones, A.S., 1979. Stability of ice caps and ice sheets resting on beds of deformable sediment. *J. Glaciol.*, 24 (90), 29–43.

Boulton, G.S., and Hindmarsh, R.C.A., 1987. Sediment deformation beneath glaciers: Rheology and geological concequences. *J. Geophys. Res.*, 92 (B9), 9059–9082.

Boulton, G.S. Dent, D.L., and Morris, E.M., 1987. Subglacial shearing and crushing, and the role of water pressures in tills from south-east Iceland. *Geogr. Ann.*, 56A (3–4), 135–145.

Boulton, G.S., Zatsepin, S., and Maillot, B., 2001. *Analysis of groundwater flow beneath ice sheets*. Swedish Nuclear Fuel and Waste Management Co. Technical Report TR-01-06.

Braithwaite, R.J., and Thomsen, H.H., 1989. Simulation of run-off from the Greenland ice sheet for planning hydro-electric power, Ilulisat/Jakobshavn, West Greenland. *Ann. Glaciol.*, 13, 12–15.

Brugman, M.M., 1986. *Water flow at the base of a surging glacier*. PhD diss. California Institute of Technology, Pasadena, USA.

Budd, W.F., 1969. The dynamics of ice masses. *ANARE Scientific Reports. Series A (IV) Glaciology. Publ. No.*, 108.

Čermák, V., 1989. Crustal heat production and mantle heat flow in Central and Eastern Europe. *Tectonophysics*, 159 (3–4), 192–215.

Clarke, G.K.C., 1987. Subglacial till: a physical framework for its properties and processes. *J. Geophys. Res.*, 92 (B9), 9023–9036.

Clarke, G.K.C., 2003. Hydraulics of subglacial outburst floods: new insights from the Spring-Hutter formulation. *J. Glaciol.*, 49 (165), 299–313.

Clarke, G.K.C., Mathews, W.H., and Pack, R.T., 1974. Outburst floods from Lake Missoula. *Quat. Res.*, 22 (3), 289–299.

Clarke, G.K.C., Collins, S.G., and Thompson, D.E., 1984. Flow, thermal structure and subglacial conditions of a surge-type glacier. *Can. J. Earth Sci.*, 21 (2), 232–240.

Clarke, G.K.C., Leverington, D., Teller, J., adn Dyke, A., 2003. Perpectives. Superlakes, megafloods, and abrupt climate change. *Science*, 301 (5635), 922–923.

Clarke, G.K.C., Leverington, D.W., Teller, J.T., Dyke, A.S., and Marshall, S.J., 2005. Fresh arguments against the Shaw megaflood hypothesis. *Quat. Sci. Rev.*, 24 (12–13), 1533–1541.

Copland, L., Harbor, J., and Sharp, M., 1997. Borehole video observation of englacial and basal ice conditions in a temperate valley glacier. *Ann. Glaciol.*, 24, 277–282.

Dahl-Jensen, D., Gundestrup, N., Gogineni, P., and Miller,H., 2003. Basal melt at NorthGRIP modeled from borehole, ice-core and radio-echo sounder observations. *Ann. Glaciol.*, 37, 207–212.

Deeley, R.M., and Parr, P.H., 1914. The Hintereis Glacier. *Phil. Mag.*, 6, 153–176.

Denton, G.E. and Sugden, D.E., 2005. Meltwater features that suggest Miocene ice-sheet overriding the Transantarctic Mountains in Victoria Land, Antarctica. *Geogr. Ann.*, 87A (1), 67–85.

Drost-Hansen, W., 1967. The water-ice interface as seen from the liquid side. *J. Colloid Interface Sci.*, 25 (2), 131–160.

Duval, P., Lipenkov, V., Barkov, N.I., and de La Chapelle, S., 1998. Recrystallization and fabric development in the Vostok ice core. *Supplement to EOS Transactions Fall 1998 Meeting, AGU*, 79 (45), F152.

Engelhardt, H., 1978. Water in glaciers: observations and theory of the behaviour of water levels in boreholes. *Z. Gletscherk. Glazialgeol.*, 14 (1), 35–60.

Engelhardt, W.F., Harrison, W.D., and Kamb, B., 1978. Basal sliding and conditions at the glacier bed as revealed by bore-hole photography. *J. Glaciol.*, 20 (84), 469–508.

Eriksson, M.G., Björnsson, H., Herzfeld, U.C., and Holmlund, P., 1993. *The bottom topography of Storglaciären. A new map based on old and new ice depth measurements analysed with geostatistical methods*. Department of Physical Geography, Stockholm University, Stockholm, Sweden, Forskningsrapport 95, 46 p.

Fahnestock, M.,Abdalati, W., Joughin, I., Brozena, J., and Gogineni, P., 2001. High geothermal heat flow, basal melt and the origin of rapid ice flow in central Greenland. *Science*, 294 (5550), 2338–2342.

Faraday, M., 1859. Mr. Faraday on the properties of ice. *Athenæum and literary gazette* (15th June), 641.

Faraday, M., 1861. Note on regelation. *Phil. Mag.*, 21 146–153.

Fischer, U., Iverson, N.R., Hanson, B., Hooke, R.LeB., and Jansson, P., 1998. Estimation of hydraulic properties of the subglacial till layer from ploughmeter measurements. *J. Glaciol.*, 44 (148), 517–522.

Fletcher, R.C., 1977. Folding of a single viscous layer: exact infinitesimal amplitude theory. *Tectonophysics*, 39 (4), 593–606.

Flowers, G.A., 2000. *A multicomponent coupled model of glacier hydrology.* PhD diss. Univ. of British Columbia, Vancouver, B.C. Canada.

Flowers, G.E., and Clarke, G.K.C., 2002a. A multicomponent coupled model of glacier hydrology. 1. Theory and synthetic examples. *J. Geophys. Res.*, 107 (B11), doi:10.1029/2001JB001122.

Flowers, G.E., and Clarke, G.K.C., 2002b. A multicomponent coupled model of glacier hydrology. 2. Application to Trapridge Glacier, Yukon, Canada. *J. Geophys. Res.*, 107 (B11), doi:10.1029/2001JB001124.

Flowers, G.E., Björnsson, H., and Pálsson, F., 2003. New insights into the subglacial and periglacial hydrology of Vatnajökull, Iceland, from a distributed physical model. *J. Glaciol.*, 29 (165), 257–270.

Flowers, G.E., Björnsson, H., Pálsson, F., and Clarke, G.K.C., 2004. A coupled sheet-conduit mechanism for jökulhlaup propagation. *Geophys. Res. Lett.*, 11, L05401, doi:10.1029/2003GL019088.

Flowers, G.E., Marshall, S.J., Björnsson, H., and Clarke, G.K.C., 2005. Sensitivity of Vatnajökull ice cap hydrology and dynamics to climate warming over the next 2 centuries. *J. Geophys. Res.*, 110, F02011, doi:10.1029/2004JF000200

Fountain, A.G., 1989. The storage of water and hydraulic characteristics of the firn at South Cascade Glacier, Washington, USA. *Ann. Glaciol.*, 13, 69–75.

Fountain, A.G., 1994. Borehole water-level variations and implications for the subglacial hydraulics of South Cascade Glacier, Washington State, U.S.A. *J. Glaciol.*, 40 (135), 293–304.

Fountain A.G., and Walder, J.S., 1998. Water flow through temperate glaciers. *Rev. Geophys.*, 36 (3), 299–328.

Fountain, A.G., Jacobel, R.W., Schlichting, R.B., Jansson, P., and Frödin, S., 2002. Englacial water flow – The absence of Röthlisberger conduits. *Eos Trans. AGU, 83(47), Fall Meet. Suppl., Abstract*, C61A-01.

Fountain, A.G., Jacobel, R.W., Schlichting, R., and Jansson, P., 2005. Fractures as the main pathways of water flow in temperate glaciers. *Nature*, 433 (7026), 618–621.

Fountain, A.G., Schlichting, R., Jansson, P., and Jacobel, R.W., 2005. Observations of englacial flow passages – a fracture dominated system. *Ann. Glaciol.*, 40, 25–30.

Fowler, A.C., 1987a. Sliding with cavity formation. *J. Glaciol.*, 33 (115), 255–267.

Fowler, A.C., 1987b. A theory of glacier surges. *J. Geophys. Res.*, 92 (B9), 9111–9120.

Fowler, A.C., and Walder, J.S., 1993. Creep closure of channels in deforming subglacial till. *Proc. Roy. Soc. Lond. Ser. A*, 441, 17–31.

Fox Maule, C., Purucker, M.E., Olsen, N., and Mosegaard, K., 2005. Heat flux anomalies in Antarctica revealed by satellite magnetic data. *Science*, 309 (5733), 464–467

Frank, F.C., 1968. Two-component flow model for convection in the Earth's upper mantle. *Nature*, 220 (5165), 350–352.

Freese, R.A., and Cherry, J.A., 1979. *Groundwater*. Prentice Hall, Englewood Cliffs, NJ.

Furlong, K.P., and Chapman, D.S., 1987. Crustal heterogeneities and the thermal structure of the continental crust. *Geophys. Res. Lett.*, 14 (3), 314–317.

Geological Survey of Finland, 1984. Quaternary deposits of Finland. 1:1000000.

Hallet, B., 1976. Deposits formed by subglacial precipitation of $CaCO_3$. *GSA Bull.*, 87 (7), 1003–1015.

Hallet, B., and Anderson, R.S., 1980. detailed glacial geomorphology of a proglacial bedrock area at Castleguard Glacier, Alberta, Canada. *Z. Gletscherk. Glaczialgeol.*, 16 (2), 171–184.

Hantz, D., and Lliboutry, L., 1983. Waterways, ice permeability at depth and water pressures at Glacier d'Argentiere, French Alps. *J. Glaciol.*, 29 (102), 227–239.

Harper, J.T., and Humphrey, N.F., 1995.Borehole video analysis of a temperate glacier's englacial and subglacial structure: Implications for glacier flow models. *Geology*, 23 (10), 901–904.

Harrison, W.D., 1972. Temperature of a temperate glacier. *J. Glaciol.*, 11 (61), 15–29.

Hock, R., 1998. Modelling of glacier melt and discharge. *Zürcher Geographische Schriften*, 70, 140 pp.

Hock, R., 2005. Glacier melt: A review on processes and their modelling. *Progr. Phys. Geogr.*, 29 (3), 362–391.

Hock, R., and Hooke, R.LeB., 1993. Further tracer studies of internal drainage in the lower part of the ablation area of Storglaciären. *GSA Bull.*, 105 (4), 537–546.

Hock, R., and Jansson, P., 2005. Modelling glacier hydrology. In: *Anderson, M.G., and McDonnell, J., (eds.), Encyclopedia of Hydrological Sciences. John Wiley & Sons, Chichester*, 4, 2647–2655.

Hock, R., Jansson, P., and Braun, L., 2005. Modelling the response of mountain glacier discharge to climate warming. In: *Huber, U.M., Bugmann, H.K.M., and Reasoner, M.A., (Eds.), 2005, Global Change and Mountain Regions (A State of Knowledge Overview), Springer, Dordrecht*, 243–252.

Hodge, S.M., 1974. Variations in sliding of a temperate glacier. *J. Glaciol.*, 13 (69), 349–369.

Hodge, S.M., 1976. Direct measurement of basal water pressure: A pilot study. *J. Glaciol.*, 16 (74), 205–218.

Hodge, S.M., 1979. Direct measurements of basal water pressures: Progress and problems. *J. Glaciol.*, 23 (89), 309–319.

Hohmann, M., 1997. Soil freezing – the concept of soil water potential. State of the art. *Cold Reg. Sci. Technol.*, 25 (2), 101–110.

Holmlund, P., 1996. Maps of Storglaciären and their use in glacier monitoring studies. *Geogr. Ann.*, 78A (2–3), 193–196.

Holmlund, P., 1988. Internal geometry and evolution of moulins, Storglaciären, Sweden. *J. Glaciol.*, 34 (117), 242–248.

Holmlund, P., and Hooke, R.LeB., 1983. High water-pressure events in moulins,Storglaciären,Sweden. *Geogr. Ann.*, 65A (1–2), 19–25.

Hooke, R.LeB., 1977. Basal temperatures in polar ice sheets: a qualitative review. *Quat. Res.*, 7, 1–13.

Hooke, R.LeB., 1981. Flow law for polycrystalline ice in glaciers: Comparison of theoretical predictions, laboratory data, and field measurements. *Rev. Geophys. Space Phys.*, 19 (4), 664–672.

Hooke, R.LeB., 1984. On the role of mechanical energy in maintaining subglacial water conduits at atmospheric pressure. *J. Glaciol.*, 30 (105), 180–187.

Hooke, R.LeB., 1989. Englacial and subglacial hydrology: A qualitative review. *Arct. Alp. Res.*, 21 (3), 221–233.

Hooke, R.LeB., 1991. Positive feedbacks associated with the erosion of glacial cirques and overdeepenings. *GSA Bull.*, 103 (8), 1104–1108.

Hooke, R.LeB., 2005. *Principles of glacier mechanics. Second Edition.* Cambridge University Press, Cambridge.

Hooke, R.LeB., and Pohjola, V.A., 1994. Hydrology of a segment of a glacier situated in an overdeepening, Storglaciären, Sweden. *J. Glaciol.*, 40 (134), 140–148.

Hooke, R.Leb., Laumann, T., and Kohler, J., 1990. Subglacial water pressures and the shape of subglacial conduits. *J. Glaciol.*, 36 (122), 67–71.

Hooke, R.LeB., Hanson, B., Iverson, N.R., Jansson, P., and Fischer, U., 1997. Rheology of till beneath Storglaciären, Sweden. *J. Glaciol.*, 43 (143), 172–179.

Hooke, R.LeB., Miller, S.B., and Kohler, J. 1988. Character of the englacial and subglacial drainage system in the upper part of the ablation area of Storglaciären, Sweden. *J. Glaciol.*, 34 (117), 228–231.

Hubbard, B. and Nienow, P., 1997. Alpine subglacial hydrology. *Quat. Sci. Rev.*, 16 (9), 939–955.

Humphrey, N.F., 1987. Coupling between water pressure and basal sliding in a linked-cavity hydraulic system. In: *Waddington, E.D., and Walder, J.S., (Eds.), The physical basis of ice sheet modelling. IAHS publ.*, 170, 105–119.

Humphrey, N., Raymond, C., and Harrison, W., 1986. Discharges of turbid water during mini-surges of Variegated Glacier, Alaska, U.S.A. *J. Glaciol.*, 32 (111), 195–207.

Humphrey, N., Kamb, B., Fahnestock, M., and Engelhardt, H., 1993. Characteristics of the bed of the lower Columbia Glacier, Alaska. *J. Geophys. Res.*, 98 (B1), 837–846.

Hunsacker, J.C. and Rightmire, B.G., 1947. *Engineering applications to fluid mechanics.* McGraw-Hill Book Co., Inc., New York.

Iken, A., 1977. Variations in surface velocities of some alpine glaciers measured at intervals of a few hours. Comparison with arctic glaciers. *Z. Gletscherk. Glazialgeol.*, 13 (1–2), 23–35.

Iken, A., 1981. The effect of the subglacial water pressure on the sliding velocity of a glacier in an idealized numerical model. *J. Glaciol.*, 27 (97), 407–421.

Iken, A., and Bindschadler, R.A., 1986. Combined measurements of subglacial water pressure and surface velocity of Findelengletscher, Switzerland: Conclusions about drainage system and sliding mechanism. *J. Glaciol.*, 32 (119), 101–119.

Iken, A., Röthlisberger, H., Flotron, A., and Haeberli, W., 1983. The uplift of Unteraargletscher at the beginning of the melt season – a consequence of water storage at the bed? *J. Glaciol.*, 29 (101), 26–47.

Iverson, N.R., Jansson, P., and Hooke, R.LeB., 1994. In-situ measurement of the strength of deforming subglacial till. *J. Glaciol.*, 40 (136), 497–503.

Iverson, N.R., Hanson, B., Hooke, R.LeB., and Jansson, P., 1995. Flow mechanism of glaciers on soft beds. *Science*, 267 (5195), 80–81.

Iverson, N.R., Baker, R.W., Hooke, R.LeB., Hanson, B., and Jansson, P., 1999. Coupling between a glacier and a soft bed: I. A relation between effective pressure and local shear stress determined from till elasticity. *J. Glaciol.*, 45 (149), 31–40.

Jansson, P., 1995. Water pressure and basal sliding, Storglaciären, Sweden. *J. Glaciol.*, 41 (138), 232–240.

Jansson, P., 1996. Dynamics and hydrology of a small polythermal valley glacier. *Geogr. Ann.*, 78A (4), 171–180.

Jansson P., Hock, R., and Schneider, T., 2003. The concept of glacier storage: A review. *J. Hydrol.*, 282 (1–4): 116–129.

Jean-Baptiste, J., Petit, J.R., Lipenkov, V.Ya., Reynaud, D., and Barkow, N.I., 2001. Helium isotope in deep Vostok ice core (Antarctica): constraints on hydrothermal processes and water exchange in the subglacial lake. *Nature*, 411, 460–462.

Jellinek, H.H.G., 1967. Liquid-like (transition) layer on ice. *J. Colloid Interface Sci.*, 25 (2), 190–205.

Johnson, J., and Fastook, J.L., 2002. Northern Hemisphere glaciation and its sensitivity to basal melt water. *Quat. Int.*, 95–96, 65–74.

Josenhans, H.W., and Zevenhuizen, J., 1990. Dynamics of the Laurentide Ice Sheet in Hudson Bay, Canada. *Marine Geol.*, 92 (1–2), 1–26.

Kamb, B., 1970. Sliding motion of glaciers: Theory and observation. *Rev. Geophys. Space Phys.*, 8 (4), 673–728.

Kamb, B., 1987. Glacier surge mechanism based on linked cavity configuration of the basal water conduit system. *J. Geophys. Res.*, 92 (B9), 9083–9100.

Kamb, B., 1991. Rheological nonlinearity and flow stability in the deforming bed mechanism of ice stream motion. *J. Geophys. Res.*, 96 (B10), 16585–16595.

Kamb, B., Raymond, C.F., Harrison, W.D., Engelhardt, H., Echelmeyer, K. A., Humphrey, N., Brugman, M.M., and Pfeffer, T., 1985. Glacier surge mechanism: 1982–83 surge of Variegated Glacier, Alaska *Science*, 227 (4686), 469–479.

Kapitsa, A.P., Ridley, J.K., Robin, G. de Q., Siegert, M.J., and Zotikov, I.A., 1996. A large deep freshwater lake beneath the ice of central East Antarctica. *Nature*, 381 (6584), 684–686.

Ketcham, V.M. and Hobbs, P.V., 1969. An experimental determination of the surface energies of ice. *Phil. Mag. Eight Ser.*, 19(162), 1161–1173.

Kleman, J., and Hättestrand, C., 1999. Frozen-bed Fennoscandian and Laurentide ice sheets during the Last Glacial Maximum. *Nature*, 402 (6757), 63–66.

Kohler, J.C., 1992. *Glacial hydrology of Storglaciären, northern Sweden*. PhD diss. department of Geology and Geophysics, University of Minnesota, USA.

Kohler, J., 1995. Determining the extent of pressurized flow beneath Storglaciären, Sweden, using results of tracer experiments and measurements of input and output discharge. *J. Glaciol.*, 41 (138), 217–231.

Lambe, T.W., and Whitman, R.V., 1969. *Soil Mechanics*. John Wiley & Sons, New York.

Lang, H., 1987. Forecasting meltwater runoff from snow-covered areas and from glacier basins. In: *Kraijenhoff, D.A., Moll, J.R., (eds.), River flow modelling and forecasting. Reidel, Dordrecht*, 99–127.

Lindeberg, G., and Ringberg, B., 1999. Image analysis of rythmites in proximal varves in Blekinge,southeastern Sweden. *GFF*, 121 (3), 182–186.

Lingle, C.S., and Brown, T.J., 1987. A subglacial aquifer bed model and water pressure dependent basal sliding relationship for a West Antarctic ie stream. In: *Van der Veen, C.J., and Oerlemans, J., (eds.), Dynamic of the West Antarctic ice sheet. Proceedings from a workshop held in Utrecht, May 6–8, 1985. D. Reidel Publishing Company, Dordrecht*, 249–285.

Lliboutry, L., 1971. Permeability, brine content, and temperature of temperate ice. *J. Glaciol.*, 10 (58), 15–30.

Lliboutry, L., 1978. Glissement d'un glacier sur un plan parsemé d'obstacles hémisphériques. *Ann. Geophys.*, 34 (2), 147–162.

Lliboutry, L., 1979. Local friction laws for glaciers: a critical review and new openings. *J. Glaciol.*, 23 (89), 67–95.

Llboutry, L., 1983. Modifications of the theory of intraglacial waterways for the case of subglacial ones. *J. Glaciol.*, 29 (102), 216–226.

Marshall, S.J., and Clarke, G.K.C., 1999. Modelling North American freshwater runoff and proglacial lake history through the last glacial cycle, *Quat. Res.*, 52 (3), 300–315.

Marshall, S.J., Björnsson, H., Flowers, G.E., and Clarke, G.K.C., 2005. Simulation of Vatnajökull ice cap dynamics. *J. Geophys. Res.*, 110, F03009, doi:10.1029/2004JF000262.

Meyer-Peter, E. and Müller, R., 1948. Formulas for bed-load transport. In: *Proceedings of the 3rd Conference. International Association of Hydraulic Research, Stockholm, Sweden*, 39–64.

Müller, F., 1962. Zonation in the accumulation area of the glaciers of Axel Heiberg Island, N.W.T., Canada. *J. Glaciol.*, 4 (33), 302–313.

Müller, F., and Iken, A., 1973. Velocity fluctuations and water regime of arctic valley glaciers. In: *Symposium on the Hydrology of Glaciers, Cambridge, England, 1969. IAHS Publ.*, 95, 165–182.

Näslund, J.-O., Rodhe, L., Fastook, J., Holmlund, P., 2003. New ways of studying ice sheet flow directions and glacial erosion by computer modeling – examples from Fennoscandia. *Quat. Sci. Rev.*, 22 (2–4), 245–258.

Näslund, J.-O., Jansson, P., Fastook, J.L., Johnson, J. and Andersson, L., 2004. The First realistic dataset on distributed geothermal heat flow for ice sheet modelling. *Abstract presented at European Geosciences Union 1st General Assembly, Nice, France, April 25-30 2004.*

Näslund, J.-O., Jansson, P., Fastook, J.L., Johnson, J. and Andersson, L., 2005. Detailed spatially distributed heat-flow data for modelling of basal temperatures and meltwater production beneath the Scandinavian ice sheet. *Ann. Glaciol.*, 40, 95–101.

Näslund, J.-O., Johnson, J.V., Pattyn, F., and Jansson, P., in prep. High Resolution Geothermal Heat Flux Data – Implications for Ice Sheet Dynamics. *J. Geophys. Res. F.*

Nienow, P., Sharp, M., and Willis, I., 1998. Seasonal changes in the morphology of the subglacial drainage system, Haut Glacier d'Arolla, Switzerland. *Earth Surf. Proc. and Landf.*, 23 (9), 825–843.

Nye, J.F., 1953. The flow law of ice from measurements in glacier tunnels, laboratory experiments, and the Jungfraufirn borehole experiment. *Proc. Roy. Soc. Lond. Ser. A*, 219 (1139), 477–489.

Nye, J.F., 1967. Theory of regelation. *Phil. Mag. Eighth Ser.*, 16 (144), 1249–1266.

Nye, J.F., 1969. A calculation on the sliding of ice over a wavy surface using a Newtonian viscous approximation. *Proc. Roy. Soc. Lond. Ser. A*, 311 (1506), 445–467.

Nye, J.F., 1973. Water at the bed of a glacier. In: *IUGG-IAHS Symposium on the Hydrology of Glaciers, Cambridge, 7–13 September, 1969. IAHS Publ.*, 95, 189–194.

Nye, J.F., 1976. Water flow in glaciers: jökulhlaups, tunnels, and veins. *J. Glaciol.*, 17 (77), 181–207.

Nye, J.F., and Mae, S., 1972. The effect of non-hydrostatic stress on intergranular water veins and lenses in ice. *J. Glaciol.*, 11 (61), 81–101.

Nye, J.F., and Frank F.C., 1973. The hydrology of the intergranular veins in a temperate glacier. In: *IUGG-IAHS Symposium on the Hydrology of Glaciers, Cambridge, 7–13 September, 1969. IAHS Publ.*, 95, 157–161.

O'Neill, K., and Miller, R.D., 1985. Exploration of rigid ice model of frost heave. *Water Resour. Res.*, 21 (3), 281–296.

Padilla, F., and Villeneuve, J.P., 1992. Modelling and experimental studies of frost heave including solute effects. *Cold Reg. Sci. Technol.*, 20 (2), 183–194.

Parker, G., 1978a. Self-formed straight rivers with equilibrium banks and mobile bed. Part 1. The sand-silt river. *J. Fluid Mech.*, 89 (1), 109–125.

Parker, G., 1978b. Self-formed straight rivers with equilibrium banks and mobile bed. Part 2. The gravel river. *J. Fluid Mech.*, 89 (1), 127–146.

Parker, G., Klingeman, P.C., and McLean, D.G., 1982. Bedload and size distribution in paved gravel-bed streams. *J. Hydraul. Div. Am. Soc. Civ. Eng.*, 108 (HY4), 544–571.

Paterson, W.S.B., 1971. Temperature measurements in Athabasca Glacier, Canada. *J. Glaciol.*, 10 (60), 339-349.

Paterson, W.S.B., 1994. *Physics of Glaciers. 3rd Edition.* Oxford, Pergamon Press.

Pattyn, F., De Brabander, S., and Huyghe, A., 2005. Basal and thermal control mechanisms of the Ragnhild Glaciers, East Antarctica. *Ann. Glaciol.*, 40, 225–231.

Petit, J.R., Basile, I., Jouzel, J., Barkow, N.I., Lipenkov, V.Ya., Vostretov, R.N., Vasiliev, N.I., and Rado, C., 1998. Preliminary investigations and implications from the 3623 m Vostok deep ice core studies. In: *Lake Vostok Study: Scientific objectives and technological requirements, International Workshop, Arctic and Antarctic Research Institute, St. Petersburg.* 43 p.

Pohjola, V.A., 1993. TV-video observations of bed and basal sliding on Storglaciären, Sweden. *J. Glaciol.*, 39 (131), 111–118.

Pollard, D., DeConto, R.M., and Nyblade, A.A., 2005. Sensitivity of Cenozoic Antarctic ice sheet variations to geothermal heat flux. *Global and Planetary Change*, 49 (1–2), 63–74.

Raymond, C.F., and Harrison, W.D., 1975. Some observations on the behaviour of the liquid and gas phases in temperate glacier ice. *J. Glaciol.*, 14 (71), 213–233.

Remy, F., and Minster, J.F., 1993. Precise altimetric topography in ice sheet flow studies. *Ann. Glaciol.*, 17, 195–200.

Reynaud, L., 1987. The November 1986 survey of the Grand Moulin on the Mer de Glace, Mont Blanc Massif, France. *J. Glaciol.*, 33 (113), 130–131.

Richards, K., 1982. *Rivers*. Methuen, London.

Robin, G. de Q., 1976. Is the basal ice of a temperate glacier at the pressure melting point? *J. Glaciol.*, 16 (74), 183–195.

Roesner, L.A., Aldrich, J.A., and Dickinson, R.E., 1988. *Storm Water Management Model User's manual version 4: EXTRAN Addendum*. US Environmental Protection Agency, Athens, Georgia. 188 p.

Rooney, S.T., Blankenship, D.D., and Bentley, C.R., 1987a. Seismic refraction measurement of crustal structure in West Antarctica. In: *McKenzie, G.D., (ed.), Gondwana Six: Structure, Tectonics, and Geophysics. American Geophysical Union, Washington, DC. Geophysical Monograph*, 40, 1–7.

Rooney, S.T., Blankenship, D.D., Alley, R.B., and Bentley, C.R., 1987b. Till beneath Ice Stream B. 2. Structure and continuity. *J. Geophys. Res.*, 92 (B9), 8913–8920.

Rooney, S.T., Blankenship, D.D., Alley, R.B., and Bentley, C.R., 1988. Seismic.reflection profiling of a widespread till beneath Ice Stream B,West Antarctica. (Abstract) *Ann. Glaciol.*, 11, 210.

Röthlisberger, H., 1972. Water pressure in intra- and subglacial channels. *J. Glaciol.*, 11 (62), 177–203.

Röthlisberger H., and Lang, H., 1987. Glacier hydrology. In: *Gurnell, A., (ed.), Glacio-fluvial sediment transfer*. London: Wiley, 207–284.

Rubin, A.M., 1995. Propagation of magma filled cracks. *Annu. Rev. Earth Planet. Sci.*, 23, 287–336.

Sawagaki, T. and Hirakawa, K., 1997. Erosion of bedrock by subglacial meltwater, Soya Coast, East Antarctica. *Geogr. Ann.*, 79A, 223–238.

Scambos, T.A., Hulbe, C., Fahnestock, M., and Bohlander, J., 2000. The link between climate warming and break-up of ice shelves in the Antarctic Peninsula. *J. Glaciol.*, 46 (154), 516–530.

Schneider, T., 2000. Hydrological processes in the wet-snow zone of glaciers: a review. *Z. Gletscherkd. Glazialgeol.*, 36 (1), 89–105.

Schneider, T., 2001. *Hydrological processes in firn on Storglaciären, Sweden.* PhD diss. Department of Physical Geography and Quaternary Geology, Stockholm University. Dissertation No. 19.

Sharp, M., Richards, K.S., Arnold, N.S., Lawson, W., Willis, I., Nienow, P., and Tison, J.-L., 1993. Geometry, bed topography and drainage system structure of the Haut d'Arolla, Switzerland. *Earth Surf. Proc. Landf.*, 18 (6), 557–571.

Shaw, J., 2002. The meltwater hypothesis for subglacial bedforms. *Quat. Int.*, 90, 5–22.

Shoemaker, E.M., 1986. Subglacial hydrology for an ice sheet resting on a deformable aquifer. *J. Glaciol.*, 32 (110), 20–30.

Shreve, R.L., 1972. Movement of water in glaciers. *J. Glaciol.*, 11(62): 205–214.

Siegert, M.J., and Glasser, N.F., 1997. Convergent flow of ice within the Astrolabe subglacial basin, Terre Adélie, East Antarctica: an hypothesis derived from numerical modelling experiments. *Polar Res.*, 16 (1), 63–72.

Siegert, M.J., Dowdeswell, J.A., Gorman, M.R., and McIntyre, N.F., 1996. An inventory of Antarctic subglacial lakes. *Antarct. Sci.*, 18 (3), 281–286.

Siegert, M.J., Kwook, R., Mayer, C., and Hubbard, B., 2000. Water exchange between the subglacial lake Vostok and the overlying ice sheet. *Nature*, 403 (6770), 643–646.

Siegert, M.J., Ellis-Evans, J.C., Tranter, M., Mayer, C., Petit, J.-R., Salamatin, A., and Priscu, J.C., 2001. Physical, chemical and biological processes in Lake Vostok and other Antarctic subglacial lakes. *Nature*, 414 (6864), 603–609.

Siegert, M.J., Carter, S., Tabacco, I., Popov, S., and Blankenship, D., 2005. A revised inventory of Antarctic subglacial lakes. *Antarct. Sci.*, 17, 453–460.

Singh, P., Spitzbart, G., Hubl, H., and Weinmeister, H.W., 1997. Hydrological response of snowpack under rain-on-snow events: A field study. *J. Hydrol.*, 202 (1–4), 1–20.

Singh, P., Huebl, H., and Weinmeister, H.W., 2000. Use of the recession characteristics of snowmelt hydrographs in the assessment of snow water storage in a basin. *Hydrol. Proc.*, 14 (1), 91–101.

Skempton, A.W., 1964. Long term stability of clay slopes. *Geotechnique*, 14 (2), 77–101

Sladen, J.A. and Wrigley, W., 1983. Geotechnical properties of lodgement till – a review. In: *Eyles, N., (ed.), Glacial geology: an introduction for engineers and earth scientists. Pergamon Press, Oxford*, 184–212.

Snow, D.T., 1968. Rock fracture spacings, openings, and porosities. *J. Soil Mech. Found. Div. Am. Soc. Civ. Eng.*, 94, 73–91.

Spring, U., and Hutter, K., 1981. Numerical studies of jökulhlaups. *Cold. Reg. Sci. Technol.*, 4 (3), 227–244.

Spring, U., and Hutter, K., 1982. Conduit flow of a fluid through its solid phase and its application to intraglacial channel flow. *Int. J. Eng. Sci.* 20 (2), 327–363.

Steffen, K., Nghiem, S.V., Huff, R., and Neumann, G., 2004. The melt anomaly of 2002 on the Greenland Ice Sheet from active and passive microwave satellite observations, *Geophys. Res. Lett.*, 31 (20), L2040210.1029/2004GL020444.

Steineman, S., 1958a. Experimentelle Untersuchungen zur Plastizität von Eis. *Beiträge zur Geologie der Schweiz. Geotechnische Serie, Hydrologie*, No. 10.

Steineman, S., 1958b. Thermodynamics and mechanics of ice at the melting point. *Union Géodesique et Géophysique Internationale, Association Internationale d'Hydrologie Scientifique. Symposium de Chamonix, 16–24 Sept. 1958. IAHS Publ.*, 47, 254–265.

Stone, D.B., and Clarke, G.K.C., 1993. Estimation of subglacial hydraulic properties from induced changes in basal water pressure:a theoretical framework for borehole response tests. *J. Glaciol.*, 39 (132), 327–340.

Terzaghi, K., and Peck, R.B., 1941. *Soil mechanics in engineering practise*. John Wiley, New York.

Thomsen, H.H., Braithwaite, R.J., Weidick, A., and Olesen, O.B., 1993. Evaluation of hydropower potential for possible future industrial use Nuuk area, West Greenland. *Rapp. Grønl. Geol. Unders.*, 159, 59–62.

Thomsen, H.H., Thorning, L., and Olesen, O.B., 1989. Applied glacier research for planning hydro-electric power, Ilulissat/Jakobshavn, West Greenland. *Ann. Glaciol.*, 13, 257–261.

Thomsen, H.H., Thorning, L., and Braithwaite, R., 1986. Vurdering af de gletscher-hydrologiske forhold på inlandsisen ved Paakitsup Akuliarusersua, Ilulisat/Jakobshavn. Arbejdsnotat. *Grønl. Geol. Unders.*, 15/12 1986.

Thomsen, H.H., Thorning, L., and Braithwaite, R., 1989. Glacier-hydrological conditions on the inland ice north-east of Jakobshavn/Ilulisat, West Greenland. *Grønl. Geol. Unders. Rapport No.* 138.

Tulaczyk, S., 1999. Ice sliding over weak, fine-grained tills: dependence of ice-till interactions on till granulometry. In: *Mickelson, D.M., and Attig, J.W., (Eds.): Glacial Processes: past and present. Boulder, CO, Geological Society of America (Special paper 337)*, 159–177.

Tulaczyk, S., Kamb, W.B., and Engelhardt, H.F., 2000. Basal mechanics of Ice Stream B, West Antarctica 2. Undrained plastic bed model. *J. Geophys. Res.*, 105 (B1), 483–494.

Turcotte, D.L., and Schubert, G., 1982. *Geodynamics*, John Wiley and Sons, New York.

Tyndall, J., and Huxley, T.H., 1857. On the structure and motion of glaciers. *Phil. Trans. Roy. Soc. Lond.*, 147 (2), 327–346.

van der Veen, C.J., 1998a. Fracture mechanics approach to penetration of surface crevasses on glaciers. *Cold Reg. Sci. Technol.*, 27 (1), 31–47.

van der Veen, C.J., 1998b. Fracture mechanics approach to penetration of bottom crevasses on glaciers. *Cold Reg. Sci. Technol.*, 27 (3), 213–223.

Waddington, E.D., 1987. Geothermal heat flux beneath ice sheets. In: *Waddington, E.D. and Walder, J.S., (Eds.): The physical basis of ice sheet modelling. IAHS Publ.*, 170, 217–226.

Walder, J.S., 1982. Stability of sheet flow of water beneath temperate glaciers and implications for glacier surging. *J. Glaciol.*, 28 (99), 273–293.

Walder, J.S., 1986. Hydraulics of subglacial cavities. *J. Glaciol.*, 32 (112), 439–445.

Walder, J.S. and Fowler, A., 1994. Channelized subglacial drainage over a deformable bed. *J. Glaciol.*, 40 (134), 3–15.

Walder, J., and Hallet, B., 1979. Geometry of former subglacial water channels and cavities. *J. Glaciol.*, 23 (89), 335–346.

Williams, G.P., 1970. Manning formula – a misnomer? *J. Hydraul. Div., Am. Soc. Civ. Eng.*, 96 (1), 193–200.

Weertman, J., 1957. On sliding of glaciers. *J. Glaciol.*, 3 (21), 38–42.

Weertman, J., 1962. Catastrophic glacier advances. *Union Géodésique et Géophysique Internationale, Association Internationale d'Hydrologie Scientifique, Commission des Neiges et des Glaces. Colloque d'Obergurgl, 10-9–18-9 1962*, 31–39.

Weertman, J., 1964. Glacier sliding. *J. Glaciol.*, 5 (39), 287–303.

Weertman, J., 1972. General theory of water flow at the base of a glacier or ice sheet. *Rev. Geophys. Space Phys.*, 10 (1), 287–333.

Weertman, J., 1973. Can a water-filled crevasse reach the bottom surface of a glacier?. In: *IUGG-IAHS Symposium on the Hydrology of Glaciers, Cambridge, 7–13 September, 1969. IAHS Publ.*, 95, 139–145.

Weertman, J. and Birchfield, G.E., 1982. Subglacial water flow under ice streams and West Antarctic ice-sheet stability. *Ann. Glaciol.*, 3, 316–320.

Wingham, D.J., Siegert, M.J., Shepherd, A., and Muir, A.S., 2006. Rapid discharge connects Antarctic subglacial lakes. *Nature*, 440 (7087), 1033–1036.

Zwally, H.J., Abdalati, W., Herring, T., Larson, K., Saba, J., and Steffen, K., 2002. Surface melt-induced acceleration of Greenland ice-sheet flow. *Science*, 297 (5579), 218–222.